A combination of palynology and geochemical proxies to investigate Pliocene environmental and climate changes in tropical West Africa and east equatorial Atlantic

---

Dissertation for the Doctoral Degree in Natural Sciences

Dr. rer. nat.

in the Faculty of Geosciences

at the University of Bremen

submitted by

Francesca Vallé

March, 2016

Gutachter:

Prof. Dr. Gerold Wefer

Prof. Dr. Heiko Pälike

Date of the Doctoral colloquium

8th June 2016

Erklärung/Declaration

Name: Francesca Vallé

Anschrift: Via Aldo Moro 11, Buccinasco (Mi), Italien

Hiermit erkläre ich, dass ich

1. die Arbeit ohne unerlaubte fremde Hilfe angefertigt habe,

2. keine anderen als die von mir angegebenen Quellen und Hilfsmittel benutzt habe und

3. die den benutzten Werken wörtlich oder inhaltlich entnommenen Stellen als solche kenntlich gemacht habe.

Francesca Vallé

“You don't develop courage by being happy in your relationships everyday.

You develop it by surviving difficult times and challenging adversity.” [Epicurus]

Table of contents

Abstract

West African's climate is governed by interactions between oceans, land and the low-latitude wind systems. In order to understand and model the development of the ongoing global warming and the future responses of the environment to it, it is necessary to investigate past time intervals during which climate was warmer than today. The Pliocene epoch is known as the last prolonged interval of Earth's history warmer than today with similar climatic boundary conditions. Most of the knowledge on low-latitudes climate conditions during the Pliocene regards the oceans and atmosphere interactions. Only few proxy records, documenting environmental conditions on the continents, such as vegetation development and hydrology, are available. This thesis aims to provide new insights into West African vegetation development during the Pliocene, in relation to climate variability. Marine sediment cores retrieved offshore West Africa have been studied by means of palynology and X-ray fluorescence scanning in order to reconstruct paleoenvironmental conditions on the African continent. Additionally, by studying dinocysts in the same sediments, and comparing with the terrestrial palynological results, Pliocene land - sea connections have been researched.

The first part of this thesis (Chapter 2) focuses on West African vegetation development and pollen transport to the east Atlantic Ocean, in relation to dust supply, aridity/humidity cycles and the NE trade winds development. Pollen records and mineral elemental ratios have been obtained from Ocean Drilling Program (ODP) Site 659 sediment cores. During the Pliocene, humid climate alternated with arid and dusty conditions in West Africa. The palynological results compared with the Ti/Ca ratios, proxy for dust supply, showed that pollen transport increased during dusty intervals while it was reduced during wetter intervals. The reconstructed vegetation dynamics showed that during the late Pliocene, shifts between woodlands, grasslands and desert occurred at orbital scale. The comparison between the pollen results, dust records and north Atlantic sea surface temperature, revealed that the NE trade winds intensified in West Africa after 2.53 Ma and during two short periods before that (~2.7 and 2.6 Ma) associated with the intensification of the Northern Hemisphere glaciations.

The second part of this thesis (Chapter 3) focuses on the relationship between paleoenvironmental changes in West Africa, the sedimentation in the east Atlantic Ocean and the shifts of the Intertropical Convergence Zone. High-resolution elemental ratios obtained for sediment cores from ODP Site 959 (off Ivory Coast) have been used as environmental proxies. From 5.4 Ma towards the early Pleistocene, a long-term decrease of river supply has been documented. The observed increase of aeolian supply off the Ivory Coast after 3.5 Ma, has been linked to a southward shift of the Intertropical Convergence Zone, at least during winter. Between 3.2 and 2.9 Ma, Site 959 dust records in agreement with other dust records from off northern Africa, suggest continent-wide aridity or larger climate variability related to maxima in orbital eccentricity.

The focus of the third part (Chapter 4) of this thesis are the possible connections between the east Atlantic Ocean and the West African vegetation changes during the Pliocene. Sea surface water conditions have been reconstructed by studying the organic-walled dinoflagellate cysts content of ODP Site 959 sediment cores. Different oceanographic conditions have been detected between the early and the late Pliocene. Upwelling was reduced during the early Pliocene, when warm waters characterized the Gulf of Guinea, before the Guinea Current was fully established. During the late Pliocene instead, several upwelling intervals occurred. Those intervals have been compared to the vegetation development in west Africa and a linkage between more arid events in northwest Africa and upwelling intervals in the Gulf of Guinea has been suggested.

Zusammenfassung

Das Klima Westafrikas wird durch die Wechselwirkungen zwischen Ozean, Landmassen und den Windsystemen der niederen Breiten bestimmt. Um die weitere Entwicklung der gerade stattfindenden globalen Erwärmung und der zukünftig daraus folgenden Umweltveränderungen zu verstehen und zu modellieren, ist es notwendig, vergangene Zeitintervallen zu untersuchen, in denen das Klima wärmer als heute war. Das Pliozän wird als letztes längeres Intervall der Erdgeschichte betrachtet, das ähnlich klimatische Randbedingungen aufweiste, aber signifikant wärmer als heute war. Der größte Teil des Wissens über die klimatischen Bedingungen niederer Breiten während des Pliozäns bezieht sich auf die Wechselwirkungen zwischen Ozeanen und Atmosphäre. Nur wenige Proxies sind verfügbar, die die Umweltbedingungen der Kontinente, wie Vegetationsentwicklung und Hydrologie, dokumentieren. Diese Arbeit zielt darauf ab, neue Einblicke in die westafrikanischen Vegetationsentwicklung und deren Bezug zu Klimaschwankungen während des Pliozäns zu liefern. Es wurden palynologische Untersuchungen und Röntgenfluoreszenzmessungen an vor Westafrika entnommenen marinen Sedimentkernen durchgeführt, um die Paläoumweltbedingungen auf dem afrikanischen Kontinent zu rekonstruieren. Zusätzlich wurden Dinozysten studiert und mit den terrestrischen palynologischen Ergebnissen verglichen, um pliozäne klimatische Kopplungen zwischen Land und Ozean zu erforschen.

Der erste Teil dieser Arbeit (Kapitel 2) konzentriert sich auf die westafrikanischen Vegetationsentwicklung und den Pollentransport im Ostatlantik und deren Bezug zu Staubeintrag, Trockenheits-Feuchtigkeits-Zyklen und Entwicklung des NE Passatwinds. Die Untersuchungen der Pollen und der mineralelementaren Verhältnisse wurden an Sedimentkernen der „Ocean Drilling Program“ (ODP) Kernstation 659 durchgeführt. Während des Pliozäns fand in Westafrika ein Wechsel zwischen feuchtem Klima und trockenen/staubigen Bedingungen statt. Der Vergleich von palynologischen Ergebnissen und Ti/Ca-Verhältnissen, einem Proxy für Staubeintrag, zeigt, dass der Pollentransport während staubiger Intervalle erhöht war, während er bei feuchten Intervallen reduziert war. Die Rekonstruktion der Vegetationsdynamik ergibt, dass es im späten Pliozän auf orbitalen Skalen zu Verschiebungen von Wald-, Wiesen- und Wüstenzonen gab. Pollenergebnisse, Staubaufzeichnungen und die Rekonstruktion der Meeresoberflächentemperaturen des Nordatlantiks zeigen, dass sich die NE Passatwinde in Westafrika nach 2,53 Ma und während zweier kurzer Phasen (ca. 2,7 und 2,6 Ma) intensivierten. Der Grund waren die verstärkten Vereisungen der Nordhemisphäre.

Der zweite Teil dieser Arbeit (Kapitel 3) konzentriert sich auf die Beziehung zwischen Paläoumweltveränderungen in Westafrika, der Sedimentation im Ostatlantik und den Verschiebungen der Innertropischen Konvergenzzone. Hochauflösende Elementverhältnisse, die vor der Elfenbeinküste an Sedimentkernen der ODP-Station 959 gemessen wurden, konnten als Umweltproxies verwendet werden. Es wird dokumentiert, dass es von 5,4 Ma bis hinein in das frühe Pleistozän zu einer langfristigen Abnahme des Flusseintrags kam. Der beobachtete Anstieg des äolischen Eintrags vor der Elfenbeinküste nach 3,5 Ma wurde durch eine (zumindest im Winter vorkommende) südliche Verschiebung der innertropischen Konvergenzzone verursacht. Zwischen 3,2 und 2,9 Ma deuten Staubaufzeichnungen in den ODP 959 Kernen - in Übereinstimmung mit anderen Staubaufzeichnungen vor Nordafrika - darauf hin, dass es zu einer kontinentweiten Trockenheitsphase oder extremeren Klimavariabilität kam, die durch Maxima in der Exzentrizität der Erdbahn verursacht wurden.

Im Mittelpunkt des dritten Teils (Kapitel 4) dieser Arbeit stehen die möglichen Verbindungen zwischen dem östlichen Atlantik und den westafrikanischen Vegetationsveränderungen während des Pliozäns. Bedingungen der Ozeanoberfläche wurden durch das Studium von Dinoflagellatenzysten an Sedimentkernen der ODP-Station 959 rekonstruiert. Es wurden ozeanographische Unterschiede zwischen dem frühen und dem späten Pliozän erkannt: Der Auftrieb nährstoffreicher Tiefenwässer war während des frühen Pliozäns reduziert, als wärmeres Wasser im Golf von Guinea vorherrschte, noch bevor der Guineastrom voll etabliert war. Im

Gegensatz dazu ereigneten sich während des späten Pliozäns mehrere Auftriebsereignisse. Diese Intervalle wurden mit der Vegetationsentwicklung Westafrikas verglichen und es wird eine Verknüpfung zwischen Trockenereignissen in Nordwestafrika und Auftriebsintervallen im Golf von Guinea vorgeschlagen.

Chapter 1

Introduction

1.1 Motivation

Earth's climate system has experienced continuous change, drifting from extremes of expansive warmth with ice-free poles, to extremes of cold with massive continental ice-sheets and polar ice caps (Zachos et al. 2001). Associate to climate fluctuations, environmental changes occurred. Those changes have been recorded in natural archives (e.g. marine and continental sediments, corals, ice-sheets, glaciers, speleothem) directly in the sediments (mineral components) or throughout organisms within the sediments (micro and macrofossils). To be able to reconstruct paleoclimate and paleoenvironmental changes thus, it is necessary to study the geological archives. Moreover, to refine climate models in use to project future climate scenarios, it is necessary to research, interpreting by means of proxy records, and modelling past warm climates (Dowsett et al., 2009).

At low-latitudes interactions between oceans, atmosphere, wind systems are strong. Africa is one the most vulnerable continents to climate change and climate variability (Boko et al., 2007) since complex oceanographic and terrestrial interplays control African climate. The warm Pliocene climate, with atmospheric CO2 concentrations similar as today or higher (e.g. Salzmann et al. 2011), has been suggested as analogue scenarios for interpreting the path of future climate warming during the 21st century (Jansen et al., 2007; Salzmann et al., 2009). Remarkably, during the Pliocene, hominin extinction, speciation, and behavioural events have been associate to African climatic changes (de Menocal, 2011).

This thesis investigates the long-term vegetation and climate changes in West Africa and in the eastern equatorial Atlantic during the Pliocene; in order to identify the links between low-latitude environmental variability to the global Pliocene climate reorganization, related to changes in the atmospheric circulation, ocean gateway closure, the Northern Hemisphere Glaciation and orbital forcings.

1.2 Study area: West Africa and east equatorial Atlantic

1.2.1 Climate, atmospheric features and rainfall

Climate over West Africa is generally determined by thermodynamic contrasts between the land (i.e., the Sahara) and ocean (i.e., the equatorial Atlantic) which determine a pronounced seasonal wind shift (Nicholson, 2013). A schematic representation of the prevailing atmospheric circulation patterns over Africa during July/August and January is shown in Figure 1. For the northern hemisphere those conditions correspond respectively to the summer and winter. The two most apparent seasonal shifts are in the pressure over the Sahara and the location of the Intertropical Convergence Zone (ITCZ) (Figure 1). During the boreal summer, an intense heat low, termed the Sahara Heat Low (Peyrillé and Lafore, 2007;

Nicholson, 2013) develops over the western Saha (figure 1). The cyclonic flow around this low includes the southwesterly “monsoon” flow to the south and the northeasterly trade to the west of its core and it controls the northward penetration of the SW monsoon into the continent (Peyrillé and Lafore, 2007; Nicholson, 2013) (Figure 1). The ITCZ migrates at around 20 °N over the continent. During winter the Sahara Heat Low is located south of the Darfur mountains (Nicholson, 2013) and the changing pressure systems make the ITCZ shifting to its southern position and NE trade winds become stronger (Figure 1).

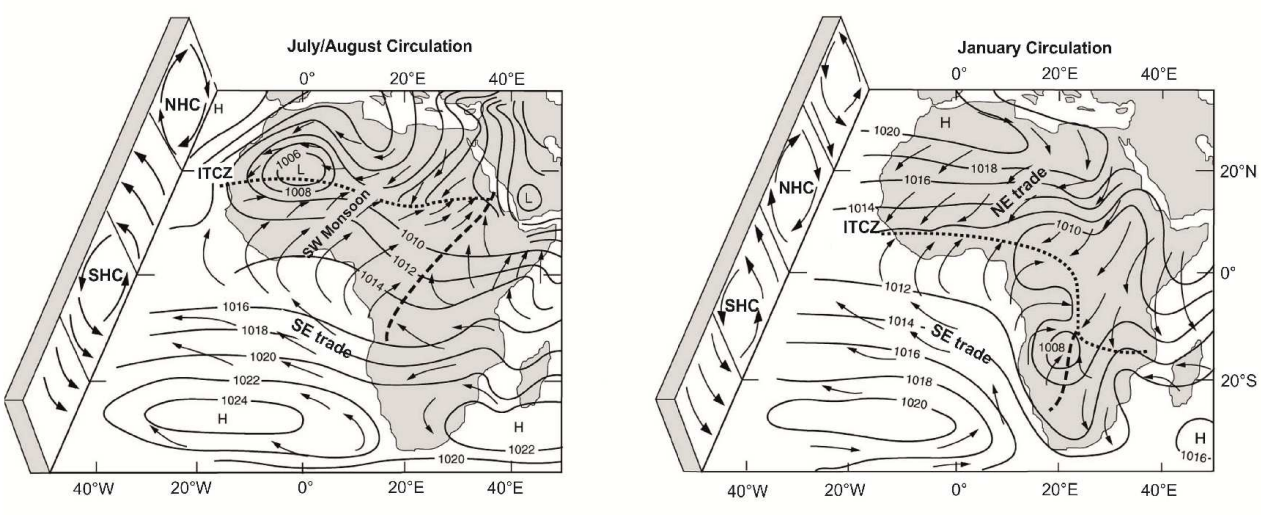

Figure 1: Schematic representation of the general patterns of low levels winds and pressure (mb) over Africa during boreal summer and winter. Dotted lines indicate the Intertropical Convergence Zone (ITCZ). Dashed lines indicate other converge zones (adapted from Gasse, 2000, after Nicholson 1996). The northern Hadley cell (NHC) and southern Hadley cell (SHC) are also indicated.

Associated to the southwest monsoon flow are the upper-level Tropical Easterly Jet (TEJ), the mid-level African Easterly Jet (AEJ), and low-level equatorial westerlies (Nicholson and Grist, 2003). In the revised view of the West African monsoon (Nicholson 2009; Nicholson, 2013) moisture available at the tropics is strongly connected to the characteristics of the African Easterly Jet and Tropical Easterly Jet, rather than by moisture convergence at the surface (Nicholson, 2009). Rainfall distribution over Africa is shown in figure 2a. Highest precipitations are found at the equatorial latitudes and decrease respectively towards northern and southern latitudes. Over southern Sahara and the northern-most Sahel, the summer rainfall is linked directly to the shifts of the ITCZ and the SW monsoon during wet years (Nicholson, 2009).

In figure 1 is also represented also the more global concept of the Hadley (northern and southern cells) cell with rising motion in the equatorial latitudes where the trade winds converge and subsidence (sinking motion) in the subtropical latitudes where the subtropical highs prevail (Nicholson, 2013). This concept is more valid for the east Atlantic ocean than for the African continent (Nicholson, 2013).

1.2.2 Vegetation

African's vegetation is zonally distributed strongly dependent on the rainfall distributions (Figure 2 a, b). White in 1983 mapped and described the African phytogeographical regions. A simplified map is shown in figure 2b. From the northern latitudes with the Sahara desert where bare soils, dunes and rocks dominate (15 in figure 2b), to zone of transition to the grasslands where aridity adapted plants grow (not distinct in figure 2b), throughout the Sahel zone (14, in figure 2b), grasslands and shrubs dominated, to the Sudanian region (3 in figure 2b), where dry forest dominate to the Guinea-Congolia/Sudanian transition zone (9, in figure 2b), where woodlands with abundant *Isoberlina* dominate, to the equatorial rain forests (1, in figure 2b). Northern of the Sahara desert (7 and 16 in figure 2b) are present vegetation rich in Mediterranean plants (e.g. *Pinus*) and steppe with abundant *Artemisia* and *Ephedra*. All flowering plants produce pollen grains. Most of the pollen grains are transported by NE trade winds, especially those from Mediterranean plants and by the African Easterly Jet, especially those from plants of the desert regions (Chenopodicaceae and Amaranthaceae), from the African continent to the east Atlantic Ocean and settle in marine sediments (Dupont, 1999a, Hooghiemstra et al., 2006). Pollen grains from plants growing in the rain forests regions, like *Alchornea* or *Rhizophora* (mangrove) are most likely transported by rivers (Dupont, 1999a and reference therein).

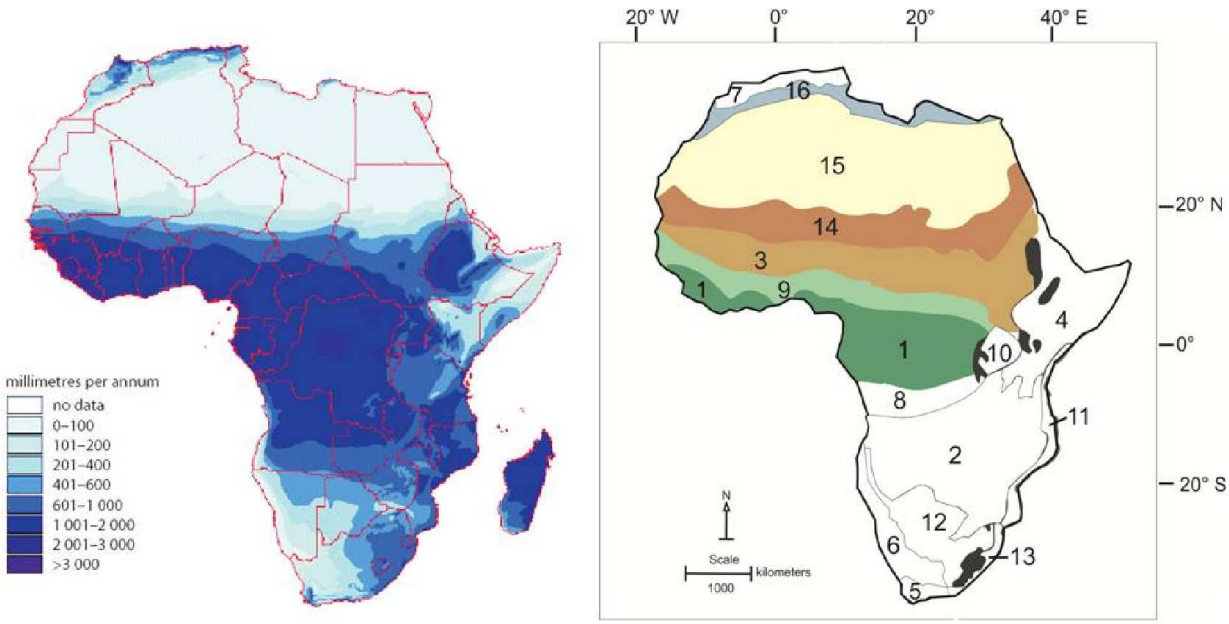

Figure 2a) Annual rainfall distribution (from: Africa Environment outlook, FAO/Agrhymet Network and ESRI). 2b) Africa's Phytogeographical regions after White (1983): 1= Guineo-Congolian center of endemism, 2 = Zambezian, 3 = Sudanian, 4 = Somalia-Masai, 5 = Cape region, 6 = Karoo-Namib, 7 = Mediterranean, 8 = Guinea-Congolia/Zambezian transition zone, 9 = Guinea-Congolia/Sudanian transition zone, 10 = Lake Victoria regional mosaic, 11 = Zansibar-Inhambane regional mosaic, 12 = Kalahari-Highveld transition zone, 13 = Tongoland-Pondoland regional mosaic, 14 = Sahel transition zone, 15 =

Sahara transition zone, 16 = Mediterranean/Sahara transition zone. Coloured regions cover the area of interest for this study.

Vegetation zones or biomes in west and south Africa changed in association to climate changes throughout the Pleistocene (Dupont, 2011). Biomes extended or retreated following climatic cycles. For examples, the Mediterranean forest area expanded during interglacials; the northern Saharan desert during glacials, and the semi-desert area in between during the transitions. Savannahs extended or shifted to lower latitudes during glacials. While the representation of the tropical rain forest fluctuated with summer insolation and precession, that of the subtropical biomes followed the pattern of glacial and interglacials (Dupont, 2011).

1.2.3 Dust formation, transport and deposition

The arid regions and the Sahara desert in northwest Africa constitute part of the largest and persistent sources of aeolian dust (e.g. Prospero et al., 1981; Prospero et al., 2002). Dust is important for several reasons. Mineral dust reaching the oceans have effects on many marine biogeochemical processes. Iron from dust, for examples, can be used by organisms where it is a limiting factor (Falkowski et al. 1998; Prospero et al., 2002). Dust has an important role in paleoclimate studies (Prospero et al., 2002); the concentration of aeolian mineral dust in deep-sea sediments (e.g. Rea, 1994; Tiedemann et al., 1989; 1994; Mulitza et al., 2009) is often used as a proxy indicator of paleoclimate aridity on the continents and of changes in the global wind systems. Generally, dust mobilization is dominated by natural sources and its activity depends on many environmental parameters, like vegetation cover and precipitation (Prospero et al., 2002). Mineral dust of northwest African regions, has different sources with different weathering conditions, which correspond to different geochemical compositions of the mineral particles (e.g. Moreno et al., 2006). Dust transport over African until reaching the east Atlantic ocean depends on winds activity of the general atmospheric circulations. Moreover, the "dust belt" (zone of dust emissions) over north Africa shifts interannually (e.g. Prospero et al., 2002). Maximum dust transport occurs in summer when large quantities of dust are carried across the Mediterranean to Europe and across the Atlantic to the Caribbean associated to the activity of the Saharan Air Layer (Sarnthein et al., 1981; Prospero et al., 2002). During winter, dust activity shifts at lower latitudes (Prospero et al., 2002) and the dry Harmattan from central Africa reach the Gulf of Guinea (Kalu, 1979). Geochemical and physical analysis of atmospheric aerosols collected along a transect off the West African coast, revealed that the majority of the aeolian sediments, deposited in the proximal equatorial Atlantic Ocean are transported by the NE trade winds (Stuut et al., 2005).

1.2.4 Oceanographic setting of east tropical Atlantic

The major surface currents offshore west Africa are wind-driven bands flowing eastward and westward (Philander, 2001). These are the Canary Current (CC), North Equatorial Current (NEC), the North Equatorial Countercurrent (NECC), the Guinea Current (GC), the Equatorial Undercurrent (EUC), the South Equatorial Current (SEC), the South Equatorial Countercurrent (SECC) (Wefer and Fisher, 1993) (figure 3). The Canary Current transports

cool waters from higher latitudes towards lower latitudes along the West African continental margin. Between 25°N-20°N gradually merges into the westward North Equatorial Current (Mittelstaedt, 1991). Around 20° and 24° N persistent upwelling occurs connected with trade wind strength; north and south of those latitudes upwelling is seasonal (Mittelstaedt, 1991) (figure 3). The NECC flows eastwards; it is stronger in summer when it is extending between 5° and 10° N strengthening the Guinea Current (Mittelstaedt, 1991). The GC brings low-saline warm waters eastward (Hisard and Merle, 1979). The EUC carries cool and highly saline waters (Hisard and Merle, 1979) and it is stronger in summer when SE trade are enhanced and the east-west equator thermocline gradient is maximum (Philander, 2001). The combined activity of winds parallel to the coast together with the shoaling of the equatorial thermocline and the reinforced EUC, develop seasonal coastal upwelling in the Gulf of Guinea (Verstraete, 1992) (figure 3). The vertical particles fluxes in upwelling areas off northwest Africa and in the Gulf of Guinea are characterized by carbonate-producing organisms (Wefer and Fisher, 1993). Along the equator, the trade winds activity causes water divergence and oceanic upwelling (Peterson and Stramma, 1991; Wefer and Fisher, 1993). The Canary current and the North Equatorial Current are part of the north Atlantic subtropical gyre (not shown in figure 3). The western boundary current of the subtropical gyre is the Gulf Stream which carries warm and saline waters from the subtropics to the higher latitudes. In the north Atlantic water masses are subjected to cooling and become more saline and denser and in localized areas in association with vertical mixing processes, they sink originating and maintaining deep water masses flowing southward, such as the oxygenated North Atlantic Deep Water (NADW) (e.g. Sarnthein et al., 1994; Rahmstorf, 2006), a key feature of the global thermohaline circulation and of the Atlantic Meridional Overturning Circulation (AMOC).

Connections between sea surface temperatures anomalies in the Gulf of Guinea and precipitations over west Africa, via atmospheric circulation and the west African monsoon, have been demonstrated (Vizy and Cook, 2001). In general, when sea surface anomalies are warm in the Gulf of Guinea, rainfall increases over the Guinean Coast, while normally cool sea surface Atlantic temperatures correspond to aridity in the tropical African areas (Norris, 1998).

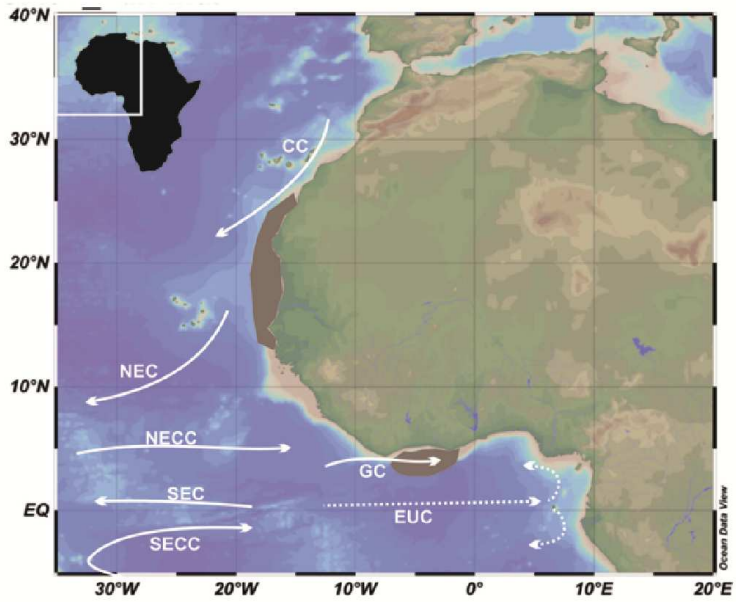

Figure 3: Features of the northeast tropical Atlantic. Surface currents are indicated with solid white arrows: CC=Canary Current, NEC=North Equatorial Current, NECC=North Equatorial Countercurrent, GC=Guinea Current, SEC=South Equatorial Current, SECC=South Equatorial Countercurrent. Dotted lines indicate subsurface currents: EUC= Equatorial Undercurrent. Seasonal upwelling areas off Cap Blanc and off the Ivory Coast/Ghana are shown with brown shaded areas (adapted from Wagner, 1998). Base map from Ocean Data View.

1.3 The Pliocene epoch

The Pliocene epoch (5.33 – 2.58 Ma ago) is divided in two stages: the Zanclean (or early Pliocene) from 5.33 to 3.6 Ma and the Piacenzian (or late Pliocene) from 3.6 to 2.58 Ma. It is a period of profound reorganizations in the Earth's climate system, during which there is a transition from relatively warm climates to cooler climates of the Pleistocene. Changes in the climate, were linked to variations of atmospheric carbon dioxide concentrations, modifications in the oceans (including closures of ocean gateways) and atmospheric circulation systems. A combination of these events are also advanced as causes for the development of four globally recognizable, glacial events, associated to sea-level drops, at ca. 4.9–4.8 Ma, at ca. 4.0 Ma, at c. 3.6 Ma, and ca. 3.3 Ma (during Marine Isotope stage, M2), which precede the intensification of the Northern Hemisphere Glaciation, at ca. 2.75 Ma (e.g. De Schepper et al., 2014).

The early Pliocene was characterized by global temperatures 2-3°C higher than today (Dowsett et al., 1996) though with small differences in atmospheric carbon dioxide concentrations (Fedorov et al., 2013). Most important for this interval are the reconstructed and modelled oceanic features which might have sustained the warmer climate. A permanent Pacific El Niño-like state, has been suggested in association to a deeper equatorial thermocline and a reduced west-east equatorial gradient (Wara et al. 2005). The reduced equatorial to subtropics gradient has been causing an expanded tropical warm pool with consequently reduced intensities of both the Hadley (Brierley et al. 2009) and the zonal Walker circulations (Wara et al. 2005; Ravelo, 2006; Brierley et al. 2009). Moreover, model results, showed for this interval, an expanded ITCZ, and increased precipitations over southwest African, east Africa and the Sahara desert (Brierley et al., 2009). In agreement with those suggested states, it has been shown that cold upwelling regions that characterize

the modern Pacific Ocean did not exist between 4.6 and 3.1 Ma (Dekens et al. 2007). A first decline of SSTs reconstructed in the Benguela upwelling systems around 3.2 Ma, suggested the same in the southern tropical Atlantic (Marlow et al., 2000).

An important event which has been suggested as linkage between low and high latitudes climate is the closure of the Central American Seaway (CAS). The shoaling of the CAS started at around 4.6 Ma (Haug and Tiedemann, 1998, Steph et al., 2006; Schmidt, 2007). Since then, warm saline waters from the western tropical Atlantic were diverted into the North Atlantic transporting heat and salt to high northern latitudes (Haug and Tiedemann, 1998), starting the intensification of the North Atlantic Deep Water (NADW) (Haug and Tiedemann, 1998; Ravelo and Andreasen, 2000; Schreck et al., 2013). Before closure of CAS, the thermohaline circulation was less efficient (Haug and Tiedemann, 1998; Billups et al., 1999). It has been thought that this led to increased moisture release in the northern North Atlantic which increased rainfall in northwest Eurasia and runoff from Siberia, leading to a freshening of the Arctic Ocean and, ultimately, to the build-up of large ice sheets in the northern Hemisphere (Driscoll and Haug, 1998) beginning at around 3.2 Ma (Jansen et al., 2000). Recently, it has been argued that the closure of CAS had not a direct impact on development the Northern Hemisphere ice sheets (De Schepper et al. 2014). Instead, it should have caused a shoaling of the thermocline, strengthening its connection with SSTs, increasing climate sensitivity during the Pliocene (Larivière et al. 2012; De Schepper et al., 2014). A gradual increase in climate sensitivity has been suggested from ~4 Ma to 2 Ma (Ravelo et al., 2004).

At the beginning of the late Pliocene, ca. 3.6 Ma, reconstructed SSTs at both high and low latitudes, record a cooling event (e.g. Naafs et al. 2010; Lawrence et al. 2009). After 3.5 Ma, temperatures in the Northern Atlantic recorded 2-3°C less than earlier (Naafs et al. 2010; Lawrence et al., 2009). The time interval between ~3.3 and 3.0 Ma is called the Mid-Pliocene Warm Period (MPWP, Dowsett, 2007) and it has been object of several modelling studies of the USGS Pliocene Research, Interpretation and Synoptic Mapping (PRISM) and within the PlioMIP framework (e.g. Haywood et al. 2010; Couteaux et al., 2012) because it has been referred as the last interval of Earth's history when global mean annual temperatures have been estimated to be 2.5°C higher than pre-industrial levels (Haywood et al., 2009) and during when continental position is similar to present one. Recent findings indicate that these higher temperatures were accompanied by only a small increase in atmospheric CO_2 suggesting a higher-than-expected sensitivity of global warming to CO2 levels (Lunt et al. 2010, Pagani et al. 2010; Seki et al. 2010) possibly due to an underestimation of the role of longer-term feedbacks such as terrestrial ecosystems on global climate. In figure 4, global Pliocene paleoclimate records and major paleoceanographic events occurred in the Atlantic and Pacific Oceans, reconstructed by means of several proxies are plotted against time. During the mid-Pliocene warm period, a strong Atlantic meridional overturning circulation (AMOC) is suggested, in causing warm conditions in the North Atlantic (Bartoli et al., 2005), which were suggested to be the main driver of humidity in tropical North Africa (deMenocal and Rind, 1993a). During the late Quaternary, West African aridity and vegetation changes

are mainly driven by AMOC variations, as postulated by Mulitza et al. (2008), Castañeda et al. (2009), Niedermeyer et al. (2009).

During the MPWP, low-latitude continental climate should thus be characterized by elevated humidity and expansion of wet biomes, such as rainforest and tree savannah. However, relatively little is known about low-latitude hydrology and the associated development of tropical vegetation during this time period. Modelling studies suggest a greatly reduced meridional temperature gradient in the North Atlantic associated with increased precipitation in Northern and East Africa and India (Lunt et al., 2007, Prange, 2008, Salzmann et al., 2008). Accordingly, in the generally warmer and moister climate of the Mid-Pliocene woodlands and tropical savannahs extended northwards far into today's arid regions (figure 5; Salzmann et al., 2008). Actual proxy records documenting these hydrologic conditions and vegetation distributions are, however, sparse. During the last 8 Ma several "green" humid periods in the Sahara have been identified (Larrasoaña et al. 2013). During these cycles interactions between vegetation cover, rainfall and dust formation are mainly controlled by the African summer monsoon oscillating in synch with Earth's orbital precession cycles (deMenocal 2011, Larrasoana et al., 2013; Zhang et al., 2014). The well-known dust records off Northwest (NW) Africa (Tiedemann et al., 1994, deMenocal, 1995), all show rhythmic (orbitally-paced) fluctuations in dust flux, which were suggested to indicate a changing forcing of aridity variations due to increasing ice volume (deMenocal, 1995, 2004). Recently, however, the paleo-environmental significance of the dust flux records was debated to be much more indicative for a transition from a relatively wet to an arid or hyper-arid climate instead of directly recording aridity (Trauth et al., 2009). Moreover, large atmospheric dust mobilization might even result from highly localized sources passing climatic threshold values instead of being indicative of aridity levels in large-scale continental areas (Prospero et al., 2002, Kröpelin et al., 2008). Dust formation and transport is linked to vegetation cover and precipitations (Prospero et al., 2002). Development of the late Pliocene vegetation of NW Africa and the Saharan-Sahelian boundary in particular, has been documented by a marine palynological record taken west of Cape Blanc, which reaches back to 3.7 Ma but not into the Early Pliocene (Leroy and Dupont, 1994). Long-term development includes changes in the floral composition of the savannah, the southward shift of the dry forest biome, and the stepwise increase of the trade winds. Millennial scale variability showed increase in the obliquity forcing of climate and vegetation after intensification of the northern Hemisphere Glaciation (NHG), probably expressing the link between low North Atlantic sea surface temperatures (SSTs) and strong North African aridity (Dupont and Leroy, 1995).

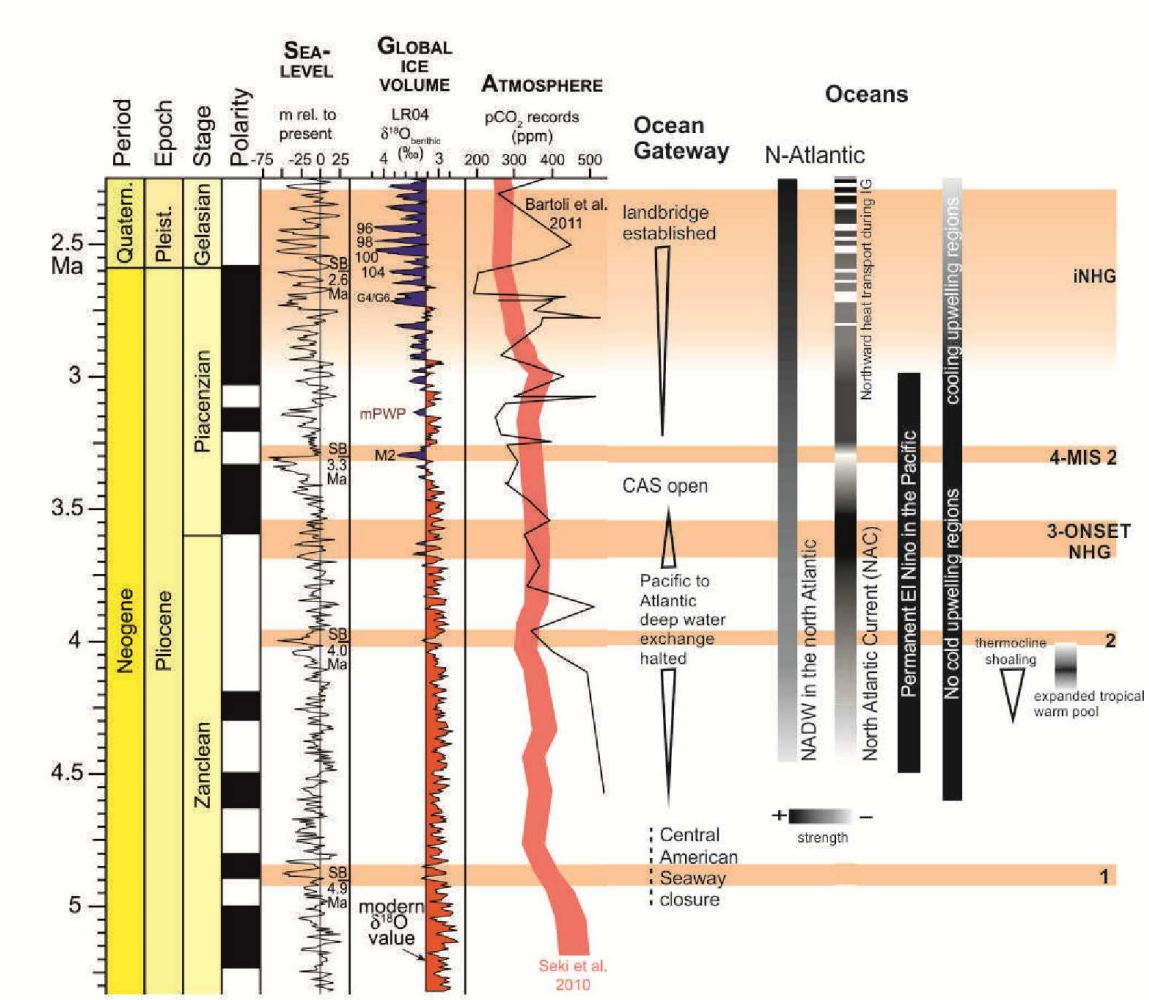

Figure 4: Pliocene global palaeoclimatic records (sea level changes, global ice volume, atmospheric carbon dioxide) together with major palaeoceanographic (gateway, currents and upwelling) events occurring in the Atlantic and Pacific Oceans and glaciations events (modified from De Schepper et al. 2014). Sea level changes are from Miller et al. 2005; global ice volume is from Lisiecki and Raymo, 2005. References for Central American Seaway closure (Haug and Tiedemann, 1998; Steph et al., 2006; Schmidt, 2007); for CAS open: De Schepper et al., 2013. For NADW enhancement: Haugh and Tiedemann, 1998; Ravelo and Andreasen, 2000; Schreck et al., 2013. For NAC: Lawrence et al., 2009,2010; Naafs et al., 2010; De Schepper et al., 2013. For Permanent El-Nino: Wara et al., 2005; For No cold upwelling and cooling of the upwelling regions: Marlow et al., 2000; Dekens, 2007. For The thermocline shoaling: Larivière et al., 2012. For the expanded warm pool: Brierley et al., 2009.

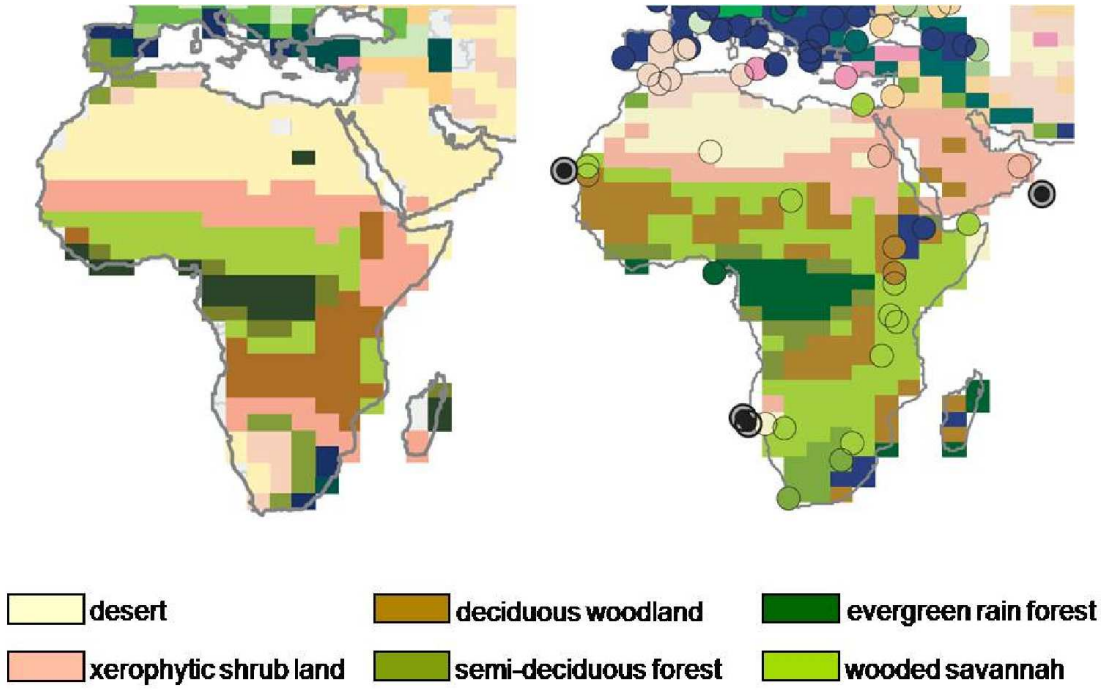

Figure 5: Reconstruction of Mid-Pliocene vegetation (right) using both data and model results compared to modern biomes (left) after Salzmann et al. (2008).

1.4 Scientific objectives

Overall, little is known about the West African environmental evolution (e.g. vegetation and hydrology) and the changes within the east Atlantic Ocean, and their connections to the global climate and oceanographic evolution throughout the Pliocene.

The main goal of this thesis is to investigate the long-term environmental and climatic evolution in West Africa and in the surface waters of the eastern equatorial Atlantic during the Pliocene epoch, in order to improve understanding of the linkages between low-latitude environmental variability and its driving forces during the global Pliocene warm climate.

Basic hypotheses were: 1) the MPWP is the result of the closure of the CAS, redirecting warm tropical waters to the North Atlantic. It caused elevated humidity and extensions of woodland and forest biomes in NW Africa; 2) NW African aridity and vegetation changes are mainly driven by AMOC variations as recently postulated by Mulitza et al. (2008), Castañeda et al. (2009) and others.

More specifically, the following questions were addressed:

1. Was the MPWP characterized by a generally warmer and wetter West African climate or were arid events just less intense?
2. What were the triggers of dust export events and how do they relate to West African climate variability?
3. Before the CAS closure, i.e., before intensification of the AMOC, was West Africa generally drier and less vegetated?
4. Which were the land-sea connections during the Pliocene?

These hypotheses and questions were tested by studying vegetation and climate (i.e. humidity versus aridity; dust activity) dynamics within the early Pliocene, before the closure of the CAS, and during the late Pliocene, including the MPWP and the intensification of the Northern Hemisphere Glaciation. Additionally, sea surface waters conditions of east Atlantic have been reconstructed and compared with continental conditions in order to establish land-sea connections.

1.5 Materials and methods

Materials used for this thesis, are briefly presented and compared in the following paragraph. After, basics concepts of the used methodologies are introduced.

1.5.1 ODP Sites 659 and 959

Marine sediments cores off west Africa used in this study have been retrieved during two Legs of the Ocean Drilling Programs (ODP). ODP Site 659 was drilled during Leg 108 in 1986 at a subtropical latitude (18°04' N) and 3070 m water depth, ~ 530 km off the coast of Mauritania (Ruddiman et al., 1987). ODP Site 959 was drilled during Leg 159 in 1995 at an equatorial latitude (3°37' N) and 2100 m water depth, ~120 km offshore of Ivory Coast (Mascle et al., 1996) (Figure 6). ODP Site 659, located out of the upwelling area off Cap Blanc it is considered as open-ocean environment site because of its low organic carbon content (Stein et al., 1989). ODP Site 959 is located within the seasonal upwelling area off Ivory Coast/Ghana (Wagner, 1998). In Figure 3, (section 1.2.4) are shown the upwelling areas off West Africa. The studied sites differ in the distance from the African coast but both are supposed to receive today small river supply (Tiedemann et al., 1989; Giresse et al., 1998). Terrigenous contents at both sites is attributed to aeolian supply (Tiedemann et al. 1989, 1994; Giresse et al. 1998; Wagner, 1998). Site 659 lies below the mid-tropospheric African Easterly Jet (AEJ) stream, which is stronger in summer (Sarnthein et al. 1981) and it is reached by the NE trade winds, thus receives dust all year round (Figure 6). Site 959 is reached by the winter dust plume of the strengthened NE trade winds and the dry Harmattan (Kalu, 1979; Prospero et al. 2002; Resh et al., 2007) (Figure 6). The age model for Site 659 is that from Tiedemann et al. (1994) which has been obtained by tuning the dust records to the northern summer insolation. For ODP Site 959 a hole-to-hole correlation, thus a composite depth record, was not available for the entire Pliocene and the chronological control was only based on biostratigraphy (Wagner, 2002). In order to be able to sample the Pliocene intervals considering coring gaps, it became necessary to develop a composite depth record and a detailed age model (see Chapter 3).

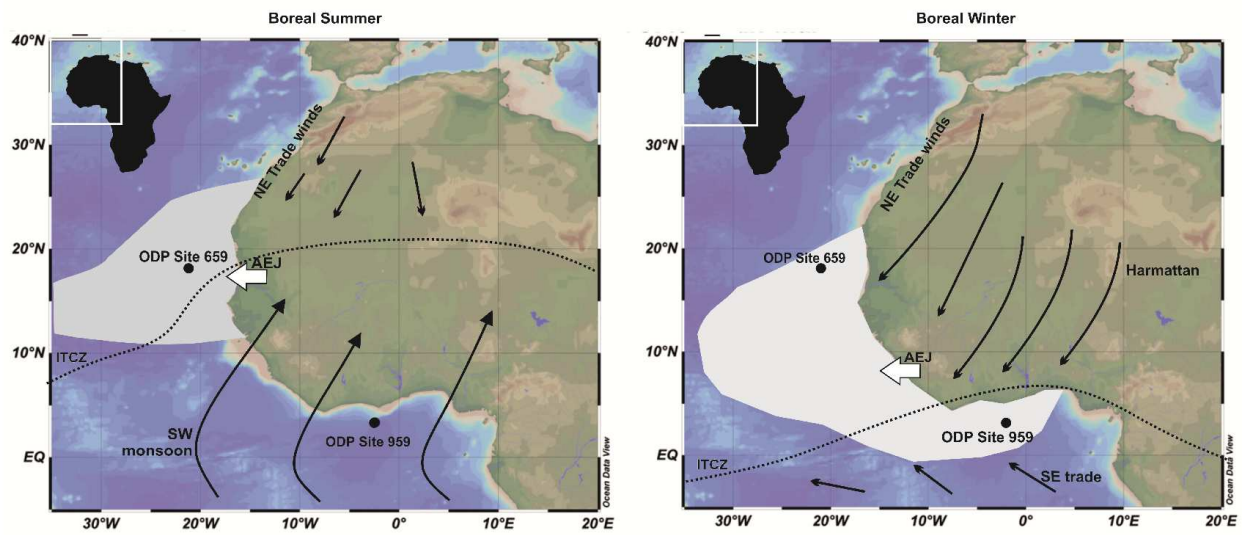

Figure 6: Location of the Ocean Drilling Program Sites 659 and 959 below summer and winter dust plumes (after Ruddimann et al., 1989). Major atmospheric features: ITCZ, NE trade winds, SE trade winds, SW monsoon and AEJ, are also shown.

1.5.2 Methodologies

1.5.2.1 Marine palynology

Marine palynology studies microfossils, included in marine sediments, that are resistant to maceral treatment (Dupont, 1999a). The walls of pollen, spores (terrestrial palynomorphs) and organic-walled dinoflagellate cysts (marine palynomorphs) are composed respectively by sporopollenin and dinosporin which are organic compounds resistant in non-oxidised conditions. Pollen data obtained from deep-sea core allow the study of vegetation dynamics over long periods, being normally continuous records (e.g. Dupont, 1999a). By studying terrestrial and marine palynomorphs in the same sediments samples direct land-sea correlations are possible.

1.5.2.1.1 Terrestrial palynomorphs

Pollen grains, fern spores, freshwater diatoms (siliceous wall), phytoliths (siliceous fragments) and charcoal from the African continent reach the east Atlantic ocean by means of aeolian or river transport. These micro-remains constitute part of the terrigenous organic matter in marine sediments. Focus of this thesis are pollen and spores. Important aspects have to be considered when analysing pollen and spores content in marine sediments: the sources and production of pollen grains, the transport to the ocean and through the water column, sedimentation processes, fossilization and accumulation in the sediments (Dupont, 1999a). Pollen production varies strongly between plant species, for example, Poaceae (grasses) produce more pollen grains than plants of the rain forests. Off west Africa, especially for open-ocean environment sites (e.g. ODP Site 659) pollen grains, are attributed to the transport of the NE trade winds and of the African Easterly Jet (AEJ) (Hooghiemstra et

al., 2006). In general, pollen transport through the water column is faster in areas of high productivity where sporomorphs are incorporated in the food chain. Moreover, time-series data of sediment traps indicate a significant correlation between the fluxes of organic carbon and lithogenic particles, with a fast and nearly unaffected sinking to the seafloor (Ratmeyer et al., 1999). Studies on surface sediments samples off west Africa showed that pollen and spores assemblages in deep-sea cores, reflect the composition of the vegetation zones, being their source areas (Hooghiemstra et al. 1986; Dupont and Agwu, 1991; Hooghiemstra et al., 2006). Furthermore, studies of marine pollen records off west Africa, covering different time slices demonstrated the extension and shifts in the latitudinal position of the phytogeographical regions (e.g. Dupont et al., 1998; 1999b; Dupont et al. 2007).

1.5.2.1.2 Marine palynomorphs: organic-walled dinoflagellate cysts

Dinoflagellates are single-celled organisms that have two distinctive flagella during at least part of their life cycle and/or a special type of nucleus called a dinokaryon (Fensome, et al., 1993). Several marine species produce fossilizable organic-walled cysts that correspond to their dormant stages. Dinoflagellates based on their feeding strategies are divided in heterotrophic taxa and autotrophic taxa (Fensome et al., 1996). Heterotrophic species produce organic-walled cysts that are more sensitive to oxidation. Autotrophic taxa produce organic-walled cysts more resistant to oxidation (e.g. Zonneveld et al. 1997). Dinoflagellates are an important component of the primary oceanic productivity, thus can be used as indicators for productivity and upwelling. Modern distribution of dinoflagellate cysts assemblages reflect the environmental conditions (e.g. salinity, sea surface temperatures, nutrient richness) of the surface waters (mostly the photic zone) where the motile form leave (e.g. Wall et al., 1977; Zonneveld et al., 2013). Therefore, fossil organic-walled dinoflagellate cysts are an important tool for paleoenvironmental reconstructions.

1.5.2.1.3 Palynological treatment

To extract the palynomorphs from the sediments a standard palynological method (Faegri and Iversen, 1989) has been applied for this study. First, for each sample of ~2 cm thickness a volume has been measured by water displacement. This is necessary for later calculation of pollen influx or accumulation rates of each taxa (pollen or dinoflagellate cyst). Additionally, a known number of indicator spores (*Lycopodium clavatum*) has been added to each sample. Afterwards, the sample was treated with ~5 % HCl to dissolve carbonates and treated with ~40 % HF to dissolve silcates for at least 48h. The residuals were not exposed to KOH or acetolysis to avoid dissolving of sensitive organic-walled dinoflagellate cysts. After neutralisation by water washing, the residuals were sieved under ultrasonic treatment using a 8 µm screen effectively holding back particles bigger than 10 µm. The sieved and cleaned residuals were stored in water. Some drops of the residual were placed with glycerol (for few slides with glycerin jelly) on a slide to allow examination with a light transmitting microscope using magnifications of 400x, and 1000x. In the same slides the numbers of indicator spores were counted to calculate the concentration of the palynomorphs per ml sediment. The

accumulation or flux rates of palynomorphs was then calculated by multiplying the concentration with the sedimentation rates.

Pollen taxa were identified following the atlas of Bonnefille and Riollet (1980), Maley, 1970; Sowunmi, 1973; 1995; Ybert, 1979, the African Pollen Database (http://apd.sedoo.fr/pollen/), as well as the reference collection of the Department of Palynology and Climate Dynamics of the University of Göttingen. The identification of dinocysts was based on published morphological descriptions from Head et al. (1989), Head (1997), Head and Westphal (1999), De Schepper and Head (2009), Warny and Wrenn (1997), Schreck et al. (2012, 2013), Morzadec-Kerfourn, (1992), McMinn (1992).

1.5.2.2. X-Ray Fluorescence core scanning

To derive paleoceanographic and paleoenvironmental information from physical and chemical characteristics of sediments it is necessary to obtain the most continuous and accurate measurements possible (Jansen et al., 1998; Röhl and Abrams, 2000). Moreover, high resolution records are necessary for looking at Milankovitch cycles signature in the sediments (Jansen et al., 1998). High-resolution down-core measurements can be obtain almost in continuous by means of X-ray fluorescence scanning (Jansen et al., 1998). Detailed XRF core scanning have already been used for high-resolution time-series studies, stratigraphic correlations, and detailed sedimentary reconstructions on different time slices (e.g. Röhl et al., 2007; Tjallingii, 2006; Westerhold et al., 2005; Westerhold and Röhl, 2006; Westerhold et al., 2012; Zeeden et al., 2013). The Avaatech X-ray Fluorescence (XRF) core scanner is a computer controlled core-scanning instrument that analyses the chemical composition of sediments directly at the surface of a split sediment core (Figure 7) (Röhl and Abrams, 2000). Therefore, XRF core scanner measurements are non-destructive and relatively fast compared to chemical analysis on discrete samples. To obtain good XRF analysis, the core surfaces must be as flat as possible (Röhl and Abrams, 2000). Therefore, before scanning, the cores must be prepared, cleaning the surface and removing cutting residues and anything that can disturb the instrument. Moreover, in order to prevent contamination and dessication of sediments, the split core surface needs to be covered by a special foil (Röhl and Abrams, 2000). The system configuration of the core scanner (Xray tube energy, detector sensibility) allows the analysis of elements from potassium (K, atomic number 19) through strontium (Sr, atomic number 38; 20 kV Xray voltage) (Röhl and

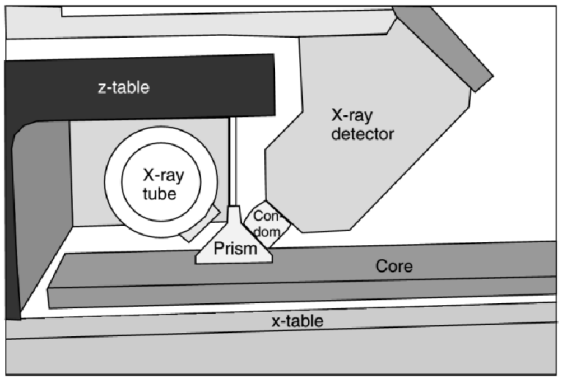

Figure 7: schematic representation of the measurement scanner of the XRF core scanner at the Marum, Bremen. The X-ray tube and the detector are oriented so that the incident beam and the detector make an angle of 45°with the surface of the sample (From Röhl and Abrams, 2000)

Abrams, 2000). The analyses are performed at predetermined positions (~measurement resolution) and counting times (Röhl and Abrams, 2000). The Xray source (the detector) is moved along the Z axis, the plastic prism is lowered on the core surface during analysis; a slit defines the dimensions of the irradiated core surface. To avoid loss of energy because of scattering in air, the area of analysis is flushed by helium. The core is moved along the X axis (Figure 7) (Röhl and Abrams, 2000). The resulting data are element intensities in counts per second (Röhl and Abrams, 2000). Element concentrations (e.g., in percent or parts per million) are not directly available, but after correlation with data from standard chemical analyses from discrete samples, these counts can be converted to element concentrations (Jansen et al., 1998; Röhl and Abrams, 2000).

For this thesis, light elemental intensities Al, Si, Ti, Fe, Ca, K, Fe, (resulted reliable, i.e. sufficient after a first measuring test) have been measured on split core surface of archive halves of ODP Site 659 and ODP Site 959 (for details regarding sections scanned, see Chapters 2 and 3) with the Avaatech XRF core scanner II at the IODP Core Repository at MARUM—Center for Marine Environmental Sciences of the University of Bremen. At ODP Site 659 the scanning resolution has been 2-cm-interval, while at ODP Site 959, it has been 1 cm interval. The instrumental settings have been the same: measurements have been collected over 1 cm^2 using a generator setting of 10kV and 20 s counting time. The split core surface was covered with a 4 µm thin SPEXCerti Prep Ultralene1 foil to avoid contamination of the XRF measurement unit and desiccation of the sediment. The data have been acquired by a Canberra X-PIPS Silicon Drift Detector (SDD; Model SXD 15C-150-500) with 150eV X-ray resolution, the Canberra Digital Spectrum Analyzer DAS 1000, and an Oxford Instruments 50W XTF5011 X-Ray tube with rhodium (Rh) target material. Raw data spectra were processed by the analysis of X-ray spectra by iterative least square software (WIN AXIL) package from Canberra Eurisys.
Elemental ratios, which are insensitive to dissolution effects (Weltje and Tjallingii, 2008; Govin et al., 2012), have been calculated and used as paleoenvironmental proxies at both sites (see next paragraph and Chapters 2 and 3).
Single Fe intensities at ODP Site 959 have been used as high-resolution record for hole-to-hole correlations and development of a composite depth record (Chapter 3).

1.5.2.2.1 Use of elemental ratios as proxies for paleoenvironmental conditions

Major elemental composition measured on continental margin sediments has been used to reconstruct terrestrial climate variations and related terrigenous input into the Atlantic in several studies (Govin et al., 2012). In general, the elemental composition in the sediments reflect different contributions and it is influenced by the environmental conditions of its sources. Most of the Ca contained in the Atlantic surface sediments can be assigned to carbonates of marine origin (e.g. Jansen et al., 1998; Arz et al., 1999; Govin et al., 2012). While the terrigenous elements vary in relations to climate conditions on the source areas and to the vehicle of transport to the oceans. The elemental composition of dust reflects its

mineralogical composition (Scheuvens et al., 2013) depending in turn on the soil types and on the climate conditions in which the soils are formed, while the mineralogy of the dust holds information about the source area (Moreno et al., 2006; Govin et al., 2012). Therefore, chemical composition of terrigenous content, associated to aeolian transport in marine sediments brings information about its source areas. Thus, for example, titanium represent an important crustal indicator and high Ti contents in aerosol samples are proposed as a marker for Saharan dust (e.g. Nicolás et al., 2008). Silicium is the most abundant element in mineral dust and mainly incorporated in quartz grains (Scheuvens et al., 2013). Elemental ratios discussed in this thesis are: iron/potassium (Fe/K) ratios, as proxy for aridity versus humidity (Chapter 2); titanium/calcium (Ti/Ca) ratios as proxy for dust (Chapters 2 and 3); titanium/aluminium (Ti/Al) ratios as proxy for aeolian vs. fluvial supply and aluminium/silicium (Al/Si) ratios as proxy for fine versus coarse grain size (Chapter 3).

1.6 Thesis Outline

The main part of this thesis consists of three manuscripts, which are either published in, submitted to or in preparation for peer-reviewed scientific journals. In the following paragraphs they are briefly summarised.

Chapter 2: Pliocene environmental change in West Africa and the onset of strong NE trade winds (ODP Sites 659 and 658).

Francesca Vallé; Lydie M. Dupont; Susanne A. Leroy; Enno Schefuß, Gerold Wefer

Published in Palaeogeography, Palaeoclimatology, Palaeoecology.

This study focuses on Pliocene vegetation dynamics in association to climate variability and the evolution of the Northeast Trade winds in west Africa by means of pollen analysis and elemental ratios, obtained with XRF-scanning, of ODP Site 659 sediment cores. By comparing Ti/Ca ratios and pollen accumulation rates the relationship between dust and pollen transport throughout the Pliocene has been investigated. A stable wet interval within the mid-Pliocene period has been recognized by changes in Fe/K ratios and pollen assemblages. The late Pliocene Site 659 pollen record has shown similar changes in vegetation composition and taxa relative abundances recorded by the nearby Site 658 pollen record. Their analogy allowed a robust reconstruction of late Pliocene west African vegetation changes. Fluctuations of pollen concentrations of trade wind indicators (*Ephedra, Artemisia, Pinus*) indicate that NE trade wind strength increased intermittently around 2.7 and 2.6 Ma, and more or less permanently since 2.5 Ma, in agreement with decreasing SST in the North Atlantic. Those results link the NE trade wind development with the intensification of the Northern Hemisphere glaciations (iNHG).

Chapter 3: Orbitally-driven environmental changes recorded at ODP Site 959 (eastern equatorial Atlantic) from the Late Miocene to the Early Pleistocene

Francesca Vallé; Lydie M. Dupont; Thomas Westerhold

submitted to International Journal of Earth Science

This study focuses on environmental changes in West Africa and sedimentation in the tropical east Atlantic in relation to orbital forcing from the late Miocene to the early Pleistocene. High-resolution XRF-scanning element intensities have been obtained for ODP Site 959. At first, correlation between Fe intensities of Site 959 Holes A, B and C, allowed the development of a composite depth record, that subsequently has been astronomically tuned detailed age model from 6.2 to 1.8 Ma. Afterwards, Ti/Ca ratios, Ti/Al ratios and Al/Si ratios records, covering also the latest Miocene interval, have been analysed and compared with other terrigenous and dust records over the east Atlantic. Enhanced run-off from the West African continent and major supply of fine material at ODP Site 959, suggest a stronger monsoon and increased precipitation during eccentricity minima during the earlier stages of the Messinian Salinity Crisis. A long-term decrease of river supply is documented after 5.4

Ma towards the early Pleistocene. After 3.5 Ma siliciclastic supply at ODP Site 959 and existing dust records from northern latitudes offshore Africa suggest that winter dust was regularly reaching the Gulf of Guinea. Enhanced continental aridity or larger climate variability corresponding with eccentricity maxima is evident between 3.2 and 2.9 Ma. The importance of eccentricity and precession (modulated by eccentricity) on the sedimentary cycles of Site 959 has been underlined.
This study gives also the stratigraphic and chronological base for next study.

Chapter 4: Pliocene land-sea connections in the east equatorial Atlantic (Gulf of Guinea): link between upwelling and aridity
Francesca Vallé; Stijn De Schepper; Lydie M. Dupont;
in preparation

This study focus on Pliocene changes in east Atlantic surface waters conditions by means of a dinoflagellate cysts record obtained at ODP Site 959. Differences in the dinoflagellate cysts assemblages indicate different surface waters conditions between the early and late Pliocene. Weak upwelling and warmer waters characterize the early Pliocene. After 3.9 Ma and throughout the late Pliocene, several upwelling intervals occur. Those changes are linked to the evolution of the Guinea Current in the Gulf of Guinea. Moreover, increased transport of neritic dinoflagellate taxa to the deep-sea Site 959 compared with terrestrial palynomorphs records could be associated to sea level changes corresponding to major Pliocene glaciation events. By comparing dinoflagellate results with palynological results obtained in the first study of this thesis (ODP Site 659) a linkage between upwelling events along the Ghanaian coast and arid phases in West Africa is suggested.

Chapter 2

Pliocene environmental change in West Africa and the onset of strong NE Trade winds (ODP Sites 659 and 658)

Francesca Vallé[1], Lydie M. Dupont[1], Suzanne A.G. Leroy[2], Enno Schefuß[1], Gerold Wefer[1]

[1]MARUM—Center for Marine Environmental Sciences, [2]Institute for the Environment, Brunel University

Keywords: Pollen, Pleistocene, Pliocene, NE trade winds, West Africa

published as: Vallé F., Dupont L. M., Leroy S.A.G., Schefuß E., Wefer G. in Palaeogeography, Palaeoclimatology, Palaeoecology 414 (2014) 403–414. dx.doi.org/10.1016/j.palaeo.2014.09.023

2.1 Abstract

Pliocene vegetation dynamics and climate variability in West Africa have been investigated through pollen and XRF-scanning records obtained from sediment cores of ODP Site 659 (18°N, 21°W). The comparison between total pollen accumulation rates and Ti/Ca ratios, which is strongly correlated with the dust input at the site, showed elevated aeolian transport of pollen during dusty periods. Comparison of the pollen records of ODP Site 659 and the nearby Site 658 resulted in a robust reconstruction of West African vegetation change since the Late Pliocene. Between 3.6 and 3.0 Ma the savannah in West Africa differed in composition from its modern counterpart and was richer in Asteraceae, in particular of the Tribus Cichorieae. Between 3.24 and 3.20 Ma a stable wet period is inferred from the Fe/K ratios, which could stand for a narrower and better specified mid Pliocene (mid-Piacenzian) warm time slice. The northward extension of woodland and savannah, albeit fluctuating, was generally greater in the Pliocene. NE trade wind vigour increased intermittently around 2.7 and 2.6 Ma, and more or less permanently since 2.5 Ma, as inferred from increased pollen concentrations of trade wind indicators (*Ephedra, Artemisia, Pinus*). Our findings link the NE trade wind development with the intensification of the Northern Hemisphere glaciations (iNHG). Prior to the iNHG, little or no systematic relation could be found between sea surface temperatures of the North Atlantic with aridity and dust in West Africa.

2.2 Introduction

An understanding of the driving forces of Pliocene climate is the aim of many studies because the middle Pliocene may constitute a geological analogue for future climate (Salzmann et al., 2011; Fedorov et al., 2013). Most of the Pliocene (Zanclean and the beginning of the Piacenzian; 5.3–~3 Ma) was characterised by global mean annual temperatures 2–4 °C higher than in preindustrial times and estimated carbon dioxide concentrations were close to modern values of up to 400 ppm (Brierley et al., 2009; Bartoli et al., 2011). Some authors claim that the so-called “permanent El Niño” state of the Pacific Ocean was one of the most important features of Pliocene warmth influencing the tropical atmosphere (Wara et al., 2005; Fedorov et al., 2006; Lawrence et al., 2006). The “permanent El Niño” is specified by a deep equatorial thermocline, a small east-to-west sea surface temperature (SST) gradient, and a reduced SST gradient between the equator and the tropics resulting in an expanded tropical warm pool in the Pacific Ocean with or without a reduced cold tongue of low equatorial SSTs (Brierley et al., 2009; Fedorov et al., 2013). These oceanic conditions would have had consequences for the atmospheric circulation in the Southern and Northern Hemispheres in the form of weaker Walker and Hadley cells (Brierley et al., 2009) implying reduced trade winds, which today contribute to create the asymmetry in the equatorial thermocline (Wara et al., 2005). Ocean– atmosphere conditions changed once the meridional temperature gradient started to increase and the tropical thermocline started to shoal (Fedorov et al., 2013). However, recent studies by O'Brian et al. (2014) and Zhang et al. (2014)question the temperature reconstructions of the West Pacific Warm Pool and Zhang et al. argue that the meridional SST gradient was already in existence in the Tortonian or Late Miocene (i.e. since 11.6 Ma). A cooling trend indicated by heavier stable oxygen isotope values of benthic foraminifers (e.g. Lisiecki and Raymo, 2005) started at around ~ 3.3 Ma. Many studies reconstructing SST in the Pacific (Wara et al., 2005; Lawrence et al., 2006; Brierley et al., 2009; Etourneau et al., 2010) reveal an increase in the meridional gradient and suggest intensification of the Hadley cell during the cooling at the Pliocene–Pleistocene transition, although the proposed timing of events varies. During the cooling the Northern Hemisphere glaciations intensified (iNHG) and the Earth's system changed from a unipolar glaciated setting to the current bipolar glaciation with a circum-Arctic synchronous ice-sheet response after 2.7 Ma (cf. Jansen et al., 1996; Ravelo et al., 2004; De Schepper et al., 2014). The influence of obliquity on climate variability became stronger (Lisiecki and Raymo, 2005). A likely explanation for the cooling is the reduction of atmospheric carbon dioxide concentrations in the order of 100 ppm between 4 and 2 Ma (Bartoli et al.,2011; Fedorov et al., 2013). Moreover, the development of strong stratification in the subarctic Pacific Ocean could have resulted in both cooling in spring and enough moisture in fall to trigger the growth of large ice sheets in North America since 2.7 Ma (Haug et al., 1999, 2005). The results of the iNHG are apparent in the North Atlantic by the southward diversion of the North Atlantic Current during glaciations (Naafs et al., 2010; Hennissen et al., 2014). These authors studied SSTs of the North Atlantic in combination

with aeolian terrestrial input from North America. The supply of plant wax in the marine sediments strongly increased during every glacial since 2.7 Ma. Glacial erosion in North America would have released dust and wax of higher plants that were transported eastwards by west winds to the North Atlantic (Naafs et al., 2012). Over the last 5 Ma the climate in Africa showed a long-term aridification trend starting around 3 Ma superimposed by alternating wet–dry cycles paced by orbital precession driving the monsoon system (Trauth et al., 2009). This trend resulted in a strong decline in tree cover in West Africa at 2.7 Ma as recorded in sediments offshore from the Niger Delta (Morley, 2000). Also in eastern Africa, vegetation became more steppe-like when grasslands expanded and aridity increased between 2.7 and 2.5 Ma (Bonnefille, 2010). Several studies proposed that the aridification in subtropical West Africa occurred parallel to the iNHG and with the intensification of northeast trade winds (deMenocal et al., 1993b; Leroy and Dupont, 1994;Tiedemann et al., 1994; deMenocal, 2004; Bonnefille, 2010). Moreover, the intensification of the trade wind system had an impact on coastal upwelling systems. Marlow et al. (2000), studying the Benguela upwelling system along the southwest coast of Namibia, suggested that the intensification of trade winds started "a positive feedback cycle" which helped in removing CO^2 from the atmosphere and started its storage in the deep ocean, thus enhancing the global Pliocene cooling trend. Concerning northwest Africa, Leroy and Dupont (1994) suggested a gradual increase of the northeast trade winds between 3.3 and 2.5 Ma. Two different mechanisms for the intensification of the trade winds have been suggested: one ties the strengthening of the atmospheric circulation to the meridional and zonal oceanic temperature gradients; the other links the strengthening of the trade winds to the iNHG. The proposed forcing mechanisms have implications for the timing and variability of the trade wind system during the Pliocene. To test which forcing is more important for the climate of West Africa and the strengthening of the NE trade winds, we investigated vegetation change, pollen transport, and the evolution of the trade wind system for the period of the Late Pliocene to Early Pleistocene (Piacenzian to Gelasian; Cohen et al., 2013) as recorded in the marine sediments retrieved offshore to the west of West Africa. We present a not-yet-published pollen record of ODP Site 659 in Section 4 comparing it with the pollen record of ODP Site 658 (Leroy and Dupont,1994) in Section 5. In Section 6 we present new XRF scanning data of ODP Site 659. Using the record of West African vegetation development as well as the dust record of ODP Site 659 (Tiedemann et al., 1994), we interpret the new XRF-scanning results of elemental ratios in ODP Site 659 sediments, which provide a high temporal resolution record of environmental change (Section 7) for two time windows (5.0–4.6 Ma and 3.6–2.5 Ma). Finally, in Section 8 we use the occurrence of pollen grains from northerly (Mediterranean and North-Saharan) sources to discuss when the NE trade winds started to intensify.

2.3 Modern setting

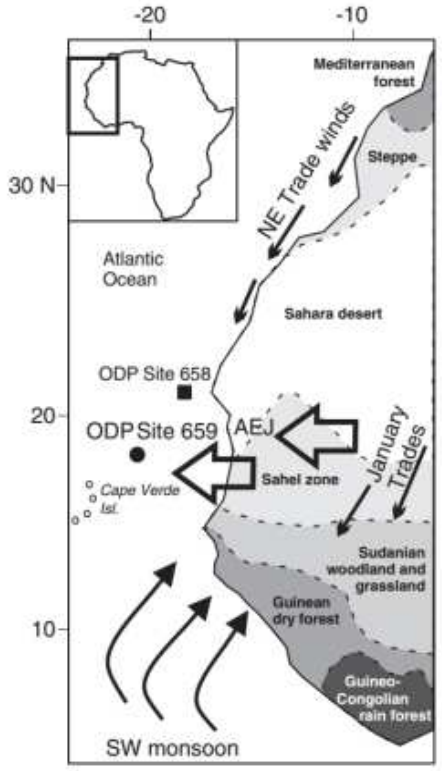

Figure 1: Present-day winds influencing West Africa and vegetation zones (Hooghiemstra et al., 2006). The position of our study site ODP Site 659 and the location of ODP Site 658, which data we used for comparison. AEJ: African Easterly Jet.

The modern atmospheric circulation over West Africa has three main components: the northeast trade winds, the African Easterly Jet (AEJ) and the southwest monsoon (Fig. 1). The NE trade winds blow at low altitudes parallel to the African coast. The AEJ blows at mid-tropospheric altitudes between 16 and 19°N during most of the year (Nicholson and Grist, 2003). Both wind systems carry mineral dust particles, pollen, spores, diatoms and organic molecules from the continent to the East Atlantic Ocean. The dust coming from the north-western fringe of the Sahara, which is transported by the trade winds is characterised by chlorite, illite (clay fraction) and pale quartz (Sarnthein et al., 1981, 1982). The clay fraction of the dust from the southern Sahara and the Sahel zones, transported by the AEJ, is enriched in kaolinite and abundant reddish-stained quartz that is rich in iron oxides and hydroxides (Sarnthein et al., 1981, 1982; Balsam et al., 1995). The pollen distribution in the marine sediments offshore of North-West Africa depends largely on the wind patterns of the NE trade winds and the AEJ (Hooghiemstra et al., 1986, 2006). The combined action of the AEJ and the high tropospheric Tropical Easterly Jet (not shown in Fig. 1) is the most important factor influencing the tropical rainbelt, which produces most of the rainfall over the Sahel, effectively independent of the Intertropical Convergence Zone (Nicholson, 2009). The vegetation in northwest Africa strongly depends on the precipitation gradient and is zonally arranged. From north to south the vegetation zones are Mediterranean forest, Steppe, Saharan desert, Sahel zone, Sudanian woodland and grassland, Guinean dry forest and Guineo-Congolian rain forest (White, 1983).

2.4 Material and Methods

Material was sampled from the sediment cores of ODP Site 659 (Ocean Drilling Program, Leg 108) that were retrieved offshore from northwest Africa (18°04 N, 21°01 W), ~ 530 km from the coast of Mauritania in 1986 (Ruddiman et al., 1987). The site is located on top of the Cape Verde Rise, at 3070 m water depth and bathed by North Atlantic Deep Water (NADW). The sediment cores are composed of carbonate oozes. The site is considered an open-marine environment site for its very low organic carbon values of less than 0.5% (Stein et al., 1989). We use the age model obtained by Tiedemann et al. (1994) whose stable oxygen isotope curve has been correlated with the benthic stack LR04 published by Lisiecki and Raymo (2005). 116 pollen samples from cores of Hole A of ODP Site 659 were palynologically analysed in 1990 by Suzanne Leroy (38), Lydie Dupont (4), Susanne Jahns (32), and Chiori Agwu (58) and, in 2011, 32 additional samples were analysed from cores 8 to 11, 14 and 15 by Francesca Vallé. Samples of 2 cm thickness (10 and 20 cm3), were prepared with standard palynological treatment using cold HCl to decalcify followed by cold HF (~ 40%) attack. The clay and organic fraction smaller than 10–12µm removed by ultrasonic sieving over an 8µm mesh. The final residues were stored in water and mounted in glycerol. To calculate concentration values, sample volume was measured by water displacement and one or two tablets containing exotic *Lycopodium* spores were added during the decalcification step. During resampling in 2011 we discovered that the cores became mouldy in storage, which left fungal hyphens in the samples after palynological preparation. Pollen grains were not visibly degraded. However, in combination with the low pollen concentration the counting of the resampled material turned out to be extremely laborious and time-consuming as hyphens were clogging the slides hiding pollen grains and *Lycopodium* spores. In order to find at least 50 pollen and spores, we analysed up to 10 slides per sample, but never managed to count more than 11% of the original sample (calculated after the counted number of *Lycopodium* spores), whereas in 1990 average counts covered ~20% (and often more than 30%) of the original sample to reach an average of 200 pollen and spores. Pollen percentages are based on the total number of pollen and spores and only calculated if counts exceeded 50 grains. To account for the low counts and the resulting uncertainties we draw confidence intervals ($\alpha = 0.05$) of the relative abundances following the method of Maher (1972). Total pollen and spore accumulation rates were calculated for all samples, using sedimentation rates re-calculated from the age model provided by Tiedemann et al. (1994). Pollen taxa were identified following the atlas of Bonnefille and Riollet (1980), the African Pollen Database (http://apd.sedoo.fr/pollen/), as well as the reference collection of the Department of Palynology and Climate Dynamics of the University of Göttingen. Pollen of shrubs and trees and other tropical elements have been placed into two groups, Sahel and forest/woodland (see Supplementary Tables 1 and 2), following the same grouping as in ODP Site 658 (Leroy and Dupont, 1994). The interpretation of the pollen record is guided by the modern distribution patterns of pollen and

spores in marine sediments offshore from NW Africa (Hooghiemstra et al., 1986, 2006). The palynological results of ODP Site 659 shown in Fig. 2 are compared with those of ODP Site 658 (Supplementary Fig. 1). XRF scanning has been performed on sediments of ODP Site 659 for a part of the Zanclean (5–4.6 Ma), the Piacenzian (3.6–2.5 Ma), and the last glacial cycle (past 0.14 Ma). We scanned intensities (number of counts per second) of the major light elements Al, Si, Ti, Fe, Ca, K, and Fe directly at the surface of the sediment cores from Hole A and Hole B of ODP Site 659 at 2 cm resolution using the Avaatech XRF core scanner II at the IODP Core Repository at MARUM—Center for Marine Environmental Sciences of the University of Bremen. A detailed description of the instrument and of the measurement techniques can be found in Röhl and Abrams (2000), Richter et al. (2006) and Jansen et al.(1998). Scanning took place in 2011 and 2013. When analysing the data, it became clear that the data scanned in 2013 showed an offset compared to those from 2011. To calculate the offset and to be able to correct for it, we rescanned selected sections and recalculated the intensities to the level of 2011 by linear regression. From the measured and corrected intensities, we calculated the natural logarithm of the elemental ratios Fe/K and Ti/Ca. Using the natural logarithm ensures symmetry of the ratios around zero (Weltje and Tjallingii, 2008; Govin et al., 2012). We carried out a linear regression analysis between dust percentages and dust accumulation rates (Tiedemann, 1991; Tiedemann et al.,1994) using ordinary least squares and Pearson's r correlation. We calculated 95% confidence intervals of slope and intercept based on direct calculation and bootstrapping (Supplementary Fig. 2). In Section 6(Tables 1 and 2), we compare the results of pollen analysis and XRF scanning statistically testing for equal mean (t-test), variance (F-test), and median (Mann–Whitney-test). To analyse cyclicity in the elemental ratio record (Section 7), we carried out a continuous wavelet transform of ln(Ti/Ca) and ln(Fe/K) using a Morlet wavelet (wave number 6). All statistical analyses were performed with the paleontological statistics package PAST vs 3.0 (Hammer et al., 2001). The significance of the power maxima over red noise has been tested using the module REDFIT (Schulz and Mudelsee, 2002) of the PAST package.

2.5 Pollen record of ODP Site 659

The pollen diagram of selected taxa is shown in Fig. 2 for the period 3.6 Ma to the present. The sediments of ODP Site 659 are poor in pollen and spores, which generally are well preserved. The pollen and spore accumulation rates fluctuate between 0 and 2000 grains per cm2 per thousand years (N/cm^2/ka) showing low values in the upper and lowermost parts of the record and high and variable ones in between. Accumulation rates of the summed pollen of *Pinus*, *Ephedra*, and *Artemisia* (TW, trade wind indicators) increase first during the Gelasian and reach maximum values in the Middle Pleistocene. The most abundant pollen taxon is Poaceae with an average value of ~30%. Other abundant pollen taxa are Caryophyllaceae and Amaranthaceae including Chenopodiaceae (=CA), Cyperaceae, Asteraceae (Liguliflorae, Tubuliflorae, and *Artemisia* pollen types), and *Ephedra* (Fig. 2). Sparsely occurring pollen taxa have been lumped into two groups, forest elements from the

Sudanian and Guinean vegetation (95 taxa, Supplementary Table 1) and pollen from Sahelian taxa (25 taxa, Supplementary Table 2). Fern spores do not exceed 20% (of the total pollen and spores) and are mainly found in the older part of the record (before 1.5 Ma) parallel to raised percentages of *Rhizophora* pollen (Supplementary Fig. 1). Moderate fern spore percentage maxima (10–20%) occur around 2.85 Ma, between 2.2 and 2.6 Ma, and around 0.95 Ma, when the representation of forest/woodland is high. The relative abundance of Poaceae pollen is high until 2.6 Ma and gradually declines thereafter (Fig. 2). Another maximum occurs shortly before 2 Ma. After 1.5 Ma grass pollen percentages are rather stable with an average of just over 20%. Pollen abundance from the Sahel and forest/ woodland is also higher prior to 1.5 Ma and declines to very low values after 0.9 Ma. The second most abundant pollen taxon is CA reaching values exceeding 50% between 2.8 and 1.4 Ma. *Artemisia* and *Ephedra* pollen percentages are high (~20%) after 0.5 Ma; other *Ephedra* pollen percentage maxima occur between 2.2 and 1.9 Ma, when *Artemisia* pollen percentages are low. Shortly before 2.5 Ma, a maximum occurs for both *Ephedra* and *Artemisia*. The Asteraceae record shows some remarkable maxima before 3 Ma, while values for Liguliflorae and Tubuliflorae are rather low throughout the rest of the Pliocene and in the Pleistocene (Fig. 2). An isolated Tubuliflorae pollen percentage maximum occurs at 1.3 Ma, but the temporal resolution of the record for this period is too coarse to draw conclusions from it. Besides low Cyperaceae pollen percentages during the past 300 ka, no trend can be found for the rest of the Cyperaceae record. Maximal values between 30 and 40% occur in both Pliocene and Pleistocene.

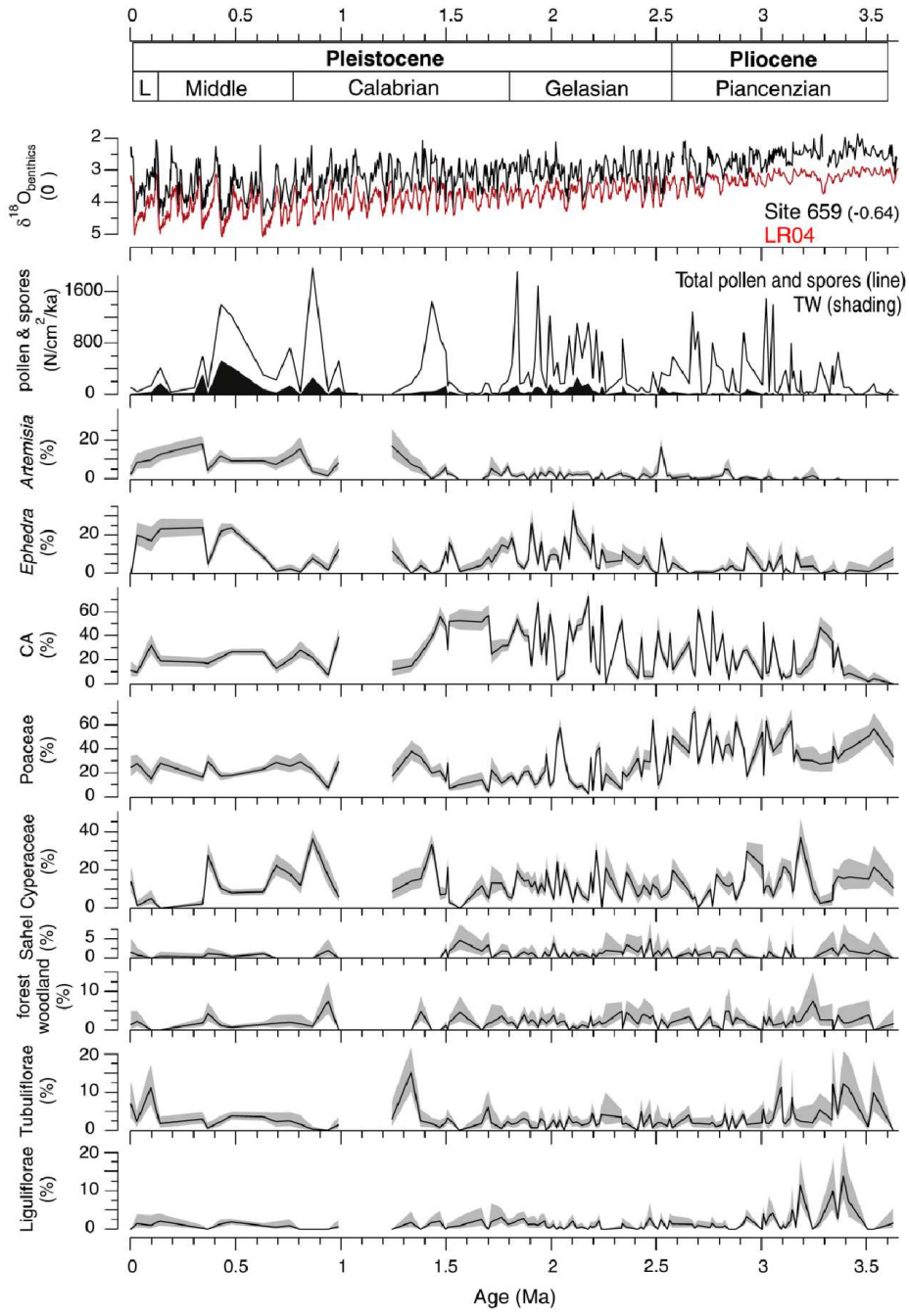

Figure 2 Pollen record of ODP Site 659. From top to bottom; chronostratigraphy version 2014/02 (Cohen et al., 2013); stable oxygen isotope stratigraphy of ODP Site 659 (upper, Tiedemann et al., 1994;$\delta^{18}O$ values of Site 659 are plotted 0.64 per mil below seawater equilibrium) compared to the global stack LR04 (lower ,Lisiecki and Raymo, 2005). Total pollen and spore accumulation rates (line); accumulation rates of trade wind transported pollen (TW; shaded black); pollen percentages of selected taxa (*Artemisia*, *Ephedra*, CA = Caryophyllaceae and Amaranthaceae, Poaceae, Cyperaceae), groups (Sahel, forest/woodland), Tubuliflorae (not including *Artemisia*), and Liguliflorae. Age model after Tiedemann et al. (1994). 95% confidence intervals of the percentage data are indicated by grey shading.

2.6 Pliocene and Pleistocene trends in West African vegetation

Before we present the results of XRF scanning we compare the pollen records of ODP Sites 659 and 658 (Leroy and Dupont, 1994) to obtain a robust interpretation of the palynological results of ODP Site 659. Age models (Tiedemann, 1991; Tiedemann et al., 1994; Leroy and Dupont, 1997) and the correlation between both sites rely on the stable oxygen isotopes of benthic foraminifera (Cibicidoides wuellerstorfi) (Supplementary Fig. 1). The pollen records of the two sites overlap between 3.7 and 1.7 Ma and between 0.8 and 0 Ma covering the Piacenzian, the Gelasian, and the Middle and Late Pleistocene (Brunhes Chron). The record of Site 659 has a lower temporal resolution and lower pollen counts resulting in relatively large error bars (given as 95% confidence intervals). The great distance of Site 659 to the coast (530 km), being almost three times as far offshore as Site 658 (200 km), results in10 times lower pollen concentrations. Moreover, sedimentation rates at Site 659 vary between 1 and 6 cm/ka and those of Site 658 range between 5 and 40 cm/ka, mostly exceeding 10 cm/ka. Despite large differences in the distance to the coast and the sedimentation rates between Sites 658 and 659, their pollen records are remarkably similar in composition and relative abundance (percentages). Within the Asteraceae three pollen taxa have been distinguished: *Artemisia*, Liguliflorae (Tribus Lactuceae after Bremer, 1994), and Tubuliflorae (the rest except for *Artemisia*). *Artemisia* pollen is mainly trade wind transported as the plants grow in the Mediterranean region and the transitional steppes between the Mediterranean and Saharan vegetation (White, 1983; Hooghiemstra et al., 1986). *Artemisia* pollen percentages show the same pattern of stepwise increasing values since the late Pliocene at both cores, i.e. an early maximum at 2.53 Ma and increased values during the past 0.5 Ma (Supplementary Fig. 1). The record for other Asteraceae pollen is remarkably different. Tubuliflorae and Liguliflorae percentage maxima are found in the Piacenzian, before 3 Ma, but the percentages remain low for the rest of the record at both ODP sites (Supplementary Fig. 1; Fig. 6). The Liguliflorae pollen grains mainly originate from species of the Tribus Cichorieae (=Lactuceae, Bremer, 1994), which nowadays are scarce in tropical West Africa (Hutchinson and Dalziel, 1963) as indicated by low pollen percentages (b10%) in modern marine sediments offshore from West Africa south of 27°N (Hooghiemstra et al., 1986). Pollen percentages of Asteraceae from modern terrestrial surface sediments are low in the central and southern Sahara and Sahel and higher Asteraceae percentages in the Sudanian savannah region of Nigeria are attributed to modern anthropogenic pressure (Lézine, 1987; Schulz, 1991). Leroy and Dupont (1994) proposed that the Liguliflorae pollen during this period would originate from savannah species and that no modern analogue for this type of savannah exists anymore. The record of ODP Site 659 also reveals increased representation of Asteraceae before 3 Ma corroborating the earlier inferences from ODP Site 658. The group of woodland/forest comprises 95 pollen taxa whose source areas are mainly in the Sudanian woodland and grassland and Guinean dry forest (Supplementary Table 1) and together make up less than 8% of the pollen assemblage. Most tropical trees produce little pollen, which is not well dispersed by wind (Dupont and Agwu, 1991). The pollen percentages for forest and woodland are slightly higher at ODP Site 659 (Supplementary Fig.

1), which is explained by its location being almost three degrees of latitude south from ODP Site 658. Percentages are somewhat higher in the Pliocene than in the Pleistocene, whose trend is similar for both cores. The Sahel group comprises 25 pollen taxa from the grassland, wooded grassland, and shrubland of the Sahel (Supplementary Table 2). Grass (Poaceae) pollen originates mainly from the Sahel and the Sudanian savannah as indicated by the modern pollen distribution in marine surface sediment samples (Hooghiemstra et al., 1986). Most maxima in the Sahel pollen co-occur with maxima in the grass pollen percentages emphasising that both groups have their main sources in the same biomes. The higher temporal resolution of the Site 658 record (Supplementary Fig. 1) reveals strong fluctuations in the grass pollen percentages, but the trends are the same in ODP Sites 659 and 658. Again the representation of grasses and Sahelian taxa is higher in the Pliocene and declines after 2.5 Ma. Between 2.3 and 1.8 Ma grass pollen percentages fluctuate strongly at Site 658, but at Site 659 only two maxima are recorded. At both sites, values are relatively low during the past 0.3 Ma The woody shrubs *Calligonum* and *Ephedra* presently grow in the northern Sahara and the transitional steppes between the desert and the Mediterranean vegetation (Knapp, 1973; White, 1983). Their pollen distribution in modern marine sediments reaches south of the latitudinal plant distribution as the result of pollen transport by the trade winds (Hooghiemstra et al., 1986). At both ODP Sites 658 and 659 *Calligonum* pollen percentages increased from 2.5 to 2.2 Ma and during the last Glacial (Supplementary Fig. 1). At Site 659 *Ephedra* pollen percentages had already increased to values over 20% at the beginning of the Pleistocene (maxima around 2.1 and around 1.9 Ma), while at Site 658 such values are reached only in the past 0.5 Ma. The higher relative abundance of *Ephedra* pollen at the southern site might indicate an increase of *Ephedra* in the Sahara south of 21°N (latitude of ODP Site 658) during the Gelasian. During the Gelasian the representation of CA is high. Sources of CA pollen are mainly along the coast and in the Sahara and many Amaranthaceae species grow on saline soils. Their pollen is distributed westwards by the easterly flow of the AEJ (Hooghiemstra et al., 1986). An increase in desert vegetation since 2.7 Ma is indicated by recurrent maxima in CA pollen percentages at ODP Sites 659 and 658 (Supplementary Fig. 1). For the period between 2.3 and 1.7 Ma, the Site 658 record shows high variability with rapidly repeating maxima. During the Middle and Late Pleistocene the CA pollen percentages are generally lower at ODP Site 659 than at Site 658. TW pollen sums up the counts of *Artemisia*, *Ephedra*, and Pinus pollen. The transport of these pollen types to ODP Sites 658 and 659 is almost exclusively by the NE trade winds (Hooghiemstra et al., 1987). Our TW group deviates from the original trade wind indicators as described by Hooghiemstra et al. (1987) and Hooghiemstra (1988) leaving out the Asteraceae other than *Artemisia*. TW pollen concentrations at Site 658 are ten times higher than at Site 659, but fluctuations and trends in the TW record run parallel at both sites (Supplementary Fig. 1; Fig. 6). Shortly before 2.5 Ma, maxima in the TW pollen concentration concurrent in both sites mark the intensification of NE trade winds at the start of the Pleistocene. Leroy and Dupont (1994) inferred earlier short periods with increased trade wind vigour, but while comparing the pollen records of ODP Site 659 and 658, we argue that the main trade wind

intensification occurred during the Pliocene- Pleistocene transition. During this period, relative abundance maxima of *Artemisia* and *Ephedra* pollen are recorded at both sites and a Pinus pollen percentage maximum is found at ODP Site 659. Increased pollen percentages of *Artemisia*, *Ephedra*, and Pinus occurred intermittently between 3.7 and 2.7 Ma, but concentrations are low. In summary, the new record of ODP Site 659 confirms the results of ODP Site 658 which have been previously interpreted as a record of the existence of a no analogue Asteraceae-rich (notably Cichorieae) savannah between 3.6 and 3.0 Ma in West Africa (Leroy and Dupont, 1994). Between 3.0 and 2.5 Ma the savannah changed in composition and periods with extended desert vegetation became more and more frequent. After 2.6 Ma, woodland and forest declined, trade winds became important, and desert vegetation further extended. Increasing the temporal resolution of our record might reveal the mechanism leading to vegetation and climate shifts associated with the intensification of the Northern Hemisphere glaciations at 2.6 Ma. Therefore, we XRF scanned sediments dated between 3.6 and 2.5 Ma (Piacenzian), between 5.0 and 4.6 (part of the Zanclean) and of the past 0.14 Ma (last glacial cycle) at an average resolution of 0.5 to 1.2 ka.

2.7 XRF scanning, results and interpretation

The major element intensities (counts per second) differentiate between terrestrial and marine origins of the elements (Fig. 3). The counts of terrigenous elements aluminium (Al), titanium (Ti), potassium (K), silicon (Si), and iron (Fe) fluctuate consistently but opposite to those of the element calcium (Ca) that is almost an order of magnitude more abundant than the most abundant terrigenous element, Fe. Intensities of all terrigenous elements including Si correlate with the dust percentage record of Tiedemann (1991). The maximum in the terrestrial elements, however, has been counted in a dark layer of sediment, dated at 3.07 Ma and recognised by Faugères et al. (1989) as one of the few turbidites reaching the Cape Verde Rise during this part of the Pliocene (marked as “T” in Fig. 3). Subsequently, we discarded the turbidite samples from further analysis. The elemental composition of dust reflects its mineralogical composition (Scheuvens et al., 2013) depending in turn on the soil types and on the climate conditions in which the soils are formed, while the mineralogy of the dust holds information about the source area (Moreno et al., 2006; Govin et al., 2012). In this study we present the variations of Fe/K and Ti/Ca ratios (Fig. 4). As the Al counts are very low, probably because of the site's great distance from the shore, we cannot use the Al/Si ratio as an indicator of dust supply (Collins et al., 2013). To interpret the changes in the ratios, we look at the implied sources of the terrigenous elements. Most of the Ca contained in the Atlantic surface sediments can be assigned to carbonates of marine origin (e.g.Jansen et al., 1998; Arz et al., 1999; Govin et al., 2012). Si is the most abundant element in mineral dust and mainly incorporated in quartz grains (Scheuvens et al., 2013). It could also be related to biogenic opal; however, opal concentration in ODP Site 659 sediments is lower than 2% and considered negligible (Tiedemann et al., 1989). Today, dust coming from the north-western fringe of the Sahara is enriched in pale quartz, illite and feldspar (Sarnthein et al., 1981) and dust coming from the southern Sahara and Sahel zone is rich in Fe-stained

quartz and kaolinite (Sarnthein et al., 1981). Ti represents an important crustal indicator and high Ti contents in aerosol samples are proposed as a marker for Saharan dust (e.g. Nicolás et al., 2008), which is often enriched in Ti. For example the source sediments of the Bodélé depression (central Sahara) exhibit high Ti/Al ratios (Scheuvens et al., 2013). Possible sources of Fe are iron oxides and hydroxides (hematite and goethite) that are a component of the distal aeolian dust, while quartz grains represent coarser grain size (Balsam et al., 1995). K is associated with many alumino silicates such as illite (Scheuvens et al., 2013) or potassium feldspar (Zabel et al., 2001) that are abundant in soils with reduced chemical weathering (Govin et al., 2012). Modern dust filter contents show that the Fe/K ratio is twice as high in dust from the savannah as from the Sahel because of the deep chemical weathering of tropical soils (Mulitza et al., 2008). To test whether the Ti/Ca ratios can be used as a dust proxy at ODP Site 659, we compared those ratios to the dust content calculated from the carbonate free siliciclastic content, which can be regarded as the terrestrial component because the Plio-Pleistocene sediments of ODP Site 659 hardly contain biogenic opal or volcanic glass (Tiedemann, 1991). The ln(Ti/Ca) is linearly correlated to the dust percentages (r2=0.82; Supplementary Fig. 2) as also observed for the last glacial cycle from ODP Site 659 (Kuechler et al., 2013). A lesser though still significant correlation (r^2= 0.54) exists between the ln(Ti/Ca) and the accumulation rates of dust; but we prefer the correlation between ln(Ti/Ca) and dust percentage as both measures concern relative abundance. The correlation is good enough to consider the ln(Ti/Ca) a proxy for dust percentages in sediments of ODP Site 659, whereby

ln Ti/Ca= 0,05 dust % - 6,9.

Some Ti/Ca ratios are particularly low during the Zanclean (Fig. 4) and the residuals from the regression display negative values (Supplementary Fig. 2). Obviously the linearity of the relationship between ln(Ti/Ca) and dust percentages breaks down at very low values of dust. When dust is scarce the dust percentages either overestimate or the ln(Ti/Ca) values underestimate the dust supply. During the last glacial cycle, the residuals are positive; here the Ti/Ca ratios are generally high while the dust percentages strongly fluctuate. For further characterisation, we compare Fe/K and Ti/Ca ratios of specific samples with their pollen content (Fig. 4). Our rationale is that while dusty periods are recorded by high Ti/Ca ratios, humid periods would be recorded by high Fe/K ratios. We put pollen samples into four different groups depending on maxima and minima in the Fe/K and Ti/Ca ratios and tested differences in total pollen accumulation rates and pollen percentages of Poaceae and CA between dusty samples (Ti/Ca maxima) and non-dusty ones (Ti/Ca minima) and between samples from wet periods (Fe/K maxima) and arid ones (Fe/K minima). The results are presented in Tables 1 (dusty vs non-dusty) and 2 (wet vs arid).

Table 1
Testing differences in total pollen accumulation rates (PAR) and percentages of grass (Poaceae) and Caryophyllaceae–Amaranthaceae (CA) between samples showing Ti/Ca maxima or minima indicating relatively dusty or non-dusty conditions, respectively. C.I., confidence interval; MW-test, Mann–Whitney test.

Pollen	Poaceae %		Ca %		Par per cm^2 per ka	
	Dusty	Non-dusty	Dusty	Non-dusty	Dusty	Non-dusty
Number	18	24	18	24	18	45
Mean	33.47	47.44	30.88	13.34	521.94	188.64
95% C.I.	28.74	40.74	21.91	8.44	352.69	92.32
	38.20	54.15	39.85	18.23	691.19	284.97
Variance	90.60	252.11	325.38	134.33	115830	102800
Median	31.13	50.37	29.57	9.55	452.79	56.22
F-test	$P < 0.05$		$P < 0.05$		$P > 0.05$	
T-test	$(P \ll 0.01)$		$(P \ll 0.01)$		$P \ll 0.01$	
MW-test	$P \ll 0.01$		$P \ll 0.01$		$P \ll 0.01$	

Table 2
Testing differences in total pollen accumulation rates (PAR) and percentages of grass (Poaceae) and Caryophyllaceae–Amaranthaceae (CA) between samples showing Fe/K maxima or minima indicating relatively wet or dry conditions, respectively. C.I., confidence interval; MW-test, Mann–Whitney test.

Pollen	Poaceae %		Ca %		Par per cm^2 per ka	
	Dry	Wet	Dry	Wet	Dry	Wet
Number	17	23	17	23	17	23
Mean	30.80	51.23	30.28	12.21	473.63	383.02
95% C.I.	26.01	46.45	19.99	8.80	293.07	206.31
	35.59	56.00	40.56	15.62	654.19	559.73
Variance	86.64	121.89	400.35	15.62	654.19	559.73
Median	30.86	51.02	30.80	10.00	406.93	191.12
F-test	$P > 0.05$		$P < 0.01$		$P > 0.05$	
T-test	$P \ll 0.01$		$(P \ll 0.01)$		$P > 0.05$	
MW-test	$P \ll 0.01$		$P < 0.05$		$P > 0.05$	

The F-test indicates that the variance for Poaceae and CA pollen percentages differs between the dusty and non-dusty groups, but the dusty and non-dusty pollen accumulation rates have about the same variance. Thus, only the result of thet-test in the accumulation rates is robust. The Mann–Whitney test, however, indicates that the medians differ significantly. Pollen accumulation rates and CA pollen percentages are higher and Poaceae pollen percentages are lower when terrestrial dust is abundant as indicated by the Ti/Ca ratio. It seems that concerning total pollen accumulation at ODP Site 659, wind transport is the most important. Pollen accumulation rates have previously been used as an indicator of the transport capacity of the wind systems (Hooghiemstra, 1988; Hooghiemstra et al., 2006). Concerning the difference between samples from humid (high Fe/K) and arid (low Fe/K) periods (Table 2), the F-test indicates that the variance in the groups for Poaceae pollen percentages and accumulation rates is about the same, but the CA pollen percentages differ

in variance. Thus the-test result is not robust for the CA percentages. Accumulation rates do not differ significantly between wet and dry periods, but Poaceae percentages are higher and CA percentages are lower during wet periods as indicated by the Fe/K ratio. We interpret these results as follows: during dusty periods more pollen is transported to the site by easterly and north-easterly winds; during wetter periods savannah grassland extended as indicated by the high Poaceae pollen percentages; during drier periods desert vegetation extended as indicated by the high CA pollen percentages. However, the pollen accumulation rates do not allow distinction between humid and arid periods, which is possibly the result of the opposing effects of increased terrestrial input and less pollen producing vegetation during arid periods.

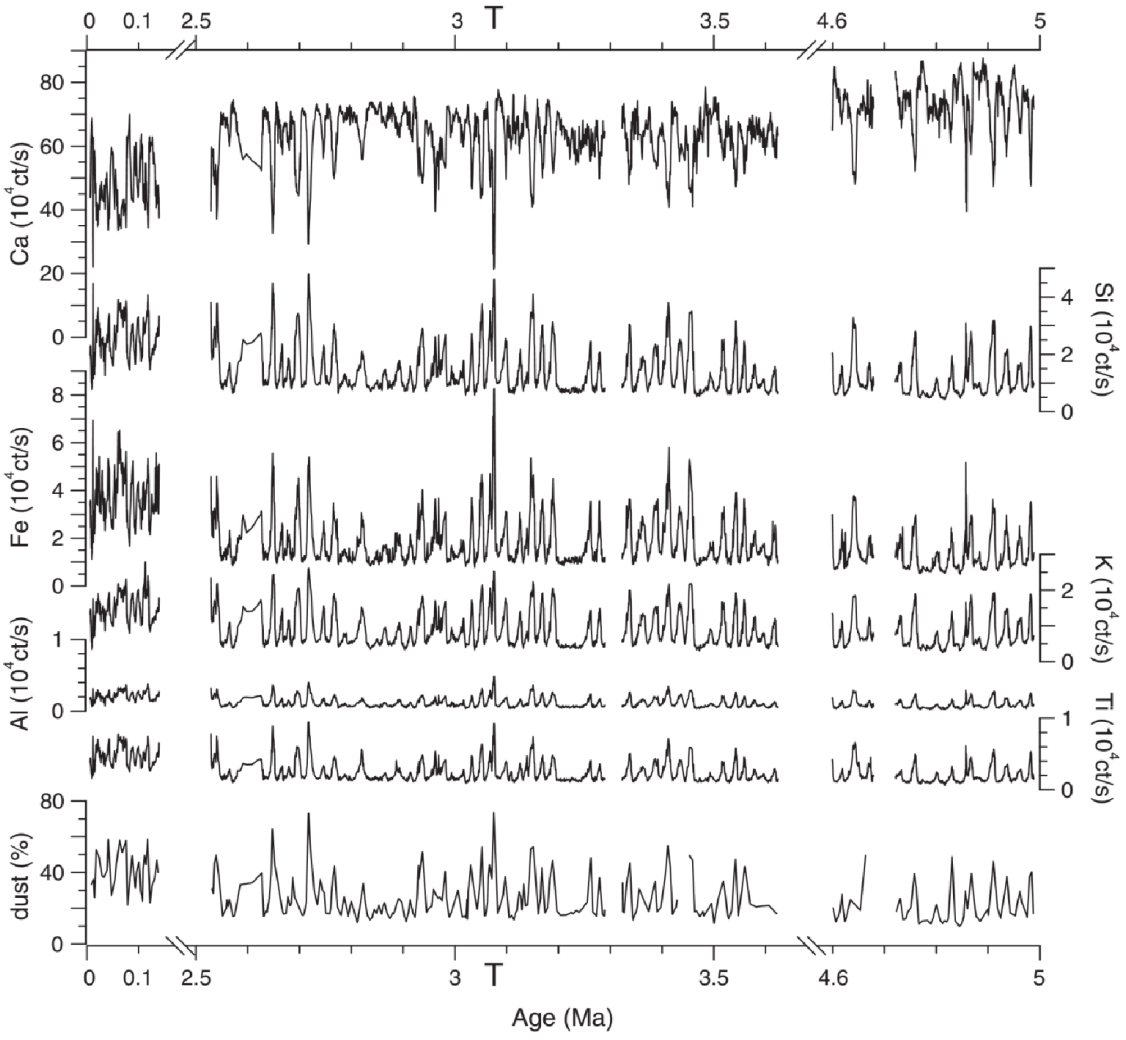

Figure 3 Major element intensities (counts per seconds) of calcium (Ca), silica (Si), iron (Fe), potassium (K), aluminium (Al), and titanium (Ti) compared with dust percentages of ODP Site 659 (Tiedemann, 1991; Tiedemann et al., 1994) for the intervals 5.0 to 4.6 Ma, 3.62 to 2.54 Ma, and 0.14 to 0 Ma. T indicates a turbidite that is discarded from further analysis.

2.8 Environmental change in West Africa prior to the iNHG

With the results of the previous section in mind, we interpret the high resolution ln(Ti/Ca) and ln(Fe/K) record of the Piacenzian and part of the Zanclean, in which we did not find enough pollen for analysis. A continuous wavelet transform traces the development in the pacing of climatic fluctuations (Fig. 5). We interpolated the data to equidistant steps of 1 ka for the period from 4.99 to 4.60 Ma and from 3.62 to 2.53 Ma. We used the age model of Tiedemann et al. (1994). Application of the alternative model of Clemens (1999), which shifts most ages older than 3 Ma by roughly one precession cycle (maximum 28 ka), leads to very similar results. Not surprisingly, variability and trends in the ln(Ti/Ca) record is similar to those inferred by Tiedemann et al. (1994) from the dust accumulation rates. The amount of dust is slightly less during the Zanclean part (5.0–4.6 Ma) than during the Piacenzian (3.6–2.6 Ma) and the dust is much less in the Pliocene compared to the last glacial cycle. The number of dust outbreaks was less during the Zanclean and increased in the Piacenzian. The power at the precession band (19–23 ka) varies between 3.6 and 2.5 Ma; power at the obliquity band (41 ka) is relatively low between 3.4 and 3.0 Ma; power at the 100 ka band shows maximum values between 4.8 and 4.6 Ma and between 3.3 and 2.9 Ma (Fig. 5). The variability and frequencies in the Fe/K ratios differ strongly from those in the Ti/Ca ratios. Fe/K ratios, indicating changes in humidity, have more high-frequency variability (significant periodicities between 2 and 3 ka) than the Ti/Ca ratios, especially during the Zanclean. This result underlines that dust is not a good indicator for aridity as its production additionally depends on the lack of vegetation and on ephemeral fluvial activity (Trauth et al., 2009). Interesting is the suborbital variability in the Fe/K ratios existing long before the iNHG suggesting that millennial cycles in tropical climate may be forced, at least in part, by processes independent from high latitude icecaps (Peterson et al., 2000). On the other hand, after 2.9 Ma power in the precession band increased indicating a role of the growing Northern Hemisphere ice-sheets on the pacing of tropical humidity cycles in West Africa. Although the short-term fluctuations in the Fe/K ratios generally agree with the pollen interpretation (see previous section), the long-term trends do not. While pollen records indicate more desert and more arid conditions during the last glacial cycle compared to the Pliocene, the average Fe/K ratios are higher in the last glacial cycle (Fig. 4). The average ln(Fe/K) value rose from 0.57 in the Zanclean to 0.78 in the Piacenzian before 3 Ma. It dropped slightly during the Piacenzian from 0.78 between 3.6 and 3.0 Ma to 0.71 between 3.0 and 2.5 Ma, but is much higher, 0.92, in the last glacial cycle. Similarly, the average dust content during the last glacial cycle is significantly higher (41%) than during the Pliocene (21% in the Zanclean and 26% in the Piacenzian). Interpreting the Fe/K long-term trend as an indication of generally increasing humidity in West Africa since the beginning of the Pliocene would be at odds with other terrestrial and marine records (e.g. Ruddiman et al., 1989; Dupont and Leroy, 1995; deMenocal, 2004; Salzmann et al., 2008) and contrary to the accepted view that Fe/K ratios become higher under wetter conditions because of the effect of weathering (Zabel et al., 2001). A more likely explanation for the rising trend in Fe/K ratios is a slow and gradual change in the source area, maybe a shift southwards as vegetation

belts moved south, from less weathered soils to deeply weathered ones that are richer in iron (Fe) and/or more depleted in potassium (K). In Fig. 6, the Ti/Ca and Fe/K ratios are compared with SST and plant wax records from IODP Site U1313 (Leg 306) in the central North Atlantic (Naafs et al., 2010, 2012). The most prolonged humid period in West Africa based on the Fe/K ratios occurred between 3.24 and 3.20 Ma. At that time temperatures in the North Atlantic at 41°N were between 22 and 20 °C (Naafs et al., 2010). During this period the terrestrial input at ODP Site 659 was very low, thus precluding a pollen record. Also the aeolian input of terrestrial material from North America in the North Atlantic was minimal during this period (Naafs et al., 2012). Fortunately, ODP Site 658–situated much nearer to the coast–does have a pollen record revealing a strong increase in the representation of woody elements of the Sudanian and Guinean vegetation (Fig. 6) and low values for elements from the desert such as *Ephedra* and CA. The period between 3.24 and 3.20 Ma is the wettest and most stable period in West Africa during the Piacenzian. Expansion of steppe and wooded grasslands during this period is reported by Bonnefille et al. (2004)for eastern Africa at the Hadar section, also suggesting wetter conditions compared to present-day arid conditions. Our data support previous modelling studies of the mid-Pliocene (mid-Piacenzian) warm period (~3.3–3.0 Ma), which reconstructed increased precipitation in subtropical Africa (Contoux et al., 2012) and indicate a smaller Sahara desert and a northward expanded woodland vegetation into today's arid region (Salzmann et al., 2008). These warmer and wetter conditions probably were similar to the ones reconstructed for the Holocene African Humid Period, between ca. 14.8 and 5.5 ka (deMenocal et al., 2000a), when the Sahara desert was covered with grasses and shrubs (COHMAP Members, 1988), palaeolakes were extended (Gasse, 2000), and the dust supply to the eastern Atlantic was drastically reduced (deMenocal et al., 2000b). In both cases (Holocene and Pliocene), eccentricity and with it the precession variability in insolation was low, but atmospheric CO2 might have been higher during the Pliocene (Laskar et al., 1993; Bartoli et al., 2011).

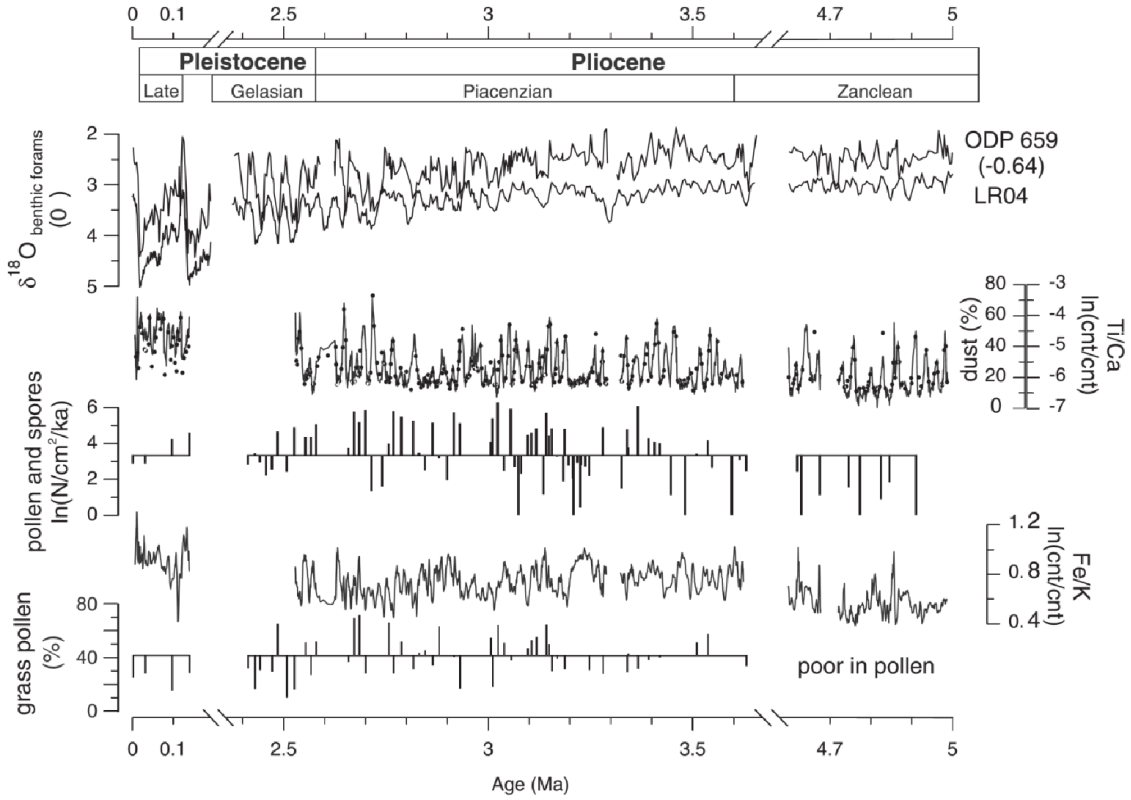

Figure 4 Comparing XRF scanning and pollen results. Chronostratigraphy version 2014/02 (Cohen et al., 2013). Stable oxygen isotopes of ODP Site 659 (Tiedemann et al., 1994) compared to the global stack LR04 (Lisiecki and Raymo, 2005).δ18O values of Site 659 are plotted 0.64 per mil below seawater equilibrium. Ti/Ca ratios (line) and dust percentages (dots) of ODP Site659 compared with the accumulation rates of total pollen and spores (bars upward and downward the mean of 3.3). Fe/K ratios (5 point moving average) compared with grass (Poaceae)pollen percentages (bars upward and downward the mean of 41). Total pollen accumulation varies with the Ti/Ca ratios (Table 1) and the dust input. Samples characterised by high Fe/K ratios mostly have more than average grass pollen percentages (Table 2).

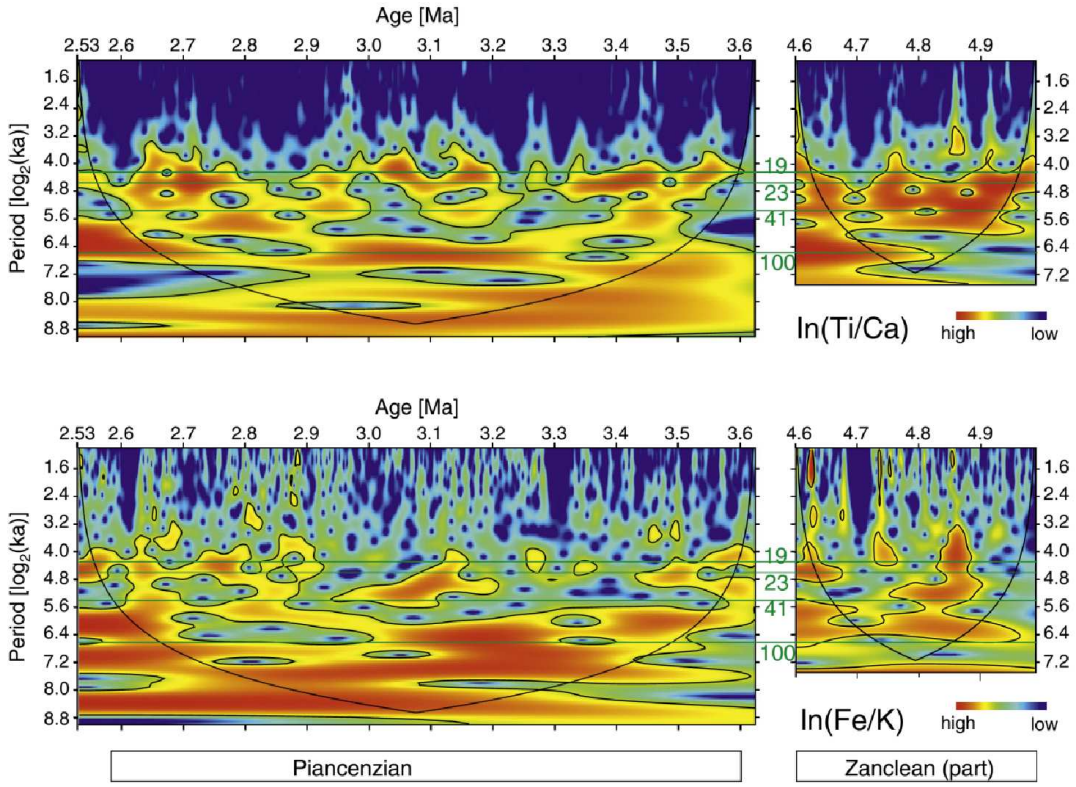

Figure 5 Continuous wavelet transform (Morlet 6) of ln(Ti/Ca) (top) and ln(Fe/K) (bottom) of ODP Site 659 for the Pliocene periods between 2.53–3.62 Ma (left) and 4.60– 4.99 Ma (right). Data are linearly interpolated to 1 ka steps using the age model ofTiedemann et al. (1994). On the X-axis age in Ma; on the Y-axis periodicities in ka on a log2-scale. Orbital periodicities are indicated by green lines. Signal power (squared correlation strength with the scaled mother wavelet) is in colour. Black contours give the significance level corresponding to p = 0.05 after a chi-squared test with the null hypothesis of a white noise model (Torrence and Compo, 1998). Cone of influence (black line) indicates the region of boundary effects.

2.9 The onset of strong NE Trade winds over Africa

Based on meridional SST differences in the equatorial Pacific (e.g. Lawrence et al., 2006), several authors suggest that enhancement of the zonal and meridional atmospheric circulation, including the trade winds, already started around 3 Ma (Wara et al., 2005; Fedorov et al., 2006). Others, however, date the strongest increase of the zonal temperature gradient much later, i.e. at 2.2–2.0 Ma (Etourneau et al., 2010; Steph et al., 2010). Concerning the latter scenario, a positive feedback cycle was possibly established around 2 Ma, in which decreasing SSTs, intensified trade winds and increased wind-driven upwelling favoured long-term sequestration of atmospheric carbon dioxide in the sediment (Marlow et al., 2000). In both cases, the strength of the trade winds is associated with the meridional SST gradient. To investigate whether the dust supply from West Africa is related to the meridional SST gradient, we compared our Ti/Ca dust record with several SST records from the Atlantic, ODP Sites 662, 607, 982 (Lawrence et al., 2009, 2010; Herbert et al., 2010), and

with the SST differences between the Equatorial Atlantic Site 662 and the North Atlantic Site 607 (Fedorov et al., 2013). We did the same with our Fe/K record to test the relationship between Atlantic SSTs and SST gradients with West African humidity between 3.5 and 2.5 Ma (not shown). We could not find any consistent correlation between the SST and our records, at least not for the period before 2.7 Ma. If there is a relationship between dust and aridity in West Africa and SST of the North Atlantic, it is not a simple one. The upwelling history offshore from Mauretania might reveal the timing of the beginning of strong NE trade winds. Grain size distribution of ODP Site 658 indicates that regular river input offluvial clays occurred prior to 3.0 Ma, which reduced stepwise between 3.0 and 2.5 Ma during glacial periods (Tiedemann et al., 1989). An early maximum of the biogenic opal at ODP Site 658 would indicate that coastal upwelling offshore from Cape Blanc began around 3 Ma suggesting an increase of the northeast trade winds by that time (Tiedemann et al., 1989). However, the three main opal maxima at ODP Site 658 fall in “warm” periods (minima in the oxygen isotope stratigraphy) and could also have been induced by river-borne nutrients instead of upwelling. Moreover, Etourneau et al. (2012) argue that upwelling globally was weak between 3 and 2.7 Ma and that in the case of the Benguela upwelling system high diatom and opal productivity in the South Atlantic occurred under weak upwelling, even stratified, conditions. The NE trade wind history probably is better recorded in the concentrations of TW pollen (Fig. 6). Comparison of the pollen records of ODP Sites 659 and 658 shows thefirst concurrent maximum in TW pollen concentration occurring at 2.53 Ma. TW pollen concentrations remain at a higher level afterwards. The TW maximum shortly before 2.5 Ma is preceded by two maxima recorded at Site 658 only (~ 2.7 and 2.6 Ma). Earlier maxima of trade wind indicators are rather ambiguous. Prior to the 2.7 Ma, before the iNHG, little or no systematic relationship occurs between SST of the North Atlantic with aridity and dust in West Africa (Fig. 6). This changes around 2.7 Ma (Marine Isotope Stage G6/G4), when, in the central North Atlantic (IODP Site U1313), the first maximum in aeolian input of n-alkanes (higher plant waxes) is registered together with a minimum in SST (Naafs et al., 2010, 2012). Naafs et al. (2012) attribute the aeolian higher plant wax supply to sources made accessible by glacial erosion and transported by westerly winds from North America. The next combined SST minima and wax maxima at Site U1313 occurred at 2.6 (Marine Isotope Stage 104) and just before 2.5 Ma (Marine Isotope Stage 100). During the glacial period of Stage G6/G4 and the two sequels around 2.6 and 2.5 Ma, aridity (decreasing Fe/K ratios) and dust levels (increasing Ti/Ca ratios) in West Africa correlate with the indication of increased NE trade winds (TW pollen concentration at Site 658). These results associate the increase of trade wind strength in West Africa to the intensification of the Northern Hemisphere glaciations.

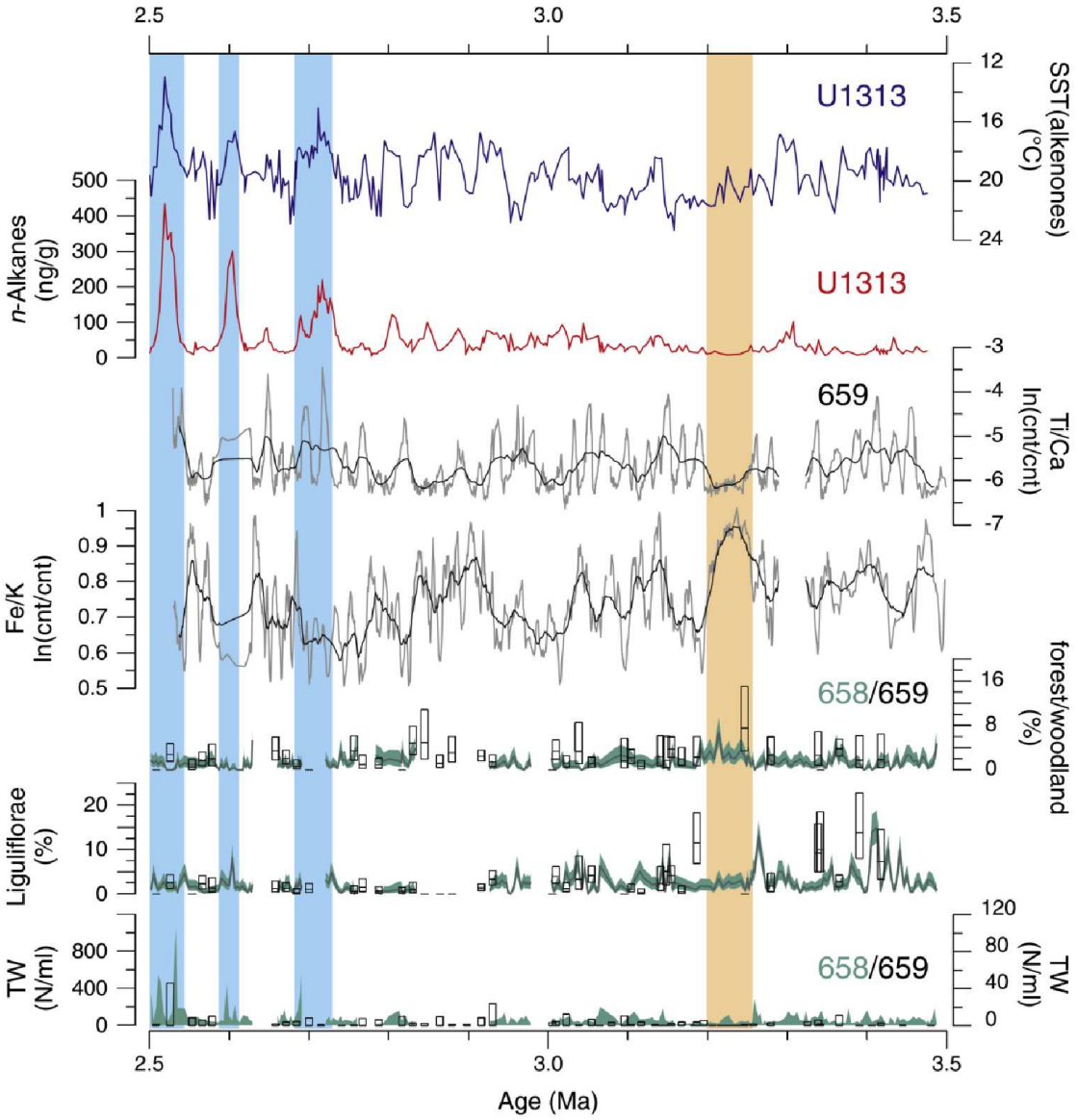

Figure 6: Comparison of Ti/Ca (thin grey line ln(Ti/Ca); thick black line ln(Ti/Ca) 31-point moving average)and Fe/K ratios (thin grey line ln(Fe/K) 5-point moving average; thick black line ln(Fe/K) 31-point moving average) of ODP Site 659 with alkenone derived SSTs (Naafs et al., 2010) and n-alkane concentration (Naafs et al., 2012) of ODP Site 306-U1313 in the North Atlantic (41°N 33°W). Note the reversed scale of the alkenone SST. Pollen percentages of forest/woodland elements and of Asteraceae Liguliflorae from ODP Sites 658 (line and shading) and 659 (boxes). 95% confidence intervals are denoted by the width of the shading (Site 658) and the length of the boxes (Site659). TW pollen concentration as an indication of NE trade wind vigour at ODP Sites 658 (shading) and 659 (boxes). Humid conditions prevailed between 3.24 and 3.20 Ma (reddish bar). Strengthening of the NE trade winds was concurrent with increased supply of plant wax (n-alkanes) to the North Atlantic during the intensification of the Northern Hemisphere Glaciations (blue bars) around 2.7, 2.6, and just before.

2.10 Conclusions

Terrestrial input to the marine sediments of ODP Site 659 is almost exclusively aeolian. The ratio between titanium and calcium expressed as ln(Ti/Ca) can serve as a proxy for dust input at the site. Pollen transport by easterly and north-easterly winds increased during dusty periods. Savannah grassland expanded during wetter periods characterised by high ln(Fe/K) values and desert vegetation expanded during drier periods characterised by low ln(Fe/K) values. During the Pliocene, humid climate alternates with arid and dusty conditions in West Africa. The longest period of warm and humid climate occurred between 3.24 and 3.20 Ma, which only covers a part– albeit the warmest one–of the mid-Pliocene (mid-Piacenzian) warm period. Comparison of the pollen records of ODP Sites 659 and 658 revealed remarkable similarities in composition adding confidence to the reconstruction of vegetation change in Pliocene West Africa. Shifts of the vegetation between woodlands, grasslands and desert occurred a orbital time scales. The long-term trend reveals a decline of woodland and forest after 2.6 Ma. The desert extended substantially since 2.7 Ma. The high relative abundance of Asteraceae Liguliflorae pollen indicates that species from the Tribus Cichorieae (=Lactuceae after Bremer, 1994) might have grown in the savannah until 3 Ma. Thefloristic composition changed and the savannah became poor in Asteraceae after 3 Ma. NE trade winds intensified in West Africa after 2.53 Ma and during two short periods before that (~2.7 and 2.6 Ma) associated with the intensification of the Northern Hemisphere glaciations. Supplementary data to this article can be found online at http://dx. doi.org/10.1016/j.palaeo.2014.09.023.

2.11 Acknowledgements

The study was financially supported by the Deutsche Forschungsgemeinschaft (DFG), grant DU221/5, and by the German Federal Administration for Education and Science (BMBF). FV thanks GLOMAR (Bremen International Graduate School for Marine Sciences). We are indebted to Susanne Jahns and Chiori Agwu for their help in the pollen analysis. We thank the Ocean Drilling Program for providing the samples. Alexus Wülbers, Walter Hale, Thomas Westerhold, Vera Lukies, and Ursula Röhl are acknowledged for helping with core handling, XRF scanning, and calibration of XRF data obtained during different sampling sessions. Mike Turner (Brunel University London) has kindly checked the English of the manuscript.

2.12 Supplementary materials

Supplementary figure 1: Comparing pollen records of ODP Sites 658 and 659. From top to bottom; stable oxygen isotope stratigraphy of ODP Sites 659 (line) and 658 (crosses) (Tiedemann, 1991, Tiedemann et al., 1994 and Leroy and Dupont, 1997). $\delta^{18}O$ values are plotted 0.64 per mil below seawater equilibrium. Concentration per ml of trade wind transported pollen (TW) and percentages for selected taxa (*Artemisia*, *Calligonum*, *Ephedra*, CA = Caryophyllaceae and Amaranthaceae, Poaceae, Sahel, forest/woodland, Asteraceae, mangrove = *Rhizophora*). Pollen taxa comprising the forest/woodland and Sahel group are given in Supplementary Tables 1 and 2, respectively. 95% confidence intervals of the percentage data are indicated by shading (ODP Site 658) or the length of the boxes (ODP Site 659).

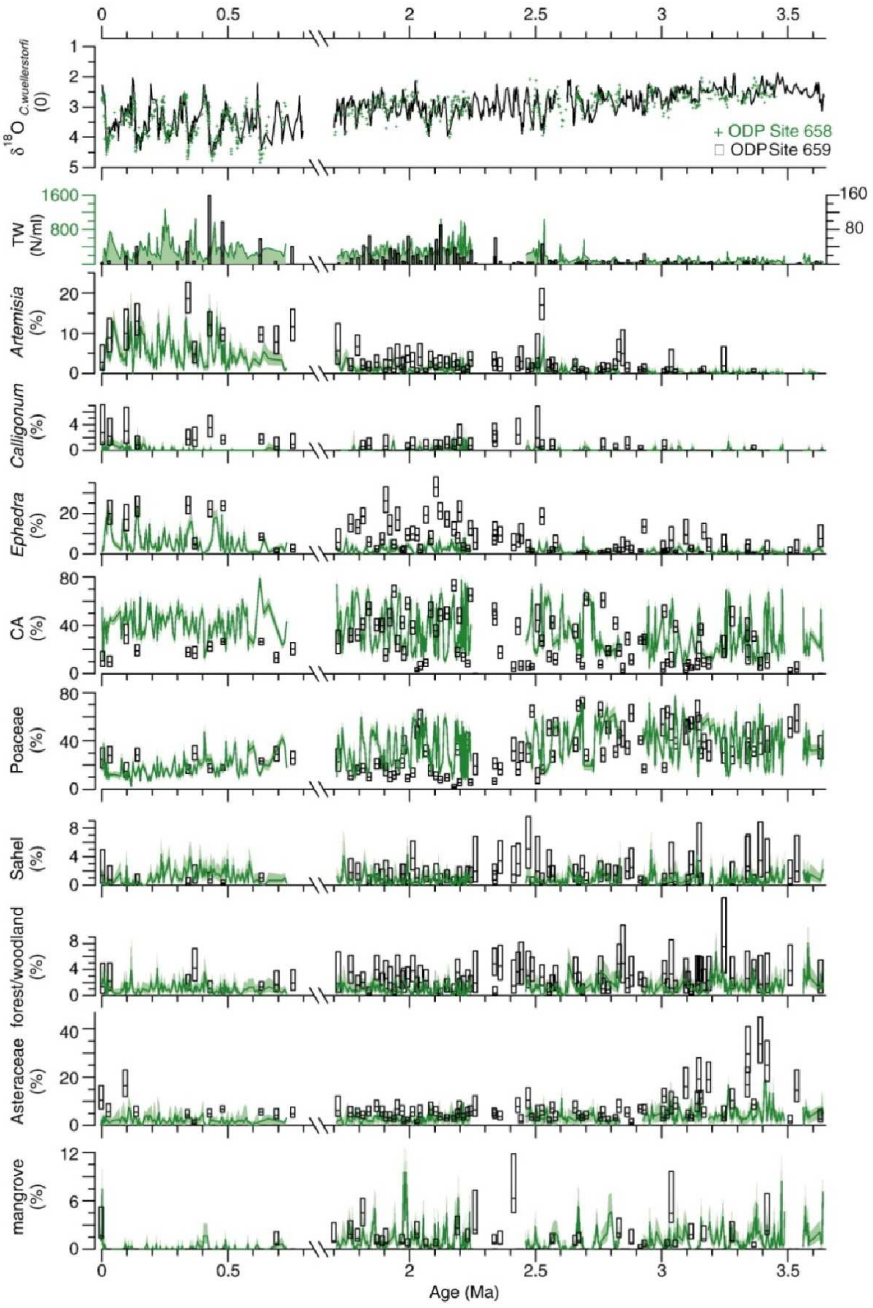

Supplementary figure 2: Linear correlation (after Hammer et al., 2001) between XRF-scanning Ti/Ca ratios and dust percentages of ODP Site 659 (Tiedemann, 1991 and Tiedemann et al., 1994). Top: X–Y-plot of ln(Ti/Ca) against dust %, linear regression and 95% confidence intervals; middle: residuals to the regression; bottom: ln(Ti/Ca) and dust percent plotted against age. Red dot (T) is the sample with the turbidite and is not included in the regression fit.

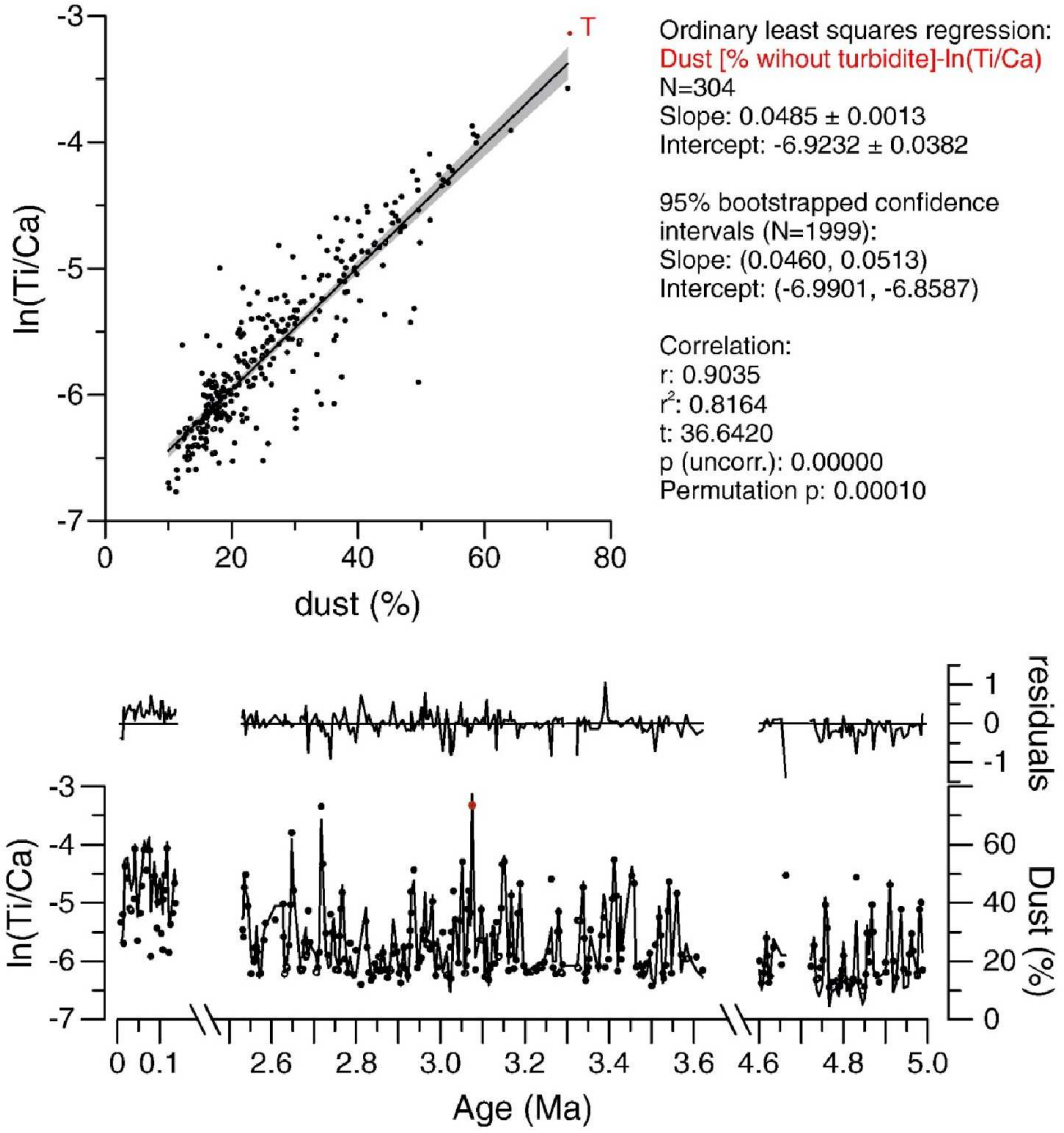

Supplementary Table 1: Pollen taxa found at ODP Site 659 and 658 grouped in “forest/woodland”. Underlined taxa have been found at both sites, bold taxa only at ODP Site 659.

Acalypha
Afzelia
Alchornea
Amphimas
Antidesma
Apocynaceae
Arecaceae
Baphia
Barleria
Berlinia
Bignoniaceae
Blepharis
Blighia
Bosqueia
Boswellia
Bridelia
Butyrospermum
Calycobolus
Cassia t.
Celastraceae
Celtis
cf. Burkea
cf. Calamus
cf. Croton
cf. Leucas
cf. Martretia
cf. Osmocarpum
cf. Spondianthus
Cissus
Cocculus
Coffea
Cola
Combretaceae/Melast.
Commicarpus
Conneraceae
Corbichonia decumbens
Corchorus/Grewia
Crossopteryx
Crudia
Delonix
Detarium
Dichrostachys
*Diodia*t.
Diospyros
Dodonaea
Drypetes molunduana t.
Elaeis guineensis
Entada
Fagara
Gaertnera
Hibiscus
Hygrophila
Hymenocardia
Hypoestes t.
Icacinaceae
Ixora
Jatropha
Justicia t.
Lannea
Leea
Macaranga
Mallotus
Manilkara
Morelia
Myrica
Myrtaceae
Nauclea
Ochnaceae
Olax
Paramacrolobium
Parinari
Pavetta
Peristrophe
Petersianthus
Phytolacaceae
Piliostigma
Protea
Pterocarpus
Pycnanthus
Rauvolvia
Rubiaceae
Rutaceae
Sabicea/Morinda
Sapium
Sapotaceae/Meliaceae
Securinega cf.virosa
Sesbania
Sherbournea
Spermacoce
Sterculia
Tetrorchidium
Trichilia
Uapaca
Virecta

Supplementary table 2: Pollen taxa found at ODP Site 659 and 658 grouped in “Sahel". Underlined taxa have been found at both sites, bold taxa only at ODP Site 659.

Acacia

Balanites

Capparidaceae

Caylusea

Chrozophora

Commiphora

Dichrostachys

Gymnosporia

Heliotropium t.

Hildebrandtia

Hyphaene

Indigofera t.

Maerua

Mitracarpus

Nyctaginaceae

Phoenix

Phyllanthus

Rhamnaceae

Rhynchosia

Salvadoraceae

Solanum

Tephrosia

Thymeleaceae

Tribulus

Zygophyllum

Chapter 3

Orbitally-driven environmental changes recorded at ODP Site 959 (eastern equatorial Atlantic) from the Late Miocene to the Early Pleistocene

Francesca Vallé, Lydie M. Dupont, Thomas Westerhold

MARUM – Center for Marine Environmental Sciences, University of Bremen, 28359 Bremen, Germany

Keywords: Pliocene; XRF core scanning; astronomical tuning; West Africa; Ivory Basin; terrestrial input

submitted to: International Journal of Earth Science. (under review)

3.1 Abstract

Paleo-records from tropical environments are important to explore the linkages between precipitation, atmospheric circulation and orbital forcing. In this study, new high-resolution XRF data from ODP Site 959 (3°37'N, 2°44'W) have been used to investigate the relationship between paleoenvironmental changes in West Africa and sedimentation in the tropical east Atlantic Ocean. Fe intensity data have been used to build a 91 meter composite depth record that has been astronomically tuned allowing the development of a detailed age model from 6.2 to 1.8 Ma. Based on this new stratigraphy we studied the variations of Ti/Al, Ti/Ca and Al/Si ratios, proxies for aeolian vs. fluvial supply, as dust indicator and fine vs. coarse grain size, respectively. We discuss sedimentation patterns at ODP Site 959 associated to the environmental changes from the late Miocene until the early Pleistocene. During the interval corresponding to the earlier stages of the Messinian Salinity Crisis our proxy records indicate enhanced run-off from the West African continent and major supply of fine material at ODP Site 959, suggesting a stronger monsoon and increased precipitation during eccentricity minima. A long-term decrease of river supply is documented after 5.4 Ma towards the early Pleistocene. From the increased values and variability of Ti/Al ratios we suggest that after 3.5 Ma dust started to reach the study site probably as a result of the southward shift of the Intertropical Convergence Zone during winter. Between 3.2 and 2.9 Ma ODP Site 959 Ti/Ca ratios exhibit three maxima corresponding to eccentricity maxima similarly to other dust records of northern Africa. This suggests continent-wide aridity or larger climate variability during that interval. Eccentricity forcing (405 kyr and 100 kyr) and precession frequencies are found in the entire studied interval. The variations of Ti/Al ratio suggest stronger seasonality between 5.8 and 5.5 Ma and after 3.2 Ma.

3.2 Introduction

Climate over the West African region is driven by changes in sea surface temperatures and wind systems since this area is dominated by the African Monsoon (Norris, 1998), which is subject to the latitudinal migration of the Intertropical Convergence Zone (ITCZ) (Ruddiman et al., 1989) and the African rainbelt (Nicholson, 2009). Although the late Miocene to Pliocene West African climate was warmer and wetter than in the Pleistocene and today, fluctuations between arid and "green" wet periods occurred since at least 8 Ma (Larrasoaña et al., 2013). During these cycles interactions between vegetation cover, rainfall and dust formation are mainly controlled by the African summer monsoon oscillating in synch with Earth's orbital precession cycles (Zhang et al., 2014; deMenocal, 2011). During more arid periods, dust supply from the African continent to the east Atlantic Ocean was enhanced while it was reduced during more wet intervals. Dust flux records at different locations offshore of West Africa indicated aeolian supply from the African continent to the east Atlantic Ocean since at least 8 Ma (Ruddiman et al., 1989). Recent modelling studies even suggest a much earlier expansion of the Sahara Desert linked to the closure of the Tethys basins dating back to the Tortonian Stage (Zhang et al., 2014). A major increase of dust supply from the Sahel and Sahara into the east Atlantic Ocean at 2.7 Ma is the result of intensified aridity in northern Africa (deMenocal, 1995; Tiedemann et al., 1994) caused by enhanced NE Trade winds associated with decreased sea surface temperatures (SST) of the North Atlantic (Vallé et al., 2014). At the same time dust records from the southern ocean (Martínez-Garcia et al., 2011) and north Atlantic also show increase in dust accumulation (Naafs et al., 2012). The latter has been related to increased dust production in North America after the intensification of the Northern Hemisphere glaciations (Naafs et al., 2012). Important indications about the response of precipitation and atmospheric circulation to past climate changes are derived from tropical paleoenvironmental records (McGee et al., 2014). Latitudinal shifts of the rainbelt and the ITCZ in relation to the cross-equatorial temperature gradient can be identified in the Pliocene records (Kuechler unpublished results). Albeit many records from subtropical northern Africa exist, the magnitude and regional variability of the African monsoon in the past are poorly constrained (McGee et al., 2014). To get new insights into the environmental evolution linked to latitudinal shifts of the rainbelt and the ITCZ in near-equatorial western Africa during the Late Miocene to Early Pleistocene we investigated the fluctuations in proxy records of siliciclastic supply at Ocean Drilling Program (ODP) Site 959 retrieved offshore of Ivory Coast. We present new high-resolution data obtained by X-Ray fluorescence (XRF) scanning of marine sediment cores. We used the iron (Fe) record to develop a detailed age model by orbital tuning. Based on this age model, we analysed the sedimentation patterns at ODP Site 959. We discuss our results together with the magnetic susceptibility and smear slides of the same site, available at the ODP Janus database, and compare them with proxy records from other ODP sites from the equatorial East Atlantic (662), the tropical East Atlantic (659) and the Arabian Sea (721/722). The modern oceanographic setting of ODP Site 959 is characterised by coastal upwelling in boreal summer as the result of the Guinea Current combined with winds flowing parallel along the coast (Verstraete, 1992). The siliciclastic component deposited at ODP Site 959 is mainly aeolian (Wagner, 1998). During boreal winter, when the ITCZ is at its southern position, the flows of the Harmattan (Kalu, 1979) and the

enhanced Northeast Trade winds reach the Gulf of Guinea carrying dust particles mostly from the north-eastern part of the Sahara desert and the Sahel zone (Kalu, 1979, Sarnthein 1981; Prospero et al. 2002) (Figure 1). The dust coming from those arid regions consists mainly of quartz grains and is enriched in silicon (Scheuvens et al., 2013, Collins et al., 2013). The grain size of dust collected off Ivory Coast/Ghana is measured between 40 and 10 µm (from fine to coarse silt) and becomes finer eastwards (Stuut et al., 2005).

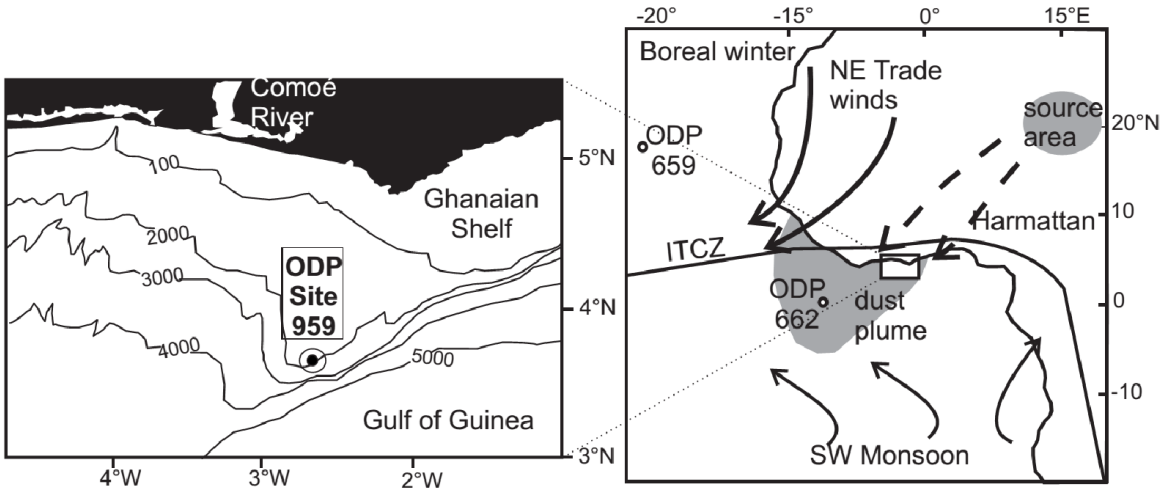

Figure 7: Left, Location of ODP Site 959. Right, Atmospheric circulation and aeolian transport over West Africa during boreal winter. Solid thick arrows represent NE Trade Winds, solid thin arrows represent SW Monsoon. Dashed arrows indicate the direction of the Harmattan. Grey areas denote the dust source area and the corresponding dust plume reaching ODP Site 959 following Kalu (1979). Redrawn from Norris (1998) and Wagner (1998). Localities of ODP site 659 and ODP site 662 used for comparison are shown with open circles.

Today, river discharge along the coastline is moderate and most of the mass gravitational flows are canalized into the Deep Ivorian Basin (Giresse et al., 1998). Fluvial material thus does not often reach Site 959 (Wagner, 1998).

3.3 Material and methods

ODP Site 959 was drilled in 1995 during Leg 159 on a small plateau on the southern shoulder of the Deep Ivorian Basin at 3°37'N, 2°44'W and 2100 m water depth, ~120 km offshore of Ivory Coast (Figure 1). The Late Miocene-Early Pleistocene sections constitute of bioturbated nannofossil-foraminifer oozes with clay and chalk starting from ~75 meter below sea floor (Mascle et al., 1996). The latest stratigraphic framework for ODP Site 959 from the Cretaceous to the Quaternary is based on shipboard biostratigraphy (Wagner, 2002). Neither magnetostratigraphy could be established at Site 959 because of the low magnetic properties of the sediments (Mascle et al., 1996), nor a hole-to-hole correlation was available for the interval of our study. We scanned from Hole 159-959A cores 3H to 9H, from Hole 159-959B cores 3H to 11H and from Hole 159-959C cores 4H to 11H by using the XRF Core Scanner II at the MARUM-University of Bremen which enables almost a continuous and non- destructive analysis of major elements (Röhl and Abrams, 2000; Röhl et al., 2007; Westerhold et al., 2007). To prevent contamination and

desiccation of the sediment, the split surface of the sections were covered with a 4 µm thin Ultralene foil. Disturbed parts of the sections were not scanned whereas overlapping sections for at least two holes were scanned in order to obtain a complete record. The measurements of the major light elements Fe, Si, Ti, Al, Ca were collected every 1 cm down-core over 1 cm using a generator setting of 10kV and 20 s counting time. The scanning data had a high signal to noise ratio. We used Fe intensity data (Area – number of total counts in 20s) to correlate between holes and to develop the age model. From the intensities of Ti, Ca, Al and Si we calculated Ti/Ca, Ti/Al and Al/Si ratios to use as environmental indicators. To ensure the symmetry of those ratios around zero, they are expressed as natural logarithms (Govin et al., 2012; Weltje and Tjallingii, 2008).

3.4 Results

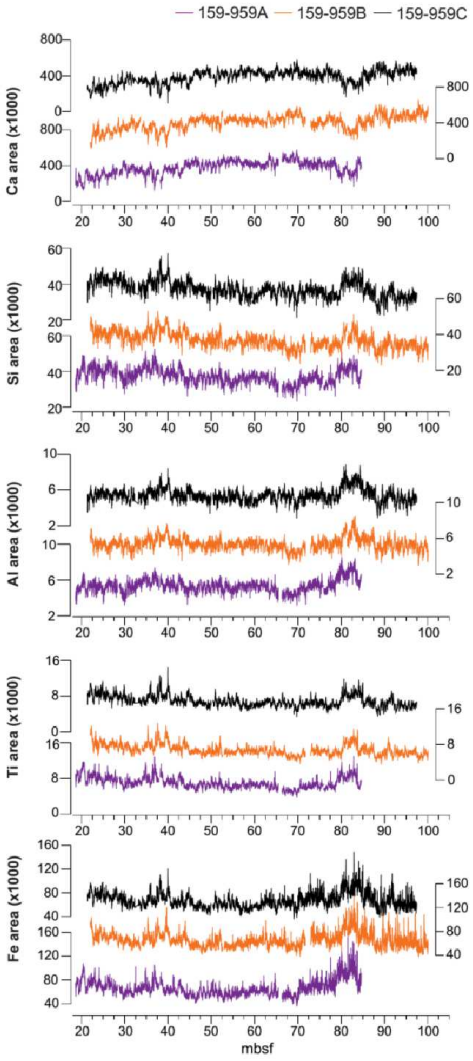

Figure 8: Element areas (intensities) against meter below sea floor (mbsf) measured with XRF scanning at 1 cm resolution for ODP Leg 159-959A (violet) Cores 3-9, 159-959B, Cores 4-11 (orange) and 159-959C cores 4-11 (black)

The intensities of iron (Fe), titanium (Ti), aluminium (Al), silicon (Si) and calcium (Ca) show similar cyclic oscillations in each of the measured holes (Figure 2). Fe, Si, Al, Ti intensities show opposite patterns to those of Ca reflecting the different origins of those elements. The measured elemental intensities are related to the concentration of the elements in the sediments. In our records Ca and Fe intensities are one order of magnitude higher than those of Si, Al and Ti. Comparison between calcium intensities and carbonate content data measured on discrete samples (Wagner, 2002) shows a linear correlation establishing that variations of Ca intensities between 250.000 and 450.000 counts per area reflect a carbonate content varying between 31 and 50%, respectively (Figure 3). The amplitude of the intensity fluctuations is higher between 34 and 45 mbsf and between 80 and 85 mbsf. Those intervals indicate a relative decrease in calcium and increase in terrigenous elements. Fe intensities show clear prominent features that we subsequently used to construct the composite depth scale. All scanning data are stored at Pangaea.de <http://doi.pangaea.de/10.1594/PANGAEA.858040>.

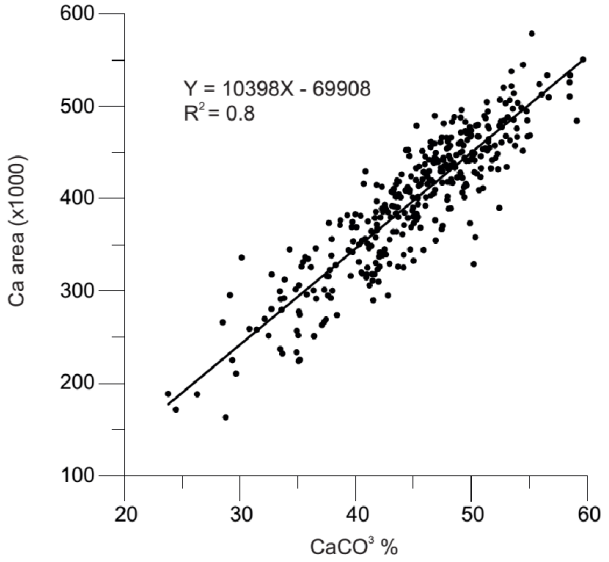

Figure 9: Correlation between XRF scanning measurements of calcium intensities and carbonate content measured on discrete samples (Wagner, 2002)

3.5 Development of the age model

High-resolution XRF core scanning data measured on multiple holes were used to build a composite depth scale for the site (e.g. Westerhold and Röhl, 2013; Westerhold et al., 2012, Westerhold et al., 2005, Evans et al., 2004). The construction of the composite depth record required several steps (see supplementary information). The cyclic patterns in the depth domain were then orbitally tuned in order to develop a high-resolution age model. After detrending the data, we proceeded with time series analysis in depth and frequency domains to establish whether the rhythms shown in the Fe composite record are related to Milankovitch cycles. As suggested by

Weedon (2003) the usage of evolutionary spectra in the depth domain allows the identification of dominant cycle periods and changes of those periods over the entire record. We chose the wavelet analysis (Morlet wave) to calculate evolutionary spectra (Torrence and Compo, 1998). Wavelet software was provided by C. Torrence and G. Compo (http://atoc.colorado.edu/research/wavelets/). Multitaper Method (MTM) power spectra (Figure 4) were calculated by the kSpectra Toolkit software from SpectraWorks using 3 tapers and a resolutionof 2 (Ghil et al., 2002). Confidence levels are based on a robust red noise estimation (Mann and Lees, 1996). Evolutionary wavelet spectra of the Site 959 Fe intensity record evidence high spectral power in parallel bands at three distinct periods (Figure 4). The dominant cycle throughout the record is 2 m long. Only between 52 and 62 rmcd this cycle becomes less evident in the wavelet spectra. Shorter cycles (1 m, 0.5 m and 0.4 m, respectively) are expressed from 52 rmcd until the base of the record. The absence of strong shifts of the period bands in the wavelet spectra indicate that rapid changes of sedimentation rate did not occur in the studied interval. We assume relatively constant sedimentation rates within three intervals; 21-50 rmcd (Figure 4a), 52-90 rmcd (Figure 4b), and 90-112.7 rmcd (Figure 4c). Multitaper spectra have been calculated for those intervals. The frequencies obtained are in accordance with the periodicities of the wavelet analysis. Frequencies around 0.5 cycle/m (2 m/cycle) of the upper interval have higher power than those of the last interval. High power around the 2-cycle/m-frequency (0.5 m/cycle) within the interval between 90 and 112.7 rmcd is linked with the high variability in the Fe intensity data. Applying the biostratigraphic ages (Supplementary Table 4) and the resulting sedimentation rates, we estimated that the 2-m-cycle represents the mean short eccentricity cycle (100 kyr), the 1-m-cycle the obliquity component (41 kyr), and the 0.5- to 0.4-m-cycles the mean precession component (21 kyr). Spectral analysis of the oldest part of the record (Fig. 4c) even indicate a split precession component (calculated frequencies of 2 and 2.4 cycle/m (0.5 and 0.4 m/cycle) corresponding to 23 and 19 kyr/cycle) but does not show a single frequency peak for the eccentricity component. Different frequencies representing eccentricity might be related to a split in the short eccentricity cycle (95 and 125 kyr/cycle). The split in the precession cycle is a strong indication for orbital forcing of the ODP Site 959 Fe record (Herbert et al., 1995; Westerhold et al., 2007). Following the metronome method of Herbert et al. (1995) we built a cyclostratigraphy by counting of cycles in the Fe data after filtering using a Gaussian band-pass filter (see supplementary information). Prior to the tuning of Fe record to orbital parameters we explored the phase relation between the terrigenous input in our study area and the orbital parameters. Tiedemann et al. (1994) found correspondence between the long eccentricity cycles (405 kyr) minima and minima in the Pliocene dust flux record at 18°N, implying that long-term aridity, linked to terrigenous supply in the east Atlantic Ocean at this latitude, responded to variations in eccentricity. Offshore southern Africa the Fe content from Miocene until the early Pliocene was increasing during wet intervals correlating to eccentricity and obliquity maxima (Vidal et al., 2002, Westerhold et al., 2005). We compared Site 959 Fe intensity data and Site 959 *C. wuellestorfi* oxygen isotope record (Norris, 1998). Although both records differ in length and resolution, we could associate high Fe intensities to high oxygen values implying a link between the Fe record and global ice volume. We, therefore, assumed a more or less constant relationship between Fe

input, eccentricity and obliquity throughout the studied interval. Hence, we preliminary tuned the Fe intensity data to the eccentricity curve La2004 (Laskar et al., 2004) correlating the minima in the eccentricity long cycles, 405 kyr (Laskar et al., 2004) to the minima in the Fe cycles (Supplementary Fig. 3). For fine-tuning we used the sum of normalized Eccentricity, Tilt and Precession (E+T-P) based on La2004 solution (Laskar et al. 2004) as a target curve applying a minimum number of tie-points (Table 3). The resulted tuned Fe record and the calculated sedimentation rate varying between 1.47 and 2.96 cm/kyr is presented in Figure 5. To verify the accuracy of our age model we compared the benthic oxygen isotope record at ODP Site 959 (Norris, 1998) and several other tuned oxygen isotope records of ODP Sites 846, 926, 982 (Shackleton et al., 1995; Shackleton and Crowhurst, 1997; Hodell et al., 2001), and the benthic oxygen isotope stack LR04 (Lisiecki and Raymo, 2005). The heavy Marine Isotope Stages CN6, Si6 and TG20 are well recognised and aligned as are the light Isotope Stages T5 and T7 (terminology after Shackleton et al., 1995). The major stepwise deglaciation from TG14 to TG9 is also recognised. However, resulting ages of Stages TG8 through TG14 are about 50 ka older at Site 959 than at Sites 926 and 982. (Supplementary Fig. 4).

Table 1. Age Model for Late Miocene-Early Pleistocene Site 959 after tuning Fe intensity data to the ETP curve.

Depth (rmcd)	Age (Ma)
21.90	1.862
22.03	1.871
25.98	2.139
27.74	2.258
38.47	2.948
42.60	3.154
45.77	3.326
47.53	3.440
55.84	3.842
61.91	4.076
76.54	4.715
80.06	4.851
83.37	5.069
87.07	5.216
89.70	5.379
91.40	5.446
96.72	5.652
101.04	5.805
103.57	5.899
109.75	6.107
112.70	6.206

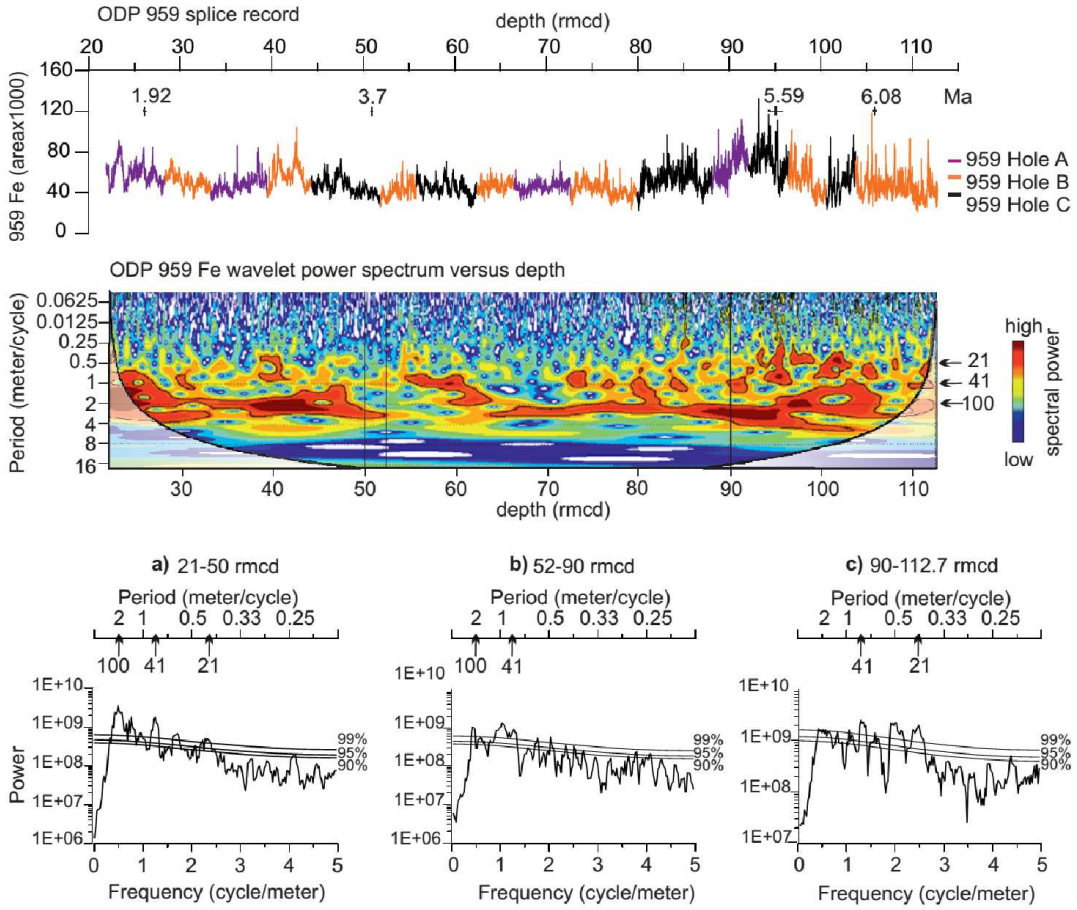

Figure 10: Top, ODP Site 959 splice record on revised composite depth in meter (rmcd). Middle, Wavelet (Morlet) power spectrum of Fe intensity in the depth domain from 21.9 to 112.7 meter composite depth (rmcd). The contours are normalized linear variances with blue representing low spectral power and red representing high spectral power. The black contour lines enclose regions with more than 95% confidence based on white noise. Shaded areas on either end indicate the cone of influence where padding with zeros influences the results. Bottom, (a-c) MTM power spectra of Fe intensity data in the depth domain for three intervals. Calculated confidence levels (90%, 95%, 99%) based on a robust red noise estimation (Mann and Lees, 1996) are shown. Multitaper Method (MTM) spectra were calculated by the kSpectra Toolkit software from SpectraWorks using 3 tapers and a resolution of 2. Prior to time series analysis Fe data were detrended, linearly resampled at 1 cm and outliers were removed.

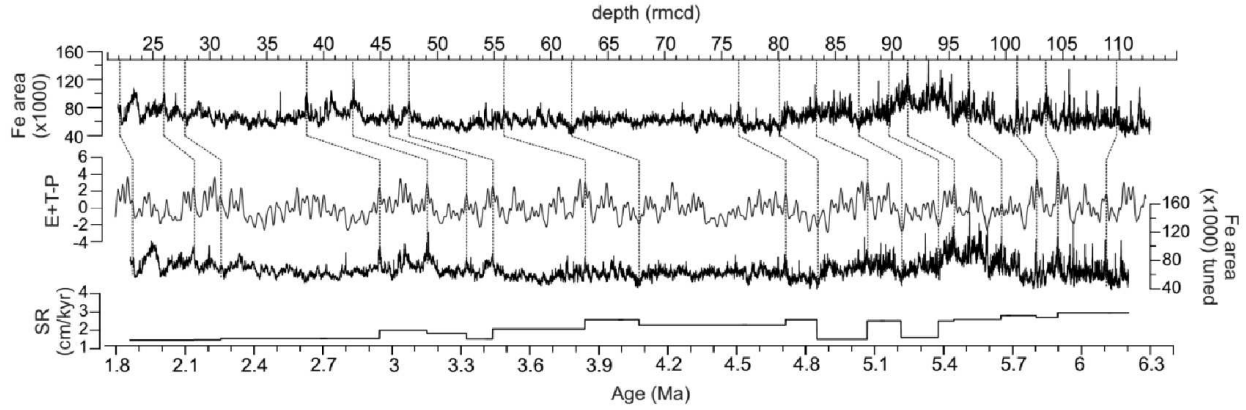

Figure 11: Fine orbital tuning of Fe intensity data (Fe area). From top to bottom: Site 959 Fe intensities on meter composite depth (rmcd); ETP curve calculated using La2004 solution (Laskar et al. 2004) and applied tie points; tuned Fe intensity data on Age and resulted sedimentation rate (SR). AnalySeries software (Paillard et al. 1996) has been used for tuning process.

3.6 Sedimentation at ODP Site 959

Calcium in the Atlantic surface sediments derives mostly from marine biogenic carbonates (Arz et al., 1999, Govin et al., 2012) whil iron, titanium, aluminium and silicon have mostly terrestrial sources. Si is the most abundant element in mineral dust where it is the main constituent of coarse quartz grains (Scheuvens et al. 2013; Collins et al., 2013). Al is linked to fine river clays (Collins et al., 2013). Possible sources of Fe are iron oxides and hydroxides (hematite and goethite) that are a component of the distal aeolian dust (Balsam et al., 1995). Ti is associated with coarse grain size minerals and due to its high content in aerosol samples,Ti has been proposed as an indicator for Saharan dust (Nicolás et al., 2008). Records of both Fe and Ti show similar patterns at Site 959, albeit Ti area values are substantially smaller. An excellent linear correlation has been found between ln(Ti/Ca) and dust percentages determined from the carbonate free siliciclastic content of sediments of ODP Site 659 (Tiedemann et al. 1994; Vallé et al, 2014). Thus, we interpret the Ti/Ca ratio mainly representing the dust supply (Arz et al. 1999); the Ti/Al ratio as a proxy of aeolian versus fluvial input (Govin et al. 2012; Zabel et al. 2001), and the Al/Si ratio being related to grain size (Collins et al. 2013). Variations of Ti/Al, Ti/Ca, Al/Si ratios are discussed below (Figure 6). As we focus on longer term trends, we present 31 point moving averages of the XRF scanning results (Figure 6).

3.6.1 Sedimentation during the Messinian Salinity Crisis

Site 959 sequence is one of the few sites in the east Atlantic that preserve a continuous record over the Messinian Salinity Crisis (MSC; Wagner, 2002), which lasted from 5.97 to 5.33 Ma (Krijgsman et al., 1999; Manzi et al., 2013). Severe carbonate dissolution occurred in the oceans during the MSC (Wagner, 2002) resulting in lower calcium intensities between 5.6 and 5.4 Ma (in Figure 2 between 80 and 85 mbsf) and a moderate to poor preservation of foraminifers during

Stages TG8 through TG14 (Norris, 1998). Note that our age model results in 50 ka older ages for this interval than the established Mediterranean time scale (Roveri et al. 2008). The relative high Ti/Ca ratios during the later stage of the MSC probably are the result of an overprint of poor carbonate preservation (Figure 6). Despite carbonate dissolution, the calculated sedimentation rates are higher than in the rest of the record (~3 cm/kyr) and the terrestrial elements (Fe, Al, Ti) of Site 959 show elevated values between 5.6 and 5.4 Ma (Figures 2 and 5) corresponding with the last stage of the MCS, in which the Mediterranean Basin was mostly isolated from the Atlantic Ocean (upper evaporites and Lago Mare facies, 5.55 - 5.33 Ma; CIESM 2008; Roveri et al., 2014). A comparable sedimentary pattern of increased terrestrial input during the later stage of the MSC has been recorded at ODP Site 1085 in the South Atlantic by Vidal et al. (2002). Increased terrestrial input is also indicated by the higher magnetic susceptibility at Site 959 during the MSC (Mascle et al., 1996). A drop in sea level might have enhanced the river supply to the site (Wagner, 2002), which today receives only little fluvial material from the Ghanaian slope explaining the low Pleistocene sedimentation rates (Giresse et al., 1998). Al/Si ratios (smaller grain sizes) are increased between 6 and 5 Ma, fluctuate around intermediate levels between 5 and 2.7 Ma and drop to lower values afterwards, suggesting that fluvial sedimentation did not cease before the Pleistocene. Schneck et al. (2010) modelled strong increase in precipitation in southern West Africa in sensitivity experiments with low sea level in the Mediterranean Basin and a desiccated basin covered with grassy vegetation. Murphy et al., (2009) found increased precipitation in southern West Africa only in the low sea experiment. Additionally, fluctuations in the amount and salinity of the Mediterranean Outflow Water could have influenced the meridional heat distribution and transport via effects on the strength and position of the Atlantic Overturning Circulation, although the effects on climate outside the North Atlantic region are small (Ivanovic et al. 2014). From the model studies a wetter climate and increased run-off in southern West Africa would be expected during the last stage of the MSC (5.55-5.33 Ma) when the connection between Mediterranean and Atlantic was restricted or severed. However, enhanced continental run-off along the West African coastline as indicated at Site 959 by lower Ti/Al ratios (more fluvial input) and higher Al/Si ratios (more fine fluvial mud) took mainly place before (5.8-5.6 Ma) and after (5.4-5.2 Ma) but not during the final stage of the MSC. On the other hand, indications of increased fluvial sedimentation correlate well with pronounced minima in the eccentricity curve (Figure 6). Thus it seems that the influence of the MSC on the climate in southern West Africa was limited and, more likely, stronger monsoon rains increased river discharge. Tropical marine areas close to the continental margin are very sensitive to changes in continental freshwater run-off, especially during wetter intervals (Beckmann et al., 2005).

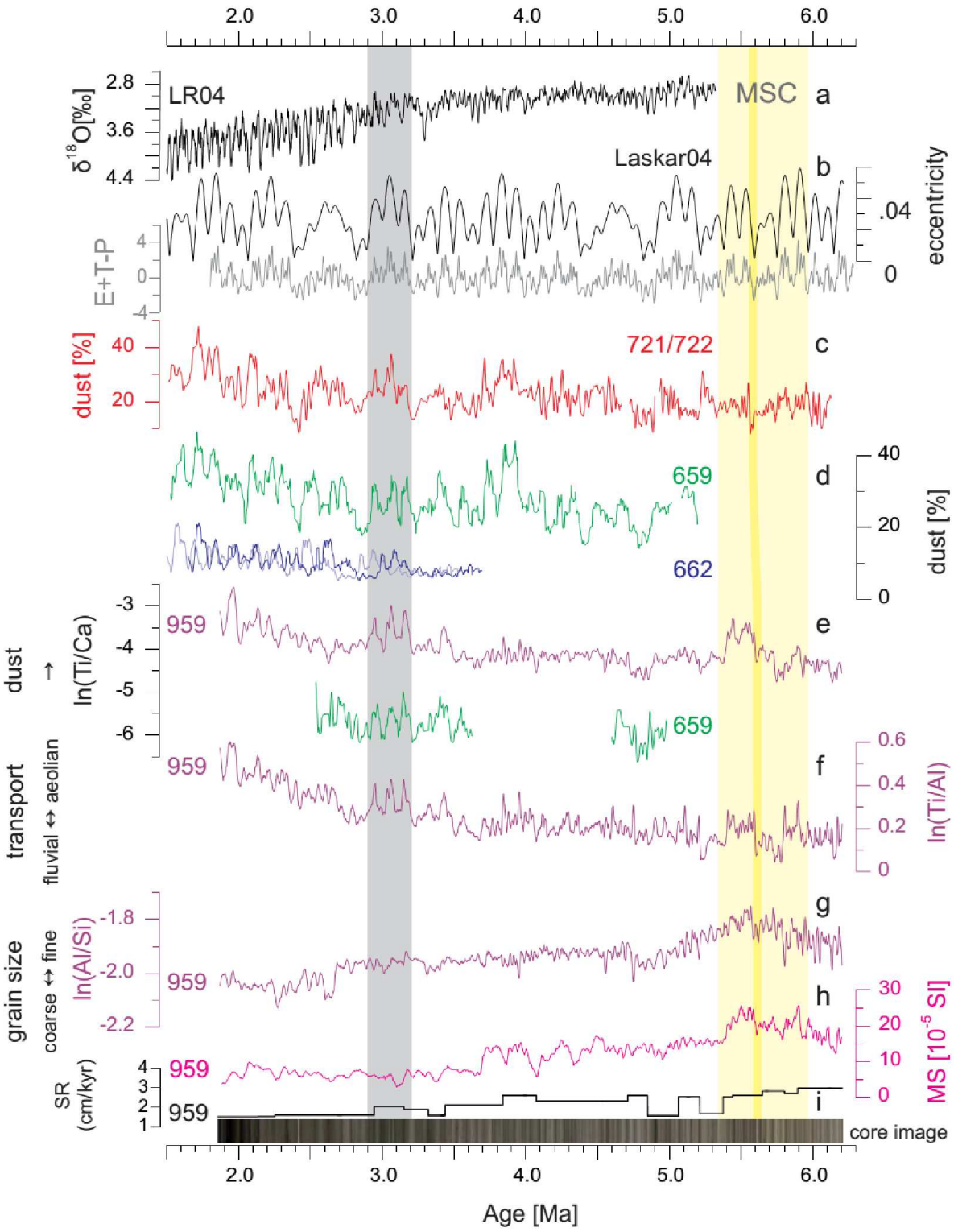

Figure 12: a, LR04 global oxygen isotope stratigraphy (Lisiecki and Raymo, 2005). b, Eccentricity (black) and E+T-P (gray) after Laskar et al. (2004). c, Estimate of dust over the Arabian Sea after magnetic susceptibility from ODP Sites 721/722 (deMenocal, 1995), in red 11pt moving average. d, Dust over the tropical East Atlantic from Site 659 (green) after Tiedemann et al. (1994) and Site 662 (blue) after Ruddiman and Janecek (1989), 11pt moving averages; light blue on the original age model, dark blue shifted by 150 kyr. e, Ti/Ca ratios after XRF

scanning of Site 959 (violet) and Site 659 (green, Vallé et al., 2014), 31pt moving averages. f, g, Ti/Al (f) and Al/Si (g) ratios of Site 959 (violet), 31pt moving average. h, magnetic susceptiblity of Site 959 (Mascle et al., 1996), in magenta 11pt moving average, age model of this study. i, Site 959 sedimentation rates (SR) and composite core image. Light yellow shading denotes the Messinian Salinity Crisis (MSC, 5.97-5.33 Ma, Manzi et al., 2014) and dark yellow shading the period 5.60-5.55 Ma (halite facies). For the period from 5.7 to 5.4 Ma our age model deviates by 0.05 Ma from the established Mediterranean chronology (supplementary information). Grey shading denotes a period with high eccentricity overlapping the mid-Pliocene Warm Period (2.9-3.2 Ma). Localities of ODP Sites 659, 662 and 959 are given in Fig. 1.

3.6.2 Long-term sedimentation changes after the MSC

After the MSC records of Ti/Ca and Ti/Al have similar patterns (Figure 6). We interpret them as a proxy for dust input and a proxy for aeolian versus fluvial supply, respectively. From 3.5 Ma the lower higher Ti/Ca and Ti/Al ratios indicate a gradual increase of windblown dust reaching Site 959 and a reduction in fluvial supply. A long-term decrease of fluvial material from the late Miocene to the early Pleistocene is also indicated by the magnetic susceptibility record (Mascle et al., 1996) and by the increase in grain size particles as indicated by the Al/Si ratios (Figure 6). A coarse resolution record of the smear slides (Mascle et al., 1996) indicates that in the windblown dust the sand fraction increased and the clay fraction decreased from 4.9 Ma on. Gradual reduction of river discharge is seemingly contradictory to the increase in moist forest and swamps between 6.5 and 3 Ma as recorded by pollen from offshore Niger Delta boreholes (Morley, 2000). However, decrease of fluvial input during the earliest Pliocene might be related to the initiation of the Guinean Current. Before the early Pliocene the West African coastline was closer to the equator, approximate at 2.5 °N (Norris, 1998) impeding the entrance of the Guinean current in the Guinea Gulf and implying a much northern position of the ITCZ relative to the coast (Norris, 1998; Wagner, 2002). This could have facilitated river supply. From the reconstruction of the thermocline using stable oxygen isotope gradients of planktonic foraminifera the initiation of the Guinea Current has been dated at ca. 4.9 Ma (Norris, 1998; Billups et al., 1999; Wagner, 2002), which amounts to ca. 5.2 Ma in the present age model. Since 3.5 Ma, a stepwise or gradual southward shift in the average southernmost position of the ITCZ during winter would have allowed the NE trade winds to reach the Gulf of Guinea. After 2.9 Ma the dust records of ODP Sites 659 and 721/722 show an increasing trend superimposed on the eccentricity fluctuations (Tiedemann et al. 1994; deMenocal 1995). The Ti/Ca ratios of ODP Site 959 increase since 2.75 Ma and the Al/Si ratios drop to a lower level at 2.7 Ma indicating coarser grain sizes. From the pollen record of ODP Site 659 it is has been concluded that NE trade winds strongly enhanced during short periods around 2.7 and 2.6 Ma and after 2.53 Ma (Leroy and Dupont, 1994; Vallé et al., 2014). Timing of the increased trade winds and synchronisation of arid phases recorded at ODP Site 659 with cold sea surface temperatures in the North Atlantic (Naafs et al, 2012) link the enhanced dust export out of northern Africa since the beginning of the Pleistocene to the intensification of the Northern Hemisphere glaciations.

3.6.3 Eccentricity forcing of the climate in northern Africa

The dust record indicates the influence of eccentricity cycles on the climate of northern Africa. In the time domain, the Ti/Ca ratios of ODP Site 959 exhibit three noticeable maxima between 3.2 and 2.9 Ma corresponding with eccentricity maxima (Figure 6). These maxima have been found in other dust records of northern Africa; at ODP Sites 659 and 662 retrieved from the East Atlantic (Ruddimann and Janecek, 1989; Tiedemann et al., 1994) as well as at ODP Site 721/722 from the Arabian Sea of (deMenocal, 1995). Those records have been plotted in Figure 6 on their original time scales, except for ODP Site 662 in the equatorial East Atlantic. The age model of Site 662 is based on biostratigraphy and not tuned (Ruddiman and Janecek, 1989); we applied to this record a shift of 150 kyrs. Correspondence of the dust records over such a large area suggests continent-wide aridity – or at least large climate variability with enhanced winds and expansion of desert-like regions to produce the dust, which seem stronger during eccentricity maxima. We note that these periods partly fall within the definition of the mid-Pliocene Warm Period (3.3-3.0 Ma; Dowsett et al. 2009) which is considered a wetter and warmer interval of the Pliocene, when savannah expanded at the expenses of the deserts as suggested by modelling results (Haywood et al., 2010). Assessment of climate variability indicated that strong seasonal variations could account for the apparent mismatch (Prescott et al 2014). In contrast, minimal dust was found in all three records (Sites 659, 721/722, 959) between 4.9 and 4.7 Ma. This minimum corresponds to one of the very long eccentricity minima in the eccentricity amplitude modulation of the early Pliocene implying smaller amplitudes of precession cycles. Dust probably did not regularly reach the Gulf of Guinea prior to 3.8 Ma. While the dust records of Site 659 (18°N East Atlantic) and Site 721/722 (17°N Arabian Sea) indicate dust outbreaks during periods with strong eccentricity, especially shortly after 4 Ma, Site 959 from the Gulf of Guinea reveals no such marked fluctuations (Figure 6). Spectral analysis of the ratios discussed confirms the cyclic fluctuations in the eccentricity bands (100 and 405 kyr). We calculated a wavelet analysis (Torrence and Compo, 1998) and REDFIT spectra (Schulz and Mudelsee, 2001). Results for ODP Site 959 Ti/Ca ratios are given in Figure 7.

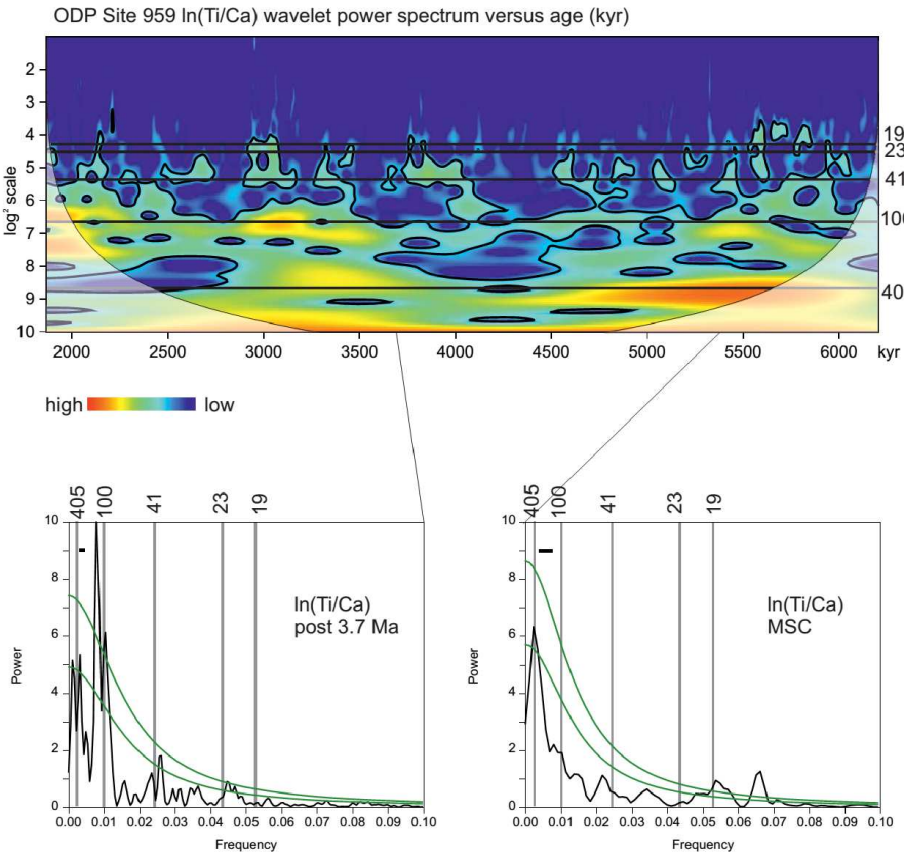

Figure 13: Top, Wavelet (Morlet) power spectrum of ln(Ti/Ca) on age in kyr. The data were detrended and linearly resampled at 1 kyr intervals. The contours are normalized linear variances with blue representing low spectral power and red representing high spectral power. The black contour lines enclose regions with more than 95% confidence based on white noise. Shaded areas on either end indicate the cone of influence where padding with zeros influences the results. Orbital periodicities are indicated. Bottom, Redfit power spectra (Schulz and Mudelsee, 2002) of ln(Ti/Ca) data on age (not resampled) for two intervals, after 3.7 Ma (left) and before 5.4 Ma (right) using Welch overlapped segment averaging (3 segments and 2x oversampling). Confidence levels (80%, 95%) are calculated using a red noise model. Grey bars denote orbital periodicities. Wavelet spectrum and Redfit spectra were calculated with PAST software (Hammer et al., 2001).

Specifically, the 405-kyr long eccentricity cycle is present in the Ti/Ca and Ti/Al dust records and the 100-kyr cycle becomes significant after 3.7 Ma. This is probably not an artefact of tuning, which was done on the Fe counts using the short eccentricity cycle and the ETP- curve. Effects of changing sedimentation rates should be cancelled out by the use of ratios instead of concentrations. Influence of eccentricity on carbonate and organic carbon records of ODP Site 959 was already found by Wagner (2002) using the original biostratigraphic age model. The impact of eccentricity on tropical climate is thought to be via the modulation of the precession, which controls the distribution of insolation between hemispheres and has strong influence on the monsoon (e.g. Kutzbach and Liu, 1997). Modelling studies has shown that both precession and obliquity intensify precipitation in northern Africa but that precession only influences the seasonal timing of the occurrence of the precipitation maximum (Tuenter et al., 2003). During eccentricity maxima the

amplitude of precession cycles is higher. Seasonality in the Northern hemisphere is enhanced during obliquity maxima coupled to a precession minimum (Tuenter et al., 2005). Recently, Marzocchi et al. (2015) modelled a full precession cycle and its consequences for the African monsoon system during the Miocene concluding that the African monsoon was already highly sensitive to orbital fluctuations during the Miocene. Indeed, Beckmann et al (2005) documented precession and eccentricity cycles in the freshwater discharge along the Ivorian Margin for the Cretaceous. If strong monsoon variability implies strong seasonality, we might interpret the Ti/Al ratios in terms of seasonality (Beckmann et al., 2005). Stronger seasonality is suggested by the deviation from the mean value of the Ti/Al ratios and would have occurred between 5.8 and 5.5 Ma, between 5.3 and 5.2 Ma and increased after 3.2 Ma (Supplementary Fig. 5). Between 3.4 Ma and 1.82 Ma, those periods of enhanced seasonality occur during obliquity maxima and precession minima according to Tuenter et al. (2005).

3.7 Conclusions

XRF scanning of cores from three drilled holes of ODP Site 959 off tropical West Africa provided high-resolution major element intensities for the Late Miocene to Early Pleistocene. Prominent features of the Fe intensity record have been used to obtain a new composite depth scale for the studied interval. The Fe intensity record exhibited cyclicity in the depth domain that could be linked to orbital cycles using spectral analysis. We fine-tuned the Fe record to the ETP (Eccentricity, Tilt, Precession) curve obtaining a detailed age model from 6.20 to 1.82 Ma. Our Ti/Al ratios suggest increased precipitation and river run-off along the western African coast during the earlier stages (lower evaporites and halite facies) but not the final ones (upper evaporites and Lago Mare facies) of the Mediterranean Salinity Crisis corresponding with eccentricity minima. Variations of elemental ratios record a long-term decrease fluvial supply of ODP Site 959 from the Late Miocene to the Early Pleistocene. This change might be related to the beginning of the Guinean Current. The comparison between siliciclastic supply at ODP Site 959 and existing dust records from northern latitudes offshore Africa suggest that winter dust was regularly reaching the Gulf of Guinea after 3.5 Ma. Between 3.2 and 2.9 Ma, the good correspondence between summer (ODP Site 659 and 771/772) and winter dust (ODP Site 959) supplies indicate enhanced continental aridity or larger climate variability corresponding with eccentricity maxima. Ti/Al record suggests increased seasonality from 3.4 Ma during obliquity maxima and precession minima. From 2.9 Ma on the trend in ODP Site 959 elemental ratios is due to the increasing effect of the forcing of Northern Hemisphere Glaciation. Time series analysis underlines the importance of eccentricity and precession (modulated by eccentricity) on the sedimentary cycles of Site 959.

3.8 Author's contribution

FV conducted the XRF measurements, developed the composite depth and astronomical age model, interpreted the results, and drafted the article; TW developed the composite depth and astronomical age model, interpreted the results, drafted and revised the article; LMD interpreted the results, drafted and revised the article.

3.9 Acknowledgements

The study was financially supported by the Deutsche Forschungsgemeinschaft (DFG), grant DU221/5. FV thanks GLOMAR (Bremen International Graduate School for Marine Sciences). We thank Ocean Drilling Program for providing the samples. Alexus Wülbers, Dr Walter Hale, Vera Lukies, and Dr Ursula Röhl are gratefully acknowledged for helping with core handling and XRF scanning.

3.10 Supplementary materials

3.10.1. Composite depth scale (rmcd) and splice

High-resolution XRF core scanning data measured on multiple holes were used to build a composite depth scale for the site (e.g. Westerhold and Röhl, 2013; Westerhold et al., 2012, Westerhold et al., 2005, Evans et al., 2004). The construction of the composite depth record required several steps. We correlated Fe intensities of Hole 959A (cores 3-9), 959B (cores 3-11) and 959C (cores 4-11) adding constant offsets to the original meter-below-sea-floor (mbsf) scale. No compression or expansion was used. The constant offsets calculated to match the cores of the three holes are presented in Supplementary Table 1. The tie points used to splice the cores over meter composite depth (mcd) have been taken where the cores showed less disturbed Fe intensity data (Supplementary Table 2). The spliced Fe record for Site 959 covers almost 91 meters (from 21.9 to 112.7 rmcd) (Supplementary Fig. 1). To allow locating samples already taken on the new composite depth scale (Westerhold et al., 2012), we adjusted the rmcd depth of the other cores outside the splice for the investigated interval. Where necessary those cores have been ‘stretched’ or ‘squeezed’ using the time-series analysis software package AnalySeries (Paillard et al., 1996) and using the new splice record as reference curve. The revised core depths with the corresponding composite depth and original depth are presented in Supplementary Table 3. The revised depths of the four selected biostratigraphic events and the resulting sedimentation rates are given in Supplementary Table 4. The cyclic patterns in the depth domain were then orbitally tuned in order to develop a high-resolution age model.

Supplementary Table 1. Offsets applied to entire cores for composite record for the three holes drilled at ODP Site 959.

Leg 159				**Leg 159**				**Leg 159**			
Site 959 Hole A				**Site 959 Hole B**				**Site 959 Hole C**			
Core	mbsf	offset(m)	mcd	Core	mbsf	Offset(m)	mcd	Core	mbsf	offset (m)	mcd
3H	18.60	2.90	21.50	**3H**	14.50	1.20	15.70	**4H**	21.30	1.29	22.59
4H	28.10	3.70	31.80	**4H**	24.00	1.83	25.83	**5H**	30.80	2.65	33.45
5H	37.60	4.62	42.23	**5H**	33.50	3.07	36.57	**6H**	40.30	2.73	43.03
6H	47.10	8.95	56.05	**6H**	43.00	4.00	47.00	**7H**	49.80	4.97	54.77
7H	56.60	9.40	66.00	**7H**	52.50	4.70	57.20	**8H**	59.30	7.64	66.94
8H	66.10	10.59	76.69	**8H**	62.00	9.61	71.61	**9H**	68.80	10.34	79.14
9H	75.60	11.24	86.84	**9H**	71.50	9.78	81.28	**10H**	78.30	10.24	88.54
				10H	81.00	11.37	92.37	**11H**	87.80	11.82	99.62
				11H	90.50	12.60	103.10				

Supplementary Table 2: Splice table.

Site	Hole	Core	Sect.	Sect. depth (cm)	mbsf	mcd		Site	Hole	Core	Sect.	Sect. depth (cm)	mbsf	mcd
U959	A	1	7	26	9.08	9.08	tie to	U959	A	2	1	0	9.10	10.00
U959	A	2	8	26	18.99	19.89	tie to	U959	A	3	1	40	19	21.90
U959	A	3	5	90	25.50	28.40	tie to	U959	B	4	2	107	26.57	28.40
U959	B	4	6	6	31.56	33.39	tie to	U959	A	4	2	9	29.69	33.39
U959	A	4	6	20	35.80	39.50	tie to	U959	B	5	2	143	36.43	39.50
U959	B	5	6	23	41.23	44.30	tie to	U959	C	6	1	127	41.57	44.30
U959	C	6	6	136	49.16	51.89	tie to	U959	B	6	4	39	47.89	51.89
U959	B	6	6	128	51.78	55.78	tie to	U959	C	7	1	101	50.81	55.78
U959	C	7	6	13	57.43	62.40	tie to	U959	B	7	4	70	57.7	62.40
U959	B	7	7	30	61.80	66.50	tie to	U959	A	7	1	50	57.10	66.50
U959	A	7	5	80	63.40	72.80	tie to	U959	B	8	1	119	63.19	72.80
U959	B	8	6	83	70.33	79.94	tie to	U959	C	9	1	80	69.60	79.94
U959	C	9	6	147	77.77	88.11	tie to	U959	A	9	1	127	76.87	88.11
U959	A	9	4	71	80.81	92.05	tie to	U959	C	10	3	51	81.81	92.05
U959	C	10	6	45	86.25	96.49	tie to	U959	B	10	3	112	85.12	96.49
U959	B	10	6	71	89.21	100.58	tie to	U959	C	11	1	96	88.76	100.58
U959	C	11	3	114	91.94	103.76	tie to	U959	B	11	1	66	91.16	103.76
U959	B	11	7	60	100.1	112.7						End of	the	splice

Supplementary Table 3. Mapping pairs of revised composite depth of the cores outside the splice record. Depths in the splice are denoted in italics. Correlation was performed with Analyseries (Paillard et al., 1996) using the splice as reference curve.

159-959A		**Splice depth**		**159-959B**		**Splice depth**		**159-959C**		**Splice depth**	
	mbsf	mcd	rmcd		mbsf	mcd	rmcd		mbsf	mcd	rmcd
3H	19	*21.90*	*21.90*	**3H**	22.16	23.36	23.32	**4H**	21.36	22.65	22.76
	25.50	*28.40*	*28.40*		22.39	23.59	23.61		21.96	23.25	23.16
4H	29.69	*33.39*	*33.39*		23.19	24.39	24.56		22.98	24.27	24.31
	35.8	*39.50*	*39.50*		23.38	24.58	24.65		23.41	24.70	24.65
	36.33	40.03	40.12		23.92	25.12	25.14		24.10	25.39	25.29
	37.08	40.78	40.97		24.13	25.33	25.33		24.68	25.97	25.79
	37.47	41.17	41.35	**4H**	24.27	26.10	26.08		24.98	26.27	26.08
5H	38.39	43.02	42.70		24.82	26.65	26.52		25.58	26.87	26.88
	39.33	43.96	43.64		25.39	27.22	27.06		25.78	27.07	27.06
	39.89	44.52	44.37		25.48	27.31	27.14		26.97	28.26	27.95
	42.12	46.75	46.75		25.74	27.57	27.61		27.28	28.57	28.35
	43.13	47.76	47.87		26.57	*28.40*	*28.40*		27.53	28.82	28.47
	43.66	48.29	48.29		31.56	*33.39*	*33.39*		28.42	29.71	29.40
	45.15	49.78	50.15		31.91	33.74	33.80		29.43	30.72	30.44
	46.49	51.12	51.78		32.54	34.37	34.51		29.66	30.95	30.71
	47.24	51.87	52.32		32.9	34.73	34.85		30.07	31.36	30.98
6H	47.97	56.92	56.50		33.44	35.27	35.46		30.46	31.75	31.41
	49.79	58.74	58.66	**5H**	34.05	37.12	37.40	**5H**	31.23	33.88	34.05
	50.70	59.65	59.45		34.52	37.59	37.69		31.81	34.46	34.49
	51.77	60.72	60.67		35.18	38.25	38.37		34.93	37.58	37.63
	52.24	61.19	61.12		36.43	*39.50*	*39.50*		35.74	38.39	38.38
	52.82	61.77	61.73		41.23	*44.30*	*44.30*		36.64	39.29	39.12
	54.13	63.08	62.94		42.55	45.62	45.71		37.41	40.06	40.04
	56.34	65.29	65.38		42.73	45.8	45.91		37.70	40.35	40.32
7H	56.91	66.31	66.35	**6H**	43.42	47.42	47.05		38.62	41.27	41.24
	57.10	*66.50*	*66.50*		43.80	47.80	47.49		40.42	43.07	43.07
	63.40	*72.80*	*72.80*		44.09	48.09	47.75	**6H**	41.57	*44.30*	*44.30*
	64.27	73.67	73.73		46.90	50.90	50.76		49.16	*51.89*	*51.89*

	64.72	74.12	74.25		47.89	*51.89*	*51.89*		49.68	52.41	52.32
	64.97	74.37	74.67		51.70	*55.70*	*55.70*	**7H**	50.43	55.40	55.53
	65.41	74.81	75.06		51.97	55.97	55.85		50.81	*55.78*	*55.78*
8H	66.56	77.15	77.36	**7H**	52.99	57.69	58.64		57.43	*62.40*	*62.40*
	67.63	78.22	78.28		53.88	58.58	59.33		57.86	62.83	62.76
	68.36	78.95	78.86		55.09	59.79	60.00		58.15	63.12	62.95
	68.81	79.40	79.31		55.63	60.33	60.46	**8H**	59.51	67.15	68.27
	69.80	80.39	80.16		56.02	60.72	60.72		60.08	67.72	68.46
	70.56	81.15	80.83		56.29	60.99	60.80		60.41	68.05	68.68
	70.71	81.30	80.94		57.25	61.95	61.70		60.64	68.28	68.97
	71.19	81.78	81.39		57.70	*62.40*	*62.40*		61.08	68.72	69.17
	72.07	82.66	82.05		60.80	*66.50*	*66.50*		61.35	68.99	69.35
	72.45	83.04	82.38	**8H**	62.83	72.44	72.61		61.62	69.26	69.64
	73.51	84.10	83.47		63.19	*72.80*	*72.80*		62.00	69.64	70.06
	73.74	84.33	83.78		70.33	*79.94*	*79.94*		62.45	70.09	70.63
	74.30	84.89	84.32		71.27	80.88	80.89		63.13	70.77	71.18
	74.53	85.12	84.58		71.56	81.17	81.20		63.31	70.95	71.51
	74.75	85.34	84.86		71.66	81.27	81.30		63.71	71.35	72.03
	75.14	85.73	85.24	**9H**	73.21	82.99	83.39		64.11	71.75	72.36
	75.69	86.28	85.81		73.78	83.56	83.83		64.77	72.41	72.62
9H	76.33	87.57	87.67		74.03	83.81	84.11		65.11	72.75	72.82
	76.87	*88.11*	*88.11*		74.86	84.64	84.86		65.40	73.04	73.03
	80.81	*92.05*	*92.05*		75.30	85.08	85.24		65.79	73.43	73.42
	82.02	93.26	93.27		76.64	86.42	86.50		66.03	73.67	73.72
	83.65	94.89	95.15		77.10	86.88	86.92		66.71	74.35	74.23
	84.57	95.81	96.14		78.38	88.16	88.07		66.91	74.55	74.47
					78.87	88.65	88.55		67.10	74.74	74.68
					79.83	89.61	89.58		67.87	75.51	75.42
					80.82	90.60	90.75		68.13	75.77	75.81
					81.28	91.06	91.06		68.41	76.05	76.29
				10H	81.72	93.09	93.14		68.95	76.59	76.58
					82.38	93.75	93.59	**9H**	69.60	*79.94*	*79.94*

	82.85	94.22	94.27		77.77	*88.11*	*88.11*
	85.12	*96.49*	*96.49*		78.23	88.57	88.51
	89.21	*100.58*	*100.58*	**10H**	79.33	89.57	89.59
	89.27	100.64	100.65		80.98	91.22	91.29
	90.20	101.57	101.72		81.81	*92.05*	*92.05*
	90.50	101.87	102.04		86.25	*96.49*	*96.49*
11H	91.05	103.65	103.63		86.66	96.90	97.01
	91.16	*103.76*	*103.76*		86.89	97.13	97.25
	100.10	*112.70*	*112.70*		87.49	97.73	97.86
				11H	88.76	*100.58*	*100.58*
					91.94	*103.76*	*103.76*
					92.27	104.09	104.13
					93.47	105.29	105.23
					93.58	105.40	105.50
					94.38	106.20	106.29
					95.19	107.01	106.95
					95.54	107.36	107.38
					96.36	108.18	108.16
					97.00	108.82	108.80
					97.33	109.15	108.98

Supplementary Table 4. Selected biostratigraphic events used for preliminary calculation of SR.

	Age (Ma)[1]	HOLE	mbsf	rmcd (this study)	SR (cm/kyr)
HO *Discoaster brouweri**	1.926	C	25	26.12±0.12	1.43
HO *Reticulofenestra pseudoumbilica**	3.700	C	48.9	51.63±0.1	1.44
HO *Discoaster quinqueramus**	5.590	B	83.84	95.24±0.73	2.31
FAD *Globorotalia margaritae***	6.080	C	94.1	106.7±0.1	2.34

[1]Age for the biostratigraphic events are from Gradstein et al. (2012)

* after Shin et al., (1998), Shin (1998), Shafik et al. (1998)

** after Norris (1998).

3.10.2. Cyclostratigraphy and orbital tuning

Following the metronome method of Herbert et al. (1995) we built a cyclostratigraphy by counting of cycles in the Fe data after filtering using a Gaussian band-pass filter (Supplementary Fig. 2). We filtered the Fe record at the eccentricity frequencies with a 30% bandwidth. We started counting eccentricity cycles at the first cycle before the Highest Occurrence (HO) of *Discoaster brouweri* (Shin et al. 1998; Shin, 1998) at 26.12 rmcd. Counting cycles was straightforward for most of the sequence except for the interval between cycle 16 and 24 were amplitudes were smaller. We counted 43 short eccentricity cycles (Supplementary Fig. 2) which correspond to a record of 4.3 Ma, assuming an average duration of 100 kyr.

We preliminary tuned the Fe intensity data to the eccentricity curve La2004 (Laskar et al., 2004) correlating the minima in the eccentricity long cycles, 405 kyr (Laskar et al., 2004) to the minima in the Fe cycles (Supplementary Fig. 3). For fine-tuning we used the sum of normalized Eccentricity, Tilt and Precession (E+T-P) based on La2004 solution (Laskar et al. 2004) as a target curve. Fe maxima were tuned to ETP maxima or Fe minima to ETP minima applying a minimum number of tie-points (Table 3 of main text).

To verify the accuracy of our age model we compared the benthic oxygen isotope record at Site 959 (Norris, 1998) and several other tuned oxygen isotope records of ODP Sites 846, 926, 982 (Shackleton et al., 1995; Shackleton and Crowhurst, 1997; Hodell et al., 2001), and the benthic oxygen isotope stack LR04 (Lisiecki and Raymo, 2005). The heavy Marine Isotope Stages CN6, Si6 and TG20 are well recognised and aligned as are the light Isotope Stages T5 and T7 (terminology after Shackleton et al., 1995). The major stepwise deglaciation from TG14 to TG9 is also recognised. However, resulting ages of Stages TG8 through TG14 are about 50 ka older at Site 959 than at Sites 926 and 982 (Supplementary Fig. 4).

Supplementary figures

Supplementary Figure 1: Core images with Fe intensity data of Site 959A (cores 3-9), 959B (cores 4-11), 959C (cores 4-11) and the Fe splice record (top) over composite depth record (rmcd). Also shown are the tie points used to obtain the splice record.

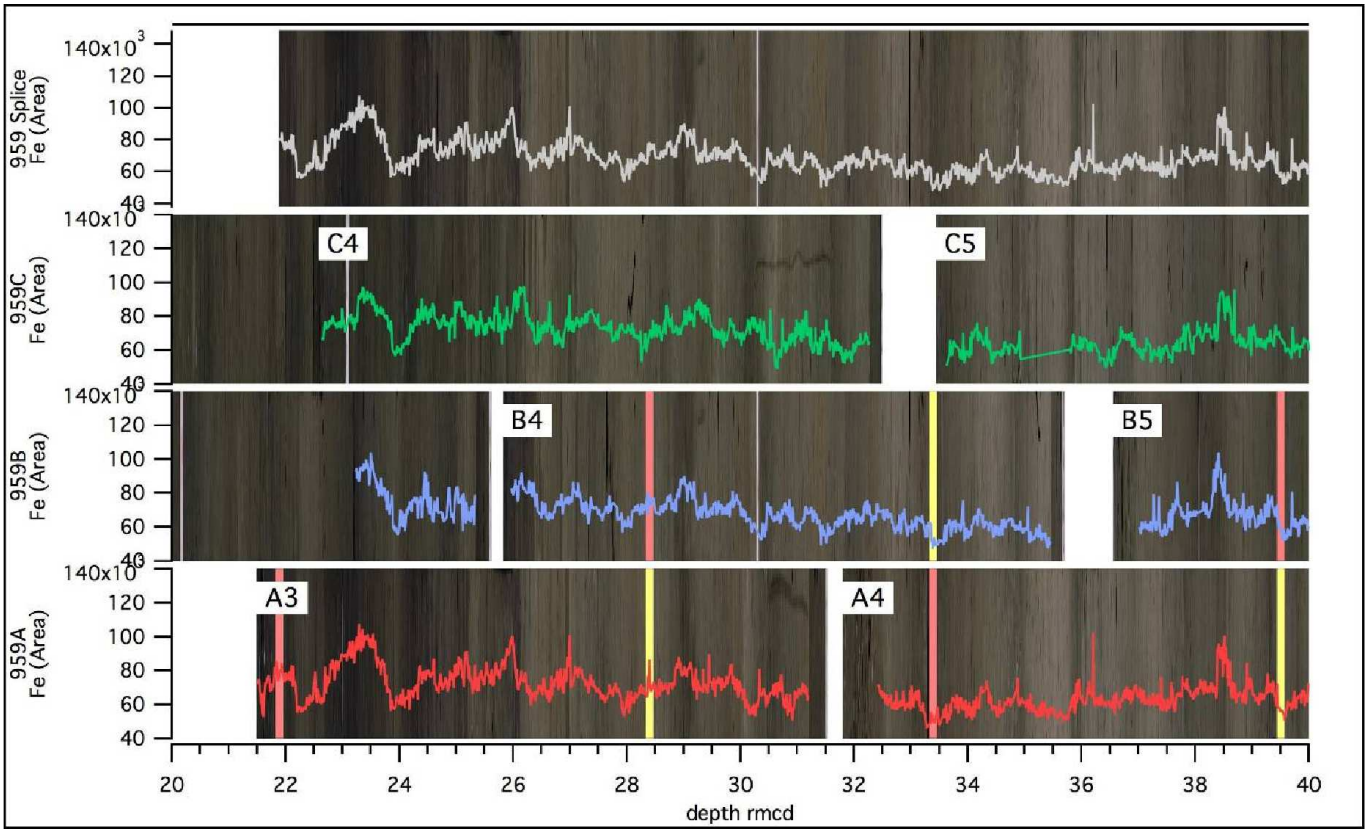

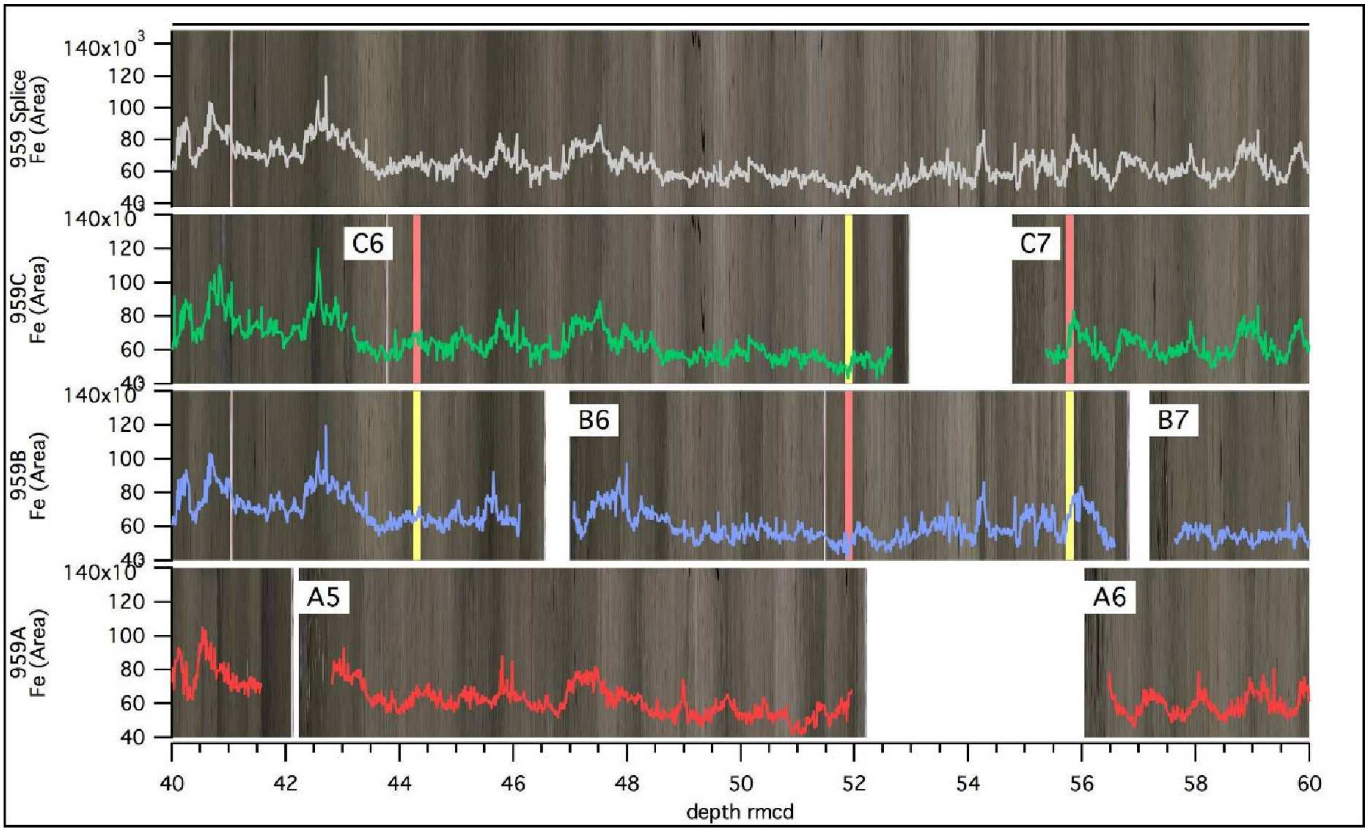
959 Splice Fe (Area)
959C Fe (Area)
959B Fe (Area)
959A Fe (Area)
140x10^3
120
100
80
60
40
C6
C7
B6
B7
A5
A6
40
42
44
46
48
50
52
54
56
58
60
depth rmcd

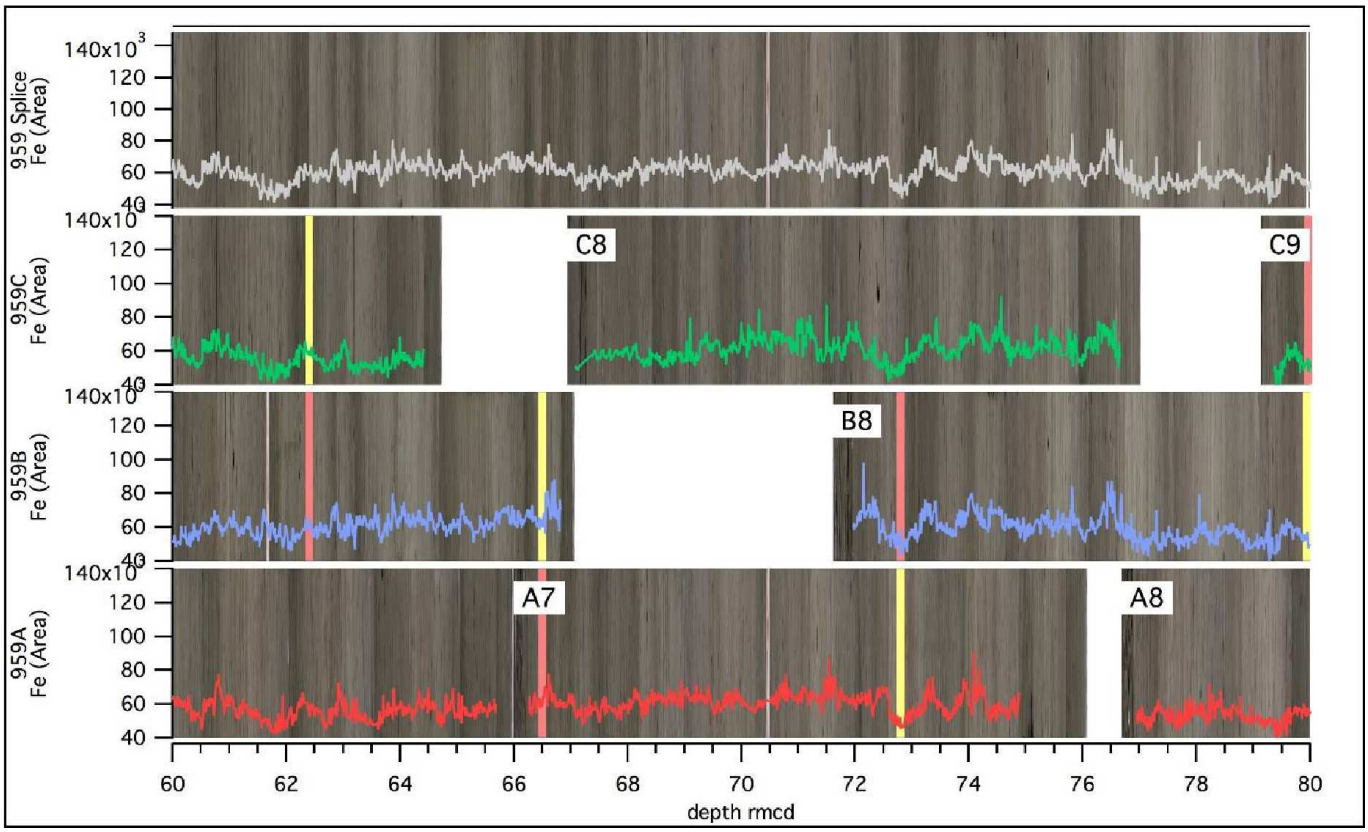
959 Splice Fe (Area)
959C Fe (Area)
959B Fe (Area)
959A Fe (Area)
140x10^3
120
100
80
60
40
C8
C9
B8
A7
A8
60
62
64
66
68
70
72
74
76
78
80
depth rmcd

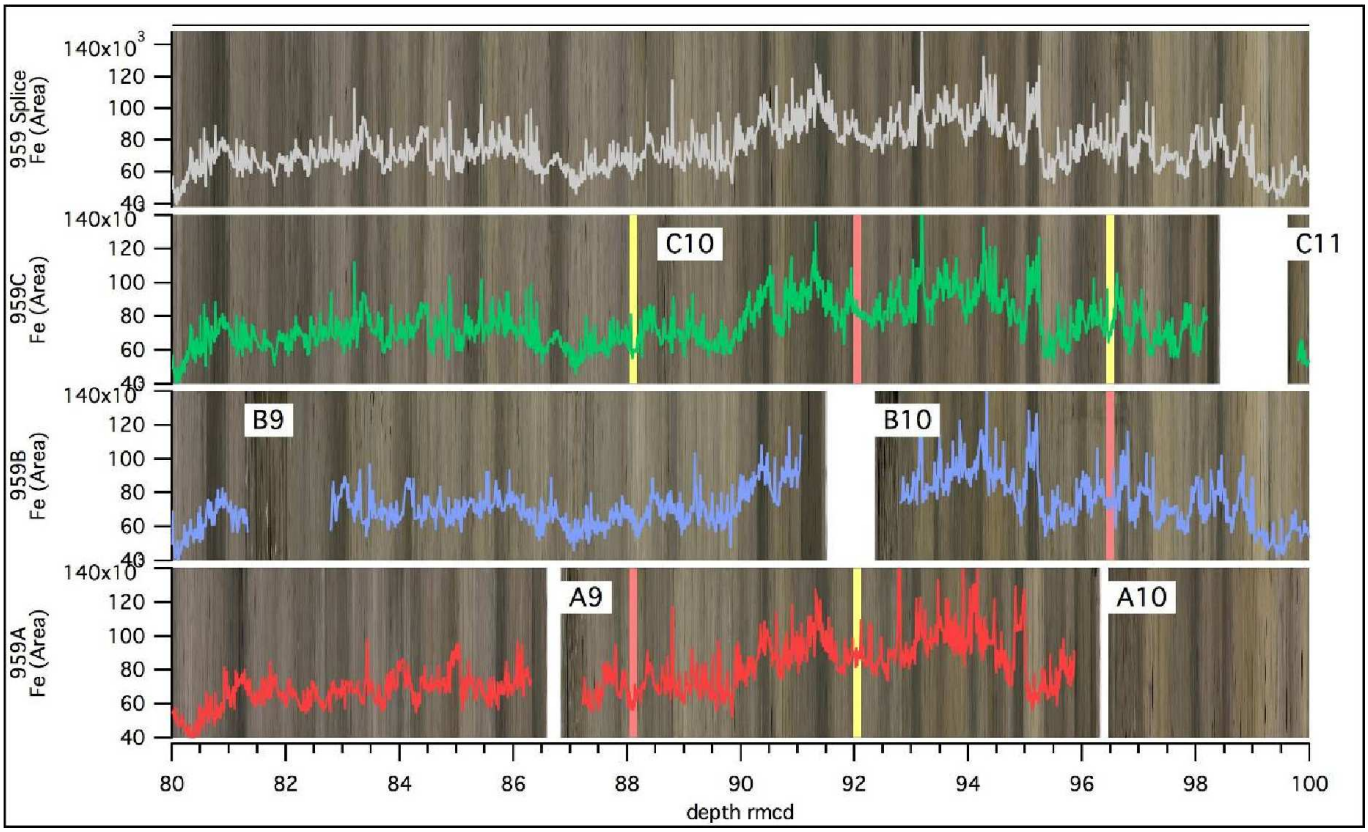
959 Splice Fe (Area)
959C Fe (Area)
959B Fe (Area)
959A Fe (Area)
140x10^3
120
100
80
60
40
C10
C11
B9
B10
A9
A10
80
82
84
86
88
90
92
94
96
98
100
depth rmcd

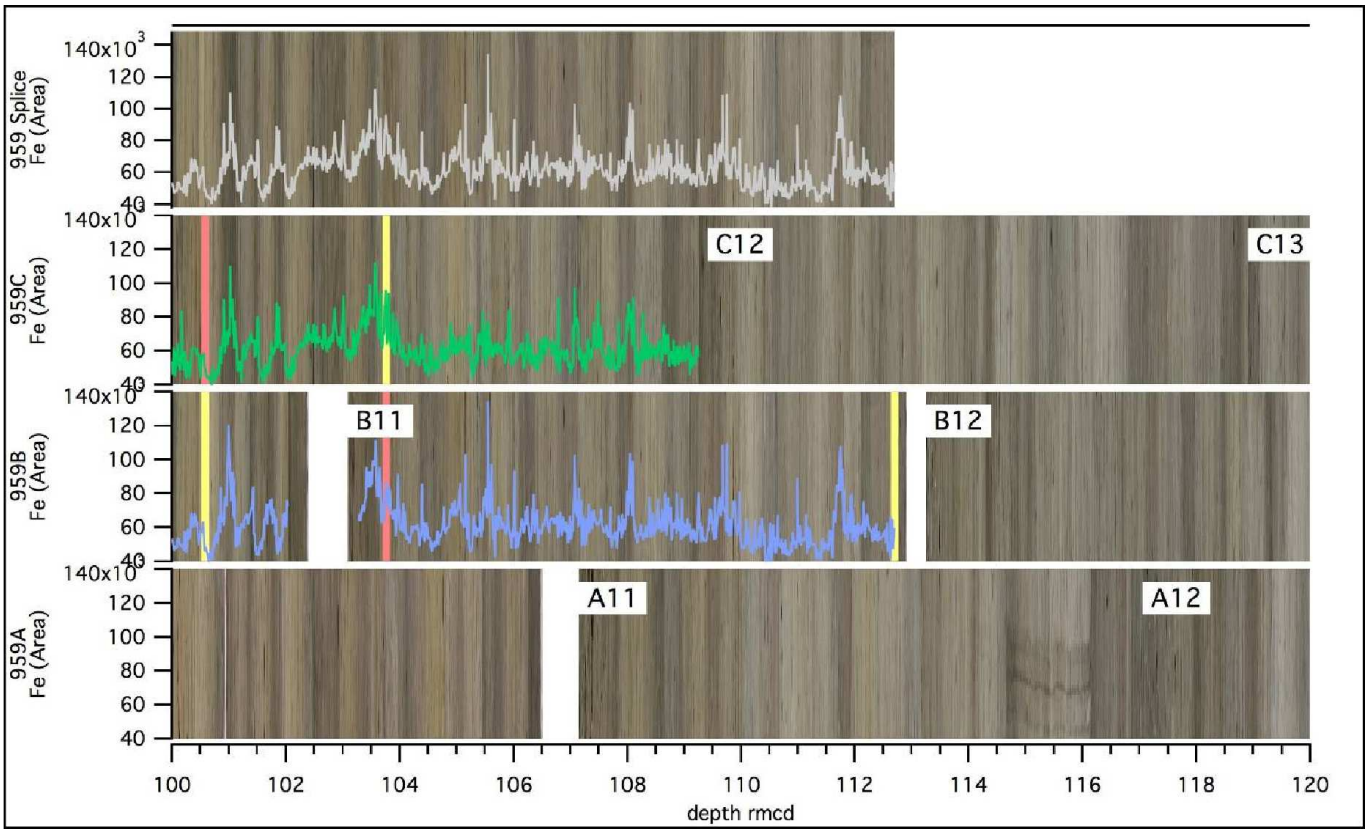
959 Splice Fe (Area)
959C Fe (Area)
959B Fe (Area)
959A Fe (Area)
140x10^3
120
100
80
60
40
C12
C13
B11
B12
A11
A12
100
102
104
106
108
110
112
114
116
118
120
depth rmcd

Supplementary Figure 2. Counting cycles (black numbers) of the Site 959 Fe composite record (rmcd, this study). Fe data (red line) are expressed as number of counts per second. Short eccentricity cycles (green line) have been extracted by Gaussian filter at the frequencies obtained for the three MTM spectra intervals keeping 30% of bandwidth. Analyseries (Paillard et al., 1996) was used for filtering the Fe record.

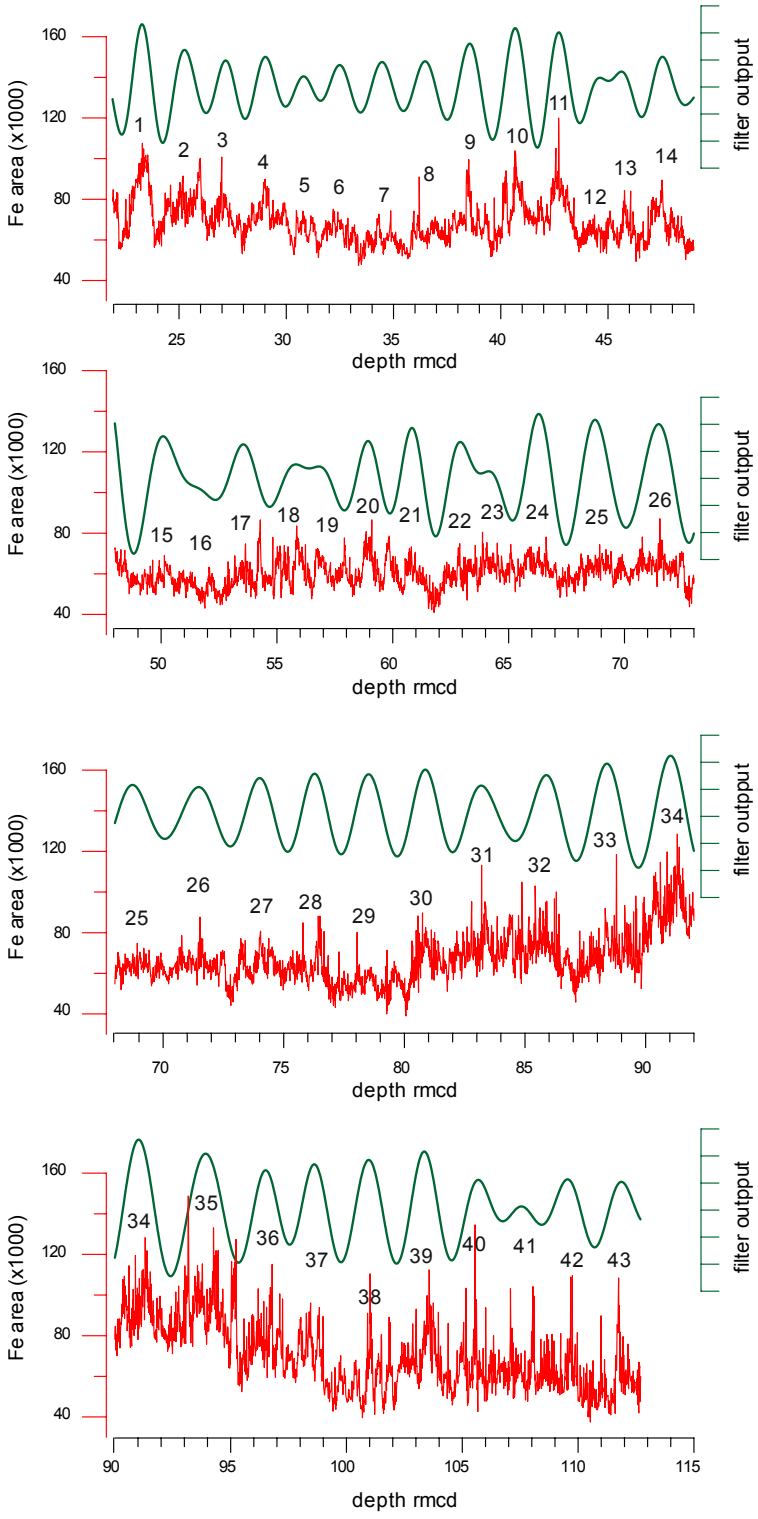

Supplementary Figure 3. Tuned Fe intensity data and Eccentricity curve La2004 (Laskar et al., 2004). Bottom, Site 959 spliced core image on age.

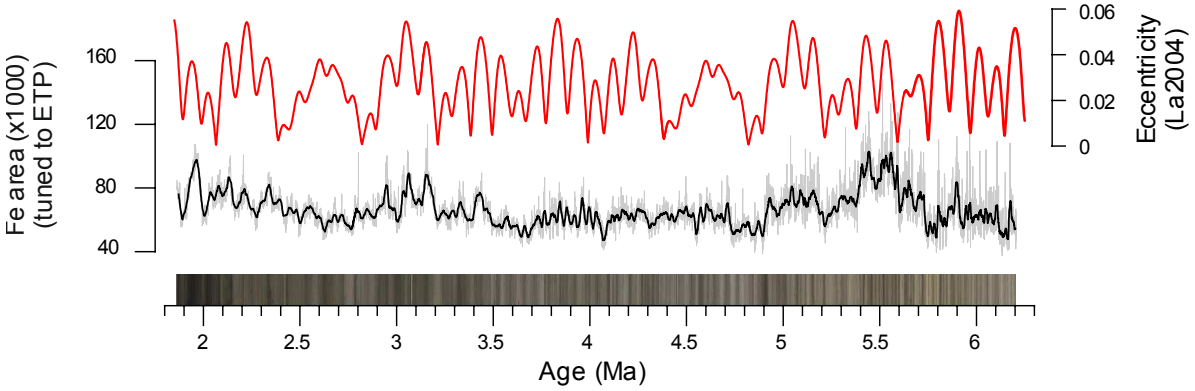

Supplementary Figure 4. Checking ODP Site 959 fine tuned age model by means of comparison between stable isotopes of benthic foraminifers. From top to bottom; $\delta^{18}O$ stack LR04 (Lisiecki and Raymo, 2005), $\delta^{18}O$ of benthic foraminifera of Site 926 (Shackleton and Crowhurst, 1997) using the revised age model of (Zeeden et al., 2013), $\delta^{18}O$ of benthic foraminifera of Site 982 (Hodell et al., 2001), $\delta^{18}O$ of benthic foraminifera of Site 846 (Shackleton et al., 1995), $\delta^{18}O$ of *C. wuellerstorfi* of Site 959 (Norris, 1998) on age of this study. Marine isotope stage terminology after Shackleton et al. (1995). Records align within 0.01 Ma but for the period between 5.7 and 5.4 Ma, where our age model results in 0.05 Ma older ages for Stages TG8 through TG14 compared to those of Sites 926 and 846. The age model of Site 982 results in a younger age for Stage TG8.

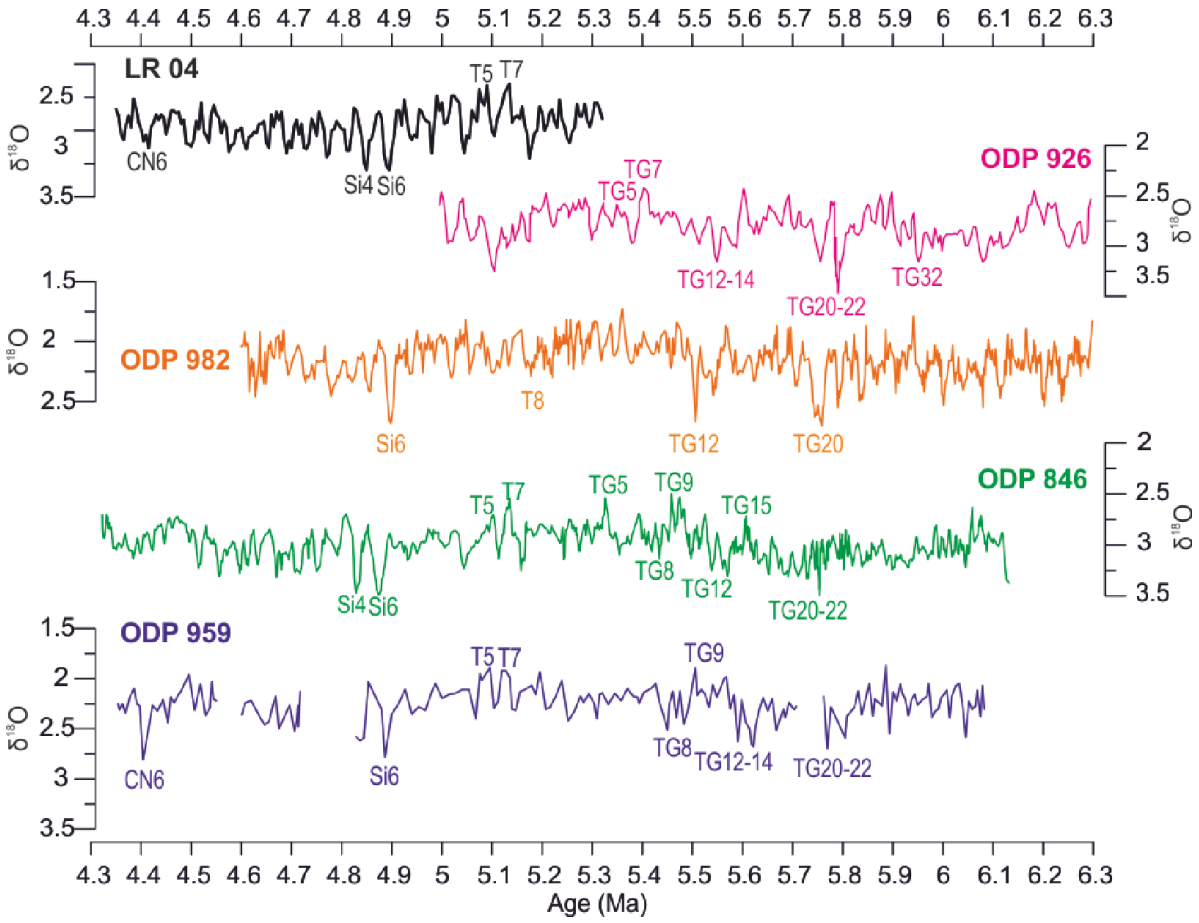

Supplementary Figure 5. From top to bottom; ln(Ti/Al) ratio, squared deviation from the mean value over the studied interval (31-point running mean), E+T-P curve, precession, obliquity, and squared deviation from the mean (7-point running mean). Insolation curves after (Laskar et al. 2004). Stronger seasonality is suggested by the squared deviation from the mean value of the ln(Ti/Al) and would have occurred between 5.8 and 5.5 Ma, between 5.3 and 5.2 Ma and increased after 3.2 Ma.

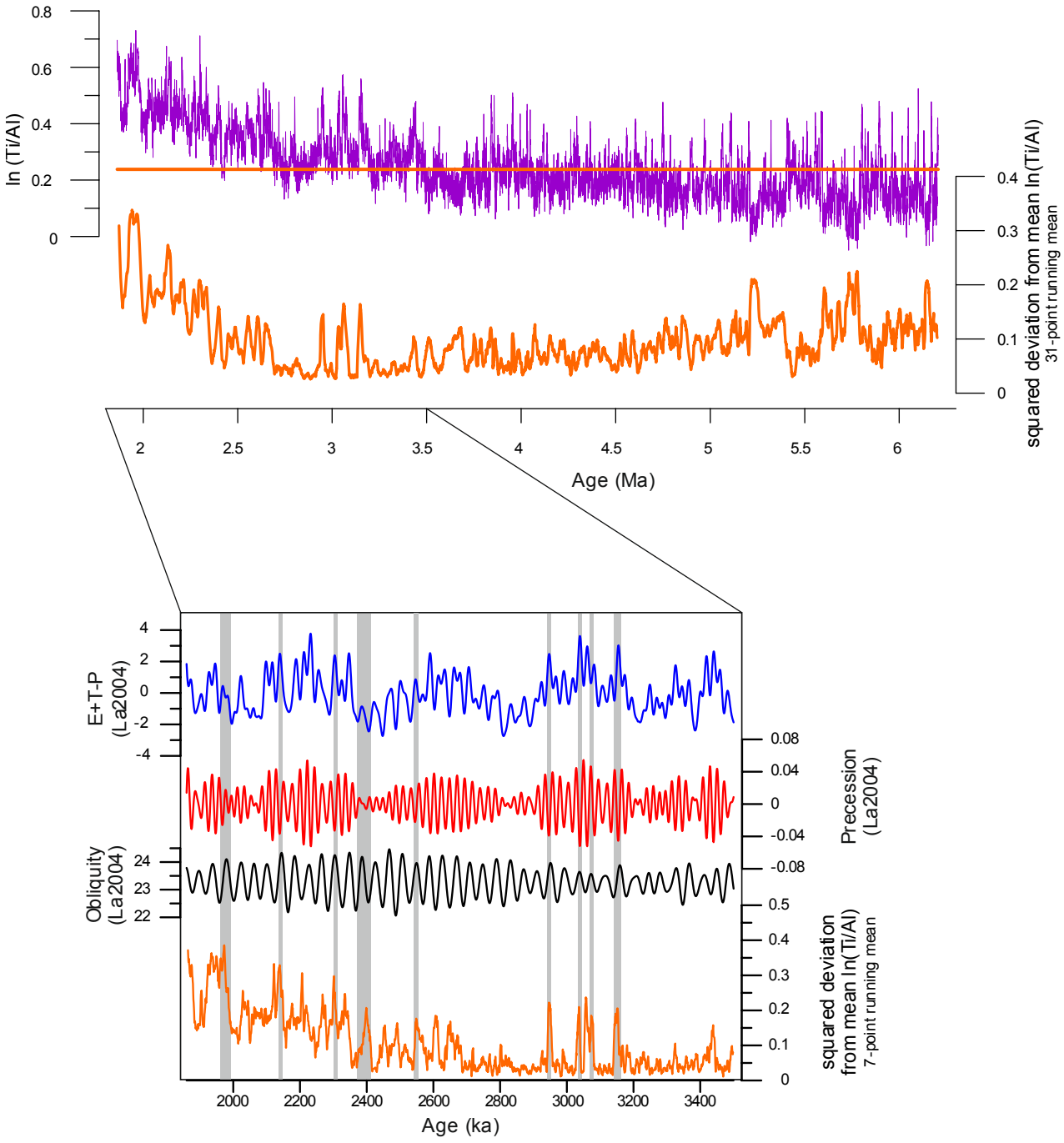

Chapter 4

Pliocene land-sea interactions in the east equatorial Atlantic (Gulf of Guinea): link between upwelling and aridity

F. Vallé[1], S. De Schepper[2], L.M.Dupont[1]*

[1] MARUM-Center for Marine Environmental Sciences, University of Bremen, [2]Uni Research Climate, Bjerknes Centre for Climate Research and Department of Earth Science, University of Bergen

In preparation

4.1 Abstract

Pliocene environmental and paleoceanographic changes in east equatorial Atlantic are investigated by means of marine palynology. The organic-walled dinoflagellate cyst record from ODP Site 959 shows differences between early Pliocene and late Pliocene in surface water productivity and temperature of the Gulf of Guinea. Upwelling was reduced in the early Pliocene before the Guinea Current was fully established. Warmer waters are suggested by the presence of the extinct genus *Batiacasphaera*. During the late Pliocene several upwelling intervals are recorded. Comparison between the Site 959 dinoflagellate cyst record and the late Pliocene vegetation development in northwest Africa suggest a link between upwelling events along the Ghanaian coast and arid phases in West Africa. Increased transport of neritic dinoflagellate taxa to the deep-sea Site 959 compared with terrestrial palynomorph records could be associated to sea level changes corresponding to major Pliocene glaciation events.

4.2 Introduction

Pliocene climate was generally warmer than today with high atmospheric carbon dioxide concentrations (e.g. Seki et al. 2010; Pagani et al. 2010; Martinez-Boti et al. 2015).Global climate underwent a gradual cooling trend from the Miocene towards the Quaternary and global sea surface temperatures gradually decreased since the Early Pliocene (c. 4.0 Ma) (Fedorov et al 2013). Also, four global glaciation events have been recognised in the Early and Late Pliocene, well before the intensification of the Northern Hemisphere Glaciations at ~2.75 Ma (De Schepper et al. 2014). Tropical climate was also quite different (Brierley et al., 2009). During the early Pliocene, the equatorial-subtropic sea surface temperature (SST) gradient was reduced together with reduced upwelling in the eastern equatorial oceans and this was coupled to a weaker atmospheric circulation (Fedorov et al. 2013). During the early Pliocene, the reduced equatorial-subtropical gradient, weakened the atmospheric circulation (Fedorov et al. 2013) and increased precipitation in tropical west and east Africa (Brierley et al. 2009) allowed an expansion of tropical rain forests and savannah, as suggested by pollen records from Niger Delta (Morley, 2000). A sedimentological record from Lake Chad indicates the presence of a freshwater lake and a

Sudanian-like climate between 6.4 and 2.3 Ma (Moussa et al., 2016). Results from both modelling experiments and pollen records suggested an expansion of the woodland into arid regions during the mid-Pliocene (Salzmann et al. 2008).

Pliocene changes of surface hydrography in the north equatorial Atlantic and of the thermocline depth in the Gulf of Guinea, including the permanent establishment of the Guinea Current, have been inferred from oxygen and carbon isotope records (Norris, 1998; Billups et al. 1999). Those changes implied a latitudinal shift of the Intertropical Convergence Zone (ITCZ) and associated changes in strength of the trade winds (Norris, 1998; Billups et al., 1999), both important characteristics of African climate. East South Atlantic SST records along the Namibian coast suggested that the Benguela upwelling system started 3.2 Ma, in association to increased trade winds activity (Marlow et al. 2000, Rosell-Melé et al. 2014).

Dinoflagellate cyst assemblages in surface sediments are a useful tool for environmental reconstructions because they reflect conditions in the surface waters (e.g. productivity) where their motile forms live (Radi et al. 2007; Holzwarth et al., 2010; Zonneveld et al. 2013). They can also be used to interpret deep-water mass ventilation changes (Zonneveld et al. 2010) and inform about transport processes (Holzwarth et al., 2010). Studies on the modern biogeographic distribution of dinoflagellate and environmental parameters characterizing the surface waters (e.g. Marret, 1994; Marret and Zonneveld 2003; Zonneveld et al. 2013; Holzwarth et al. 2010) aid the paleoecological interpretation of extant dinoflagellate species (Holzwarth et al. 2010, De Schepper et al. 2011) and palaeoenvironmental reconstruction (e.g. Head and Westphal, 1999;. De Schepper et al. 2009; De Schepper et al., 2013). Comparison between dinoflagellate cyst and pollen results allow establishing land-sea connections (Dupont et al., 1998; Dupont et al., 1999).

Pliocene dinoflagellate cyst records have been used to document palaeoclimate and hydrographical changes in the North Atlantic (De Schepper et al. 2009, De Schepper et al. 2013) However, only a single Pliocene dinoflagellate cyst record is available for the east equatorial North Atlantic (Durugbo et al. 2011). We present a new Pliocene dinoflagellate cyst record for the east equatorial Atlantic Ocean Drilling Program (ODP) Site 959 between 4.94 and 4.56 Ma and between 3.92 and 2.96 Ma, after the Guinea Current was established in the Gulf of Guinea (Norris, 1998). By comparing dinoflagellate results with terrestrial proxies we discuss changes in surface waters and upwelling in terms of changes within the Gulf of Guinea and place them in the global Pliocene environmental and climate evolution of West Africa and the east equatorial Atlantic.

4.3. Modern regional environmental setting

4.3.1 Climate and atmospheric setting

Climate over tropical West Africa is controlled by monsoon circulation and trade winds (NE and SE). Both are linked to the seasonal latitudinal migration of the Intertropical Convergence Zone (ITCZ) (Figure 1). The ITCZ migrates between about 2°N and 12°N over the eastern equatorial Atlantic and between 8°N and 24°N over the continent (Nicholson and Grist, 2003). During boreal summer, the ITCZ reaches its northernmost position between July and September. The SE trade winds grow more intense over the Gulf of Guinea and become the SW monsoon system that influences the West African continent (Leroux, 1983). During boreal winter when the ITCZ is at its

southernmost position, the enhanced NE trade winds and the dry Harmattan (Kalu, 1979; Trauth et al. 2009) reach over the Gulf of Guinea, carrying dust particles and terrestrial palynomorphs mostly coming from the NE part of the Saharan desert and the Sahel zone (Kalu, 1979, Sarnthein, 1981).

4.3.2 Oceanography

The main surface and subsurface currents flowing in the eastern tropical Atlantic and Guinea Gulf are shown in Figure1. The Guinea Current (GC) is a coastal current which transports low-saline, warm waters towards the east and overlies the Equatorial Undercurrent (EUC). The eastward flowing EUC is a subsurface current that carries cool and highly saline waters into the Gulf of Guinea, making the thermocline beneath the Guinea Current particularly intense (Hisard and Merle 1980). The North Equatorial Counter Current (NECC), which is more intense during summer, feeds the Guinea Current (Hisard and Merle 1980; Norris, 1998). An important westward current is the South Equatorial Current (SEC) which brings warm waters towards the Brazilian Coast and influences the countercurrent system (Hisard and Merle, 1980). During boreal summer, when ITCZ is at its northern position, the combined action of enhanced SE trade winds and stronger NECC strengthens the Guinea Current (Figure 1) and shoals of the thermocline allowing the EUC to bring cool waters in the Gulf of Guinea (Verstraete, 1992). SSTs in the Gulf of Guinea fluctuate seasonally between 24°C (summer) and 30 °C (winter) (Figure 1).

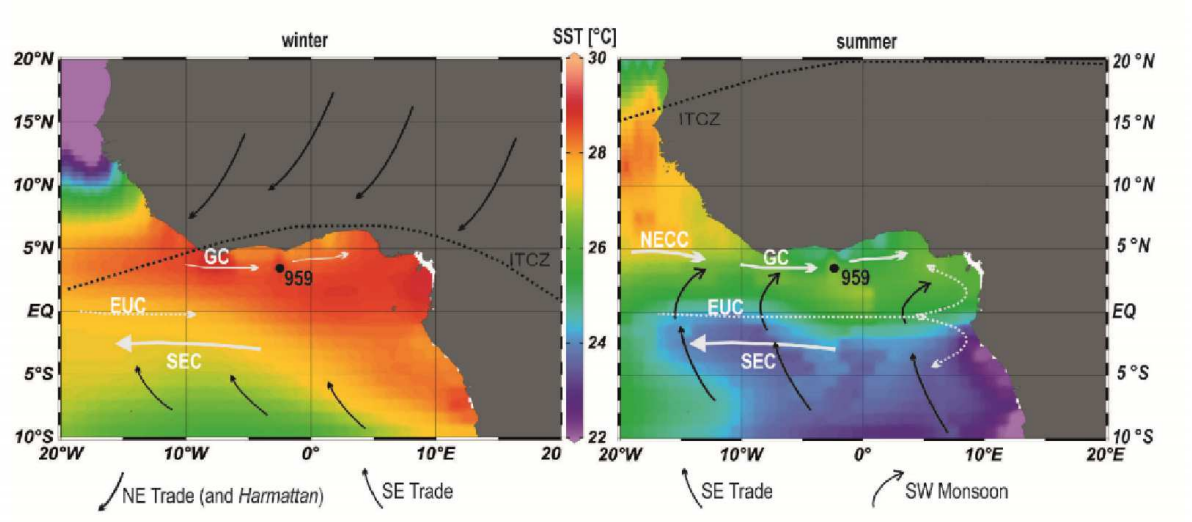

Figure 14: Maps of the study area showing the average position of the ITCZ, the associated wind systems (black arrows), sea surface temperatures (Ocean Data View, U.S. NODC World Ocean Atlas 2009) and surface (white continuous arrows) subsurface currents (dashed arrow) (after Norris, 1998) during boreal winter and boreal summer. GC=Guinea Current; NECC= North Equatorial Countercurrent; EUC=Equatorial Undercurrent; SEC=South Equatorial Current; Location of ODP Site 959 is indicated by the black dot.

4.3.3 Present distribution of dinoflagellate cyst taxa

The modern biogeographical distribution of dinoflagellate cysts in the surface sediments is mainly controlled by the prevailing surface water parameters (temperature, salinity, nutrients), but also

preservation and transport (e.g. Marret and Zonneveld, 2003, Zonneveld et al. 2013). In the Gulf of Guinea, the dinoflagellate cyst assemblages in surface sediments are mainly correlated with water depth and sea-surface salinity, rather than SSTs (Marret, 1994). Sediment surface samples assemblages are dominated by *Brigantedinium*, *Spiniferites delicatus* and *Lingulodinium machaerophorum* (Marret, 1994). *Brigantedinium,* which groups all round brown cysts, is a cosmopolitan taxon (Marret and Zonneveld, 2003) that generally has higher relative abundances in nutrient-rich surface waters characteristic of upwelling zones (Marret, 1994; Marret and Zonneveld, 2003). High percentages of *S. delicatus* are associated with upwelling (Marret, 1994). *L. machaerophorum* is characteristic of low salinity surface waters and can be considered an indicator for river discharge (Marret 1994; Holzwart et al. 2010). It also shows highest relative abundances near active upwelling cells, especially during upwelling relaxation, when water masses are already stratified but still preserve high-nutrient levels (Marret and Zonneveld, 2003; Zonneveld et al. 2013). Next to these dominant taxa, typical tropical species like *Operculodinium israelianum*, *Tuberculodinium vancampoae* and *Polysphaeridium zoharyi* occur in the Gulf of Guinea. These last three taxa are often considered to indicate estuarine environments (Morzadec-Kerfourn, 1992). *Selenopemphix nephroides* and *S. quanta*, reported as inner to outer-neritic species, are also found but with low relative abundances (Marret, 1994). The highest dinoflagellate cyst concentrations (> 10,000 cysts per ml) within the Gulf of Guinea are found off the Ghanaian coast, where seasonal upwelling occurs (Marret, 1994). Finally, *Impagidinium* spp. and *Nematosphaeropsis labyrinthus*, indicators of oceanic conditions (Zonneveld et al. 2013), have also been recorded in the Gulf of Guinea.

4.4. Material and methods

4.4.1 Materials

Site 959 was drilled on a shoulder of the Deep Ivorian Basin at 3°37'N, 2°44 W and 2100 m water depth (Mascle et al., 1996) (Figure 1). Because of its location Site 959 should not be subjected to mass gravitational flow from the Ghanaian slope (Giresse et al. 1998). Pliocene sections consist of bioturbated nannofossil and foraminifer oozes with clay and chalk (Mascle et al., 1996). Site 959 is located at the depth of the upper mixing zone between the North Atlantic Deep Water (NADW) and the intermediate water masses. It is thus subject to changes of different deep-water masses and the thermohaline circulation (Billups et al. 1999, Giresse et al., 1998).

Material was collected from the Pliocene parts of ODP Site 959 Holes A, B and C based on the composite depth record (meter composite depth, mcd) obtained by correlation of high-resolution element intensities (Vallè et al., submitted to IJES). The ODP Site 959 age model for the Pliocene has been obtained by astronomical tuning of the Fe intensities, measured by XRF scanning, to the Eccentricity-Tilt-Precession (ETP) target curve (Vallé et al., submitted to IJES). A total of 41 samples were taken: 20 samples from the Zanclean Stage at the intervals 4.94–4.56 Ma (from 81.43 to 73.05 mcd), and 3.92–3.66 Ma (from 57.96 to 51.98 mcd), and 21 samples from the Piacenzian Stage between 3.59 and 2.96 Ma, (from 50.73 to 38.76 mcd).

4.4.2 Methods

4.4.2.1 Palynological methods

The 41 samples were processed using a standard palynological treatment with cold HCl (~10%) to decalcify the sediment, followed by cold HF (~ 40%) to dissolve silicates. After two days of HF treatment, residues were neutralized by water washing. No KOH was added. Residuals have been ultrasonic sieved on a 8µm mesh to reduce the clay fraction. The residue is stored in water and mounted on a slide using glycerine jelly and sealed with nail polish. Several slides per sample were counted under a light microscope at 400× magnification to a minimum of 50 dinocysts.

To calculate concentration values, sample volume was measured by water displacement and two tablets containing exotic *Lycopodium clavatum* spores were added at the beginning during the decalcification step. Accumulation rates of individual taxa, groups and total cysts (cysts*cm^{-2}*kyr^{-1}) were calculated by multiplying concentration values with calculated sedimentation rates. Pollen and spores were counted in the same slides as dinoflagellate cysts. Since the numbers of terrestrial palynomorphs did not exceed 50 in most of the samples, we only use the total pollen and spores accumulation rates as indicator of continental input.

The identification of dinocysts was based on published morphological descriptions from Head et al. (1989), Head (1997), Head and Westphal (1999), De Schepper and Head (2009), Warny and Wrenn (1997), Schreck et al. (2012, 2013), Morzadec-Kerfourn, (1992), McMinn (1992); nomenclature is after Fensome et al. (2008) and Paez-Reyes and Head, (2013).

Resistant cyst and sensitive cyst accumulation rates have been calculated in order to estimate dinocyst preservation after deposition (Versteegh and Zonneveld, 2002) and as an indication of productivity (Versteegh and Zonneveld, 2002; Zonneveld et al., 2010). The Protoperidinioid (P) over Protoperidinioid plus Gonyaulacoid (G) ratios have been calculated to obtain an indication of surface water nutrients richness. Moreover, the neritic (N) over neritic plus oceanic (O) cyst ratio (N/O index) has been calculated to gain information about transport from the neritic to the oceanic environment.

4.4.2.2 Numerical analysis

Subdivision of the entire dinoflagellate cyst record was calculated by stratigraphically constrained cluster analysis CONISS (Grimm, 1987) with Tilia software 2.0.2 (Grimm, 2004). We ran the analysis on the relative abundances of all taxa after square root transformations. A preliminary Detrended Correspondence analysis indicated that a linear response could be assumed between the dinoflagellate data and the ecological gradients. We conducted a principal component analysis (PCA) using a dispersion matrix on the dinoflagellate cyst percentage data to explore the relationship between dinoflagellate cyst species and samples throughout the time studied. We ran the PCA on 22 selected taxa occurring at least twice and grouped together *Achomosphaera/Spiniferites* spp., *Impagidinium* spp. and *Selenopemphix* spp. (Table 1). Abundance data were pre-transformed with Hellinger transformation (Borcard et al., 2011). DCA and PCA have been performed with the Vegan package (Oksanen et al., 2015) using R software (R Development Core Team, 2008).

4.5. Results

4.5.1 Pliocene dinocyst assemblages, zonation and accumulation rates

In total, 42 dinoflagellate cyst taxa have been identified in the Pliocene sediments of ODP Site 959 (Table 1).

Table 1. Identified organic-walled dinoflagellate cyst taxa.

Brigantedinium spp.	protoperidinioid
Ataxiodinium confusum	gonyaulacoid
Barssidinium pliocenicum	protoperidinioid
Batiacasphaera micropapillata	gonyaulacoid
Batiacasphaera hirsuta	gonyaulacoid
Batiacasphaera sphaerica	gonyaulacoid
Bitectatodinium sp.	gonyaulacoid
Capisocysta sp.	gonyaulacoid
Corrudinium harlandii	gonyaulacoid
Dubridinium sp.	protoperidinioid
Echinidinium sp.	protoperidinioid
Edwardsiella sexispinosa	gonyaulacoid
Hystrichokolpoma rigaudiae	gonyaulacoid
Invertocysta lacrymosa	gonyaulacoid
Lingulodinium machaerophorum	gonyaulacoid
Nematosphaeropsis sp.	gonyaulacoid
Nematosphaeropsis labyrinthus	gonyaulacoid
Nematosphaeropsis lativittata	gonyaulacoid
Nematosphaeropsis cf. rigida	gonyaulacoid
Operculodinium israelianum	gonyaulacoid
Operculodinium janduchenei	gonyaulacoid
Cysts *of Protoceratium reticulatum* (Paez-Reyes and Head, 2013)	gonyaulacoid
Operculodinium sp.	gonyaulacoid
Pyxidinopsis reticulata	gonyaulacoid
Polysphaeridium zoharyi	gonyaulacoid
Tectatodinium pellitum	gonyaulacoid
Trinovantedinium sp.	protoperidinioid
Tuberculodinium vancampoae	gonyaulacoid
Dapsilidinium pseudocolligerum	gonyaulacoid
Dinocyst taxa grouped	
***Achomosphaera/Spiniferites* spp.**	gonyaulacoid
Achomosphaera spp.	
Spiniferites mirabilis	
Spiniferites ramosus	
Spiniferites spp.	
***Impagidinium* spp.**	gonyaulacoid

Impagidinium aculeatum	
Impagidinium patulum	
Impagidinium paradoxum	
Impagidinium sp.	
***Selenopemphix* spp.**	protoperidinioid
Selenopemphix brevispinosa	
Selenopemphix cf. undulata	
Selenopemphix nephroides	
Selenopemphix quanta	
Selenopemphix sp.	

The relative abundance of 22 selected or grouped taxa on which we ran PCA analysis are presented in Figure 2 and Table 2, and their absolute accumulation rates are shown in Figure 3. The Pliocene dinoflagellate cyst assemblages are alternatively dominated by *Brigantedinium* spp. and *Achomosphaera/Spiniferites* spp. in association with typical tropical water species (Figure 2). The entire studied interval has been divided in seven zones using CONISS. Zones are called "Ep" for Early Pliocene and "Lp" Late Pliocene.

Ep 1, 4.94–4.85 Ma. This zone is distinct due to the high percentage of *L. machaerophorum* and relatively low percentage of *Brigantedinium* and *Achomosphaera/Spiniferites* spp. *B hirsuta* shows also relatively high percentages (~10%) which increase towards the top of the zone (Figure 2). At 4.91 Ma, the highest percentage of *L. machaerophorum* corresponds to the highest peak of total dinocyst accumulation in the entire record with $7.9*10^3$ cysts*cm^{-2}*kyr^{-1} and all taxa show high accumulation rates (Figure 3).

Ep 2, 4.85–4.68 Ma. The beginning of the zone shows the presence of *N. labyrinthus* and relative high percentages of *Impagidinium* spp., taxa that today have affinity for oceanic environments (e.g. Zonneveld et al. 2013). *B. hirsuta* shows its percentage maximum. Percentages of these three taxa decrease afterwards whereas two peaks of *Achomosphaera/Spiniferites* spp. occurred interrupted by a maximum of *Brigantedinium* spp. (Figure 2). In the upper part of this zone, *P. zoharyi* and *T. vancampoae* occur in low percentages, and *T. vancampoae* has a relatively high accumulation rate that is slightly lower than the maximum in the previous zone (Figure 3). *Operculodinium* species are generally not abundant, but *O. israelianum* shows two peaks. The total dinocyst accumulation rates decrease.

Ep 3: 4.68–4.56 Ma. In this zone, *Brigantedinium* spp. becomes dominant whereas *Achomosphaera/Spiniferites* spp. decreases. There is a slight increase of *Selenopemphix* spp. and a decrease of relative abundances of *B. hirsuta*, which disappears completely from the record at the end of this zone. At the end of the zone *B. micropapillata* has a single peak up to 30% of the total assemblage. The accumulation rate of this zone remains almost constant, with a mean value of $1.2*10^3$ cysts*cm^{-2}*kyr^{-1} (Figure 3).

Ep 4: 3.92–3.59 Ma. For most of the zone *Brigantedinium* spp. shows relative abundances higher than 35%. In contrast, *Achomosphaera/Spiniferites* spp. shows its lowest percentages of the entire record. *Selenopemphix* spp. increases from the beginning of the zone reaching their highest values

of ~20%. An increasing trend in relative abundances is also shown in cysts of *Protoceratium reticulatum* (Figure 2). *Impagidinium* show a decreasing trend from 12% to 2%. *P. zoharyi* shows two small peaks at the beginning of the zone and at 3.72 Ma. *Invertocysta lacrymosa* shows two distinct peaks, one at the base and one at the top of the zone. *L. machaerophorum* is present in very low relative abundances only.

Lp 1: 3.59–3.47 Ma. During this interval, the *Achomosphaera/Spiniferites* spp. curve reaches its highest percentage (60%) and highest accumulation rate over the studied interval. In contrast, *Brigantedinium* spp. shows its lowest relative abundances. *Selenopemphix* spp. percentages decreased abruptly and remained low. This zone is marked also by two peaks of *P. zoharyi* interrupted by a peak of. *L. machaerophorum*. At the end of the zone there are peaks of percentages and accumulation rates of *I. lacrymosa* and *Capisocysta* sp. Total dinocyst accumulation rates reach the highest values of the sequence apart from the first peak in the early Pliocene zone.

Lp 2: 3.47–3.22 Ma. This zone is characterized by two peaks of *Brigantedinium* spp. before its decline at the end of the zone, alternated by two peaks of *Achomosphaera/Spiniferites* spp. *Selenopemphix* spp. show low percentages throughout the zone with a small increase towards the top of the zone. At around 3.35 Ma *Brigantedinium* spp., *Impagidinium* spp., *N. labyrinthus* show high accumulation rates. At the end of the zone *L. machaerophorum* shows a percentage maximum.

Lp 3: 3.22–2.96 Ma. Brigantedinium spp. show increasing percentages and do not drop below 20%. *Selenopemphix* spp. shows almost constant relative abundances around 5%. *Achomosphaera/Spiniferites* spp. show approximately constant percentage values and accumulation rates. Between 3.16 and 3.07 Ma, increase of relative abundances of *Operculodinium* species (Figure 2) and their accumulation rates, especially of *O. israelianum*, correspond to increasing values of total dinocyst accumulation rates (Figure 3). At the end of the zone, *Impagidinium* spp. shows a peak.

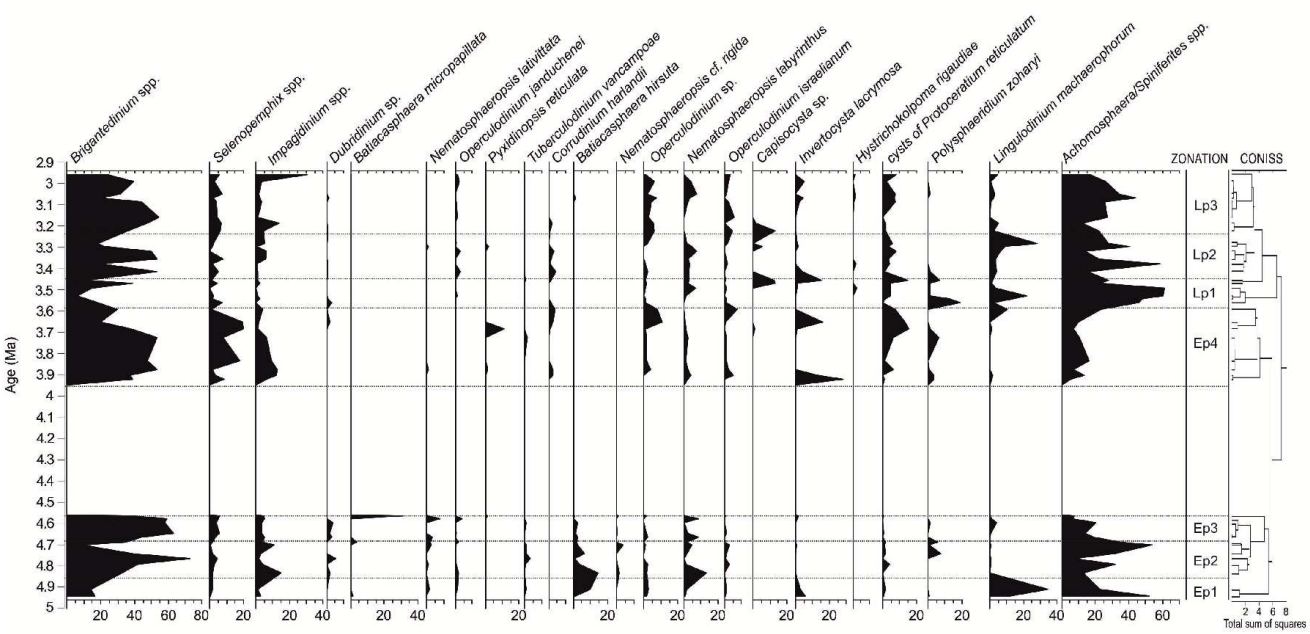

Figure 2: Relative abundances (%) of 22 dinoflagellate cysts plotted against age. Zonation is based on CONISS (Grimm, 1987). Dinocysts taxa are ordered according to PC1, from more positive to negative scores.

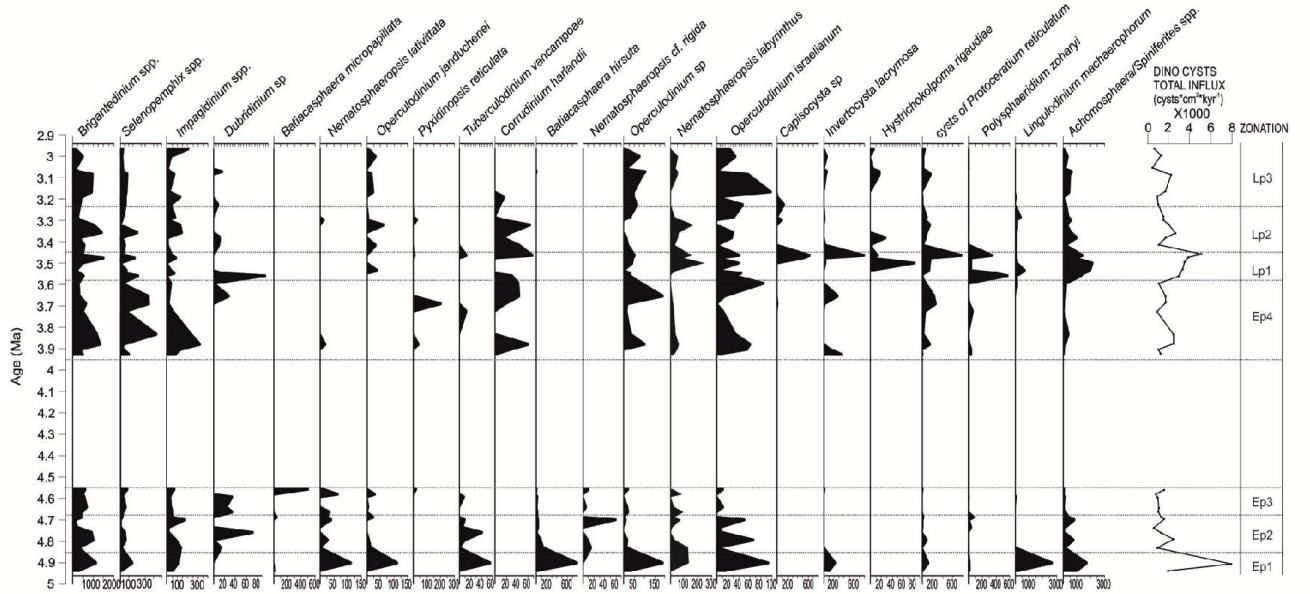

Figure 3: Accumulation rates of 22 taxa and total dinocysts accumulation rates. Dinocysts taxa are ordered according to PC1, from more positive to negative scores. Note the scale is different.

4.5.2 Accumulation rates of resistant and sensitive cysts, P/G ratios

Dinoflagellate cysts can be selectively degraded by oxygen-rich water masses at the water-sediment layer, especially when sedimentation rates are low (Versteegh and Zonneveld, 2002). We calculated accumulation rates of resistant (R) and sensitive (S) dinoflagellate considering *Impagidinium* spp., *N. labyrinthus,* cysts of *P. reticulatum* as resistant taxa and *Echinidinium* sp., *Brigantedinium* spp., *Selenopemphix* spp. as sensitive taxa (Versteegh and Zonneveld, 2002) (Figure 4). High accumulation rates of sensitive dinoflagellate cysts indicate that throughout the studied sequence, there are ten intervals where preservation is good. Protoperidinioid (P) and Gonyaulacoid (G) taxa considered for the P/G ratios are indicated in Table 1. During intervals of good preservation, Protoperidinioid (P) cysts dominate over Gonyaulacoid (G) cysts (Figure 4, pale yellow rectangles) except for the interval around 4.91 Ma (dark yellow rectangle in Figure 4). The resistant cyst accumulation rate, sometimes used as productivity proxy (e.g. Versteegh and Zonneveld, 2002; Zonneveld et al., 2010), shows a gradual decline during the early Pliocene, while the sensitive cyst accumulation rates show stronger variability. From 3.9 to 3.56 Ma both R and S accumulation rates show similar fluctuations. Sensitive accumulation rates fluctuate but never reach values of zero.

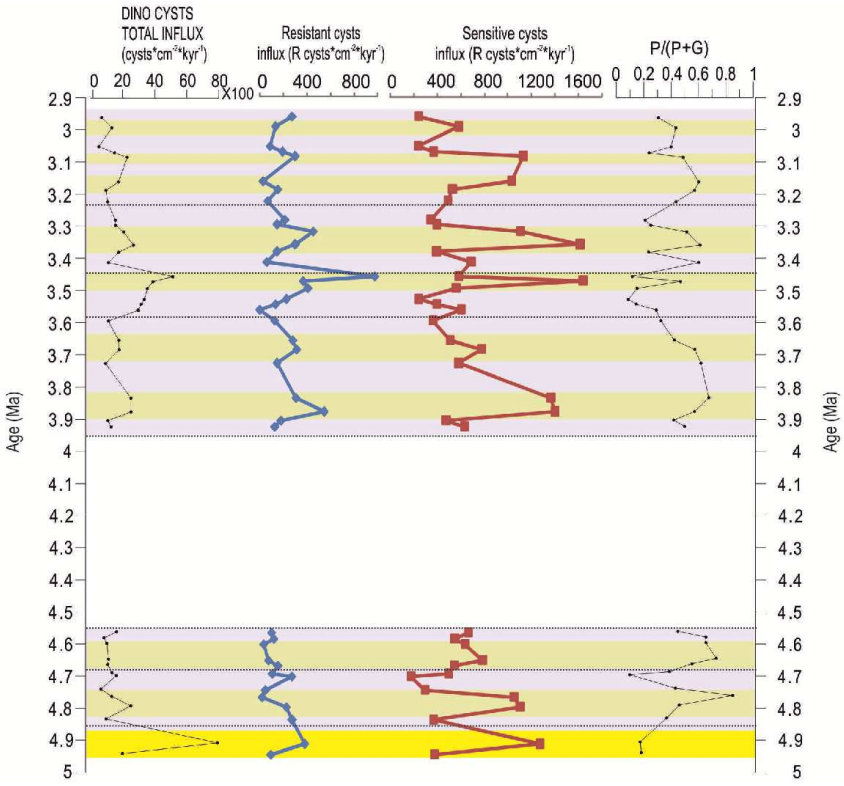

Figure 4: Resistant and sensitive dinocyst accumulation rates and P/P+G ratio. Pale yellow rectangles indicate good preservation. Dark yellow rectangle indicates good preservation but low P/(P+G) (see text).

4.5.3 PCA analysis of dinoflagellate cyst record, N/O index

The first two principal components (Figure 5) explain 25.8% (PC1) and 13% (PC2) of the total variance, respectively, and are statistically significant according to the broken stick criterion (Legendre and Legendre, 2003). The remainder of the variance can be attributed to different ecological gradients (e.g. salinity) influencing the assemblages or to the variance of a single dinoflagellate taxon. In PC1, *Brigantedinium* and *Selenophemphix* spp*.,* have high positive scores (Table 2) while *Achomosphaera/Spiniferites* spp. and *Lingulodinium machaerophorum* show low negative scores. By comparing the first component to the P/G ratios (Figure 5), we explain the first component as indicating nutrient-rich surface waters. *Impagidinium* spp. score positively on PC1 (Table 2), although it is thought to be an indicator of open oceanic conditions, which are usually oligotrophic. The calculated N/O index (neritic and oceanic taxa are listed in Table 4) is presented in Figure 5. During the early Pliocene high values of N/O index suggest predominant neritic conditions, at 4.9 Ma and between 4.8 and 4.6 Ma. Between 3.9 and 3.7 Ma lower N/O values indicate more oceanic conditions. Between 3.7 and 3.4 Ma small fluctuations of the index indicate more stable neritic conditions. During three intervals, between 3.4 and 3.3 Ma, at around 3.2 Ma, and after 3 Ma oceanic conditions prevail; lower values of N/O index correspond to positive scores on PC1 (Figure 5) and intervals of nutrient rich water masses as suggested from P/G ratios (yellow intervals in Figures 4 and 5). All samples of the first early Pliocene interval, 4.94-4.56 Ma, show positive loadings on PC2. This is also the case at 3.8 Ma, between 3.56 and 3.49 Ma (Figure 5, Table 3), between 3.4 and 3.3 Ma and in one sample at 3.16 Ma while all other samples show negative scores. The samples with more negative scores are associated to high percentages and accumulation rates of *Invertocysta lacrymosa* (Figures 2, 3). Though it seems more difficult to interpret PC2, we hypothesize that this component is reflecting a shift in assemblages from Early Pliocene to Late Pliocene (Table 3).

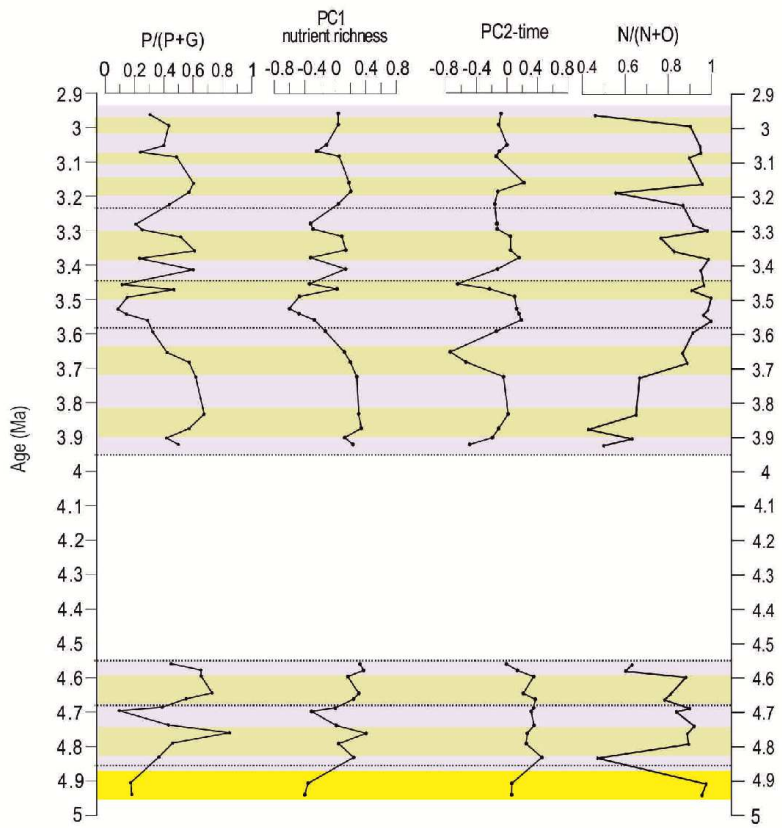

Figure 5: sample score in PC1 (nutrient richness) and PC2 (time) compared with the P/P+G ratio and N/(N+O) index.

Table 2. Scores of selected cyst taxa on PC1

Dinocysts	PC1 scores
Brigantedinium spp.	0.51
Selenopemphix spp.	0.18
Impagidinium spp.	0.17
Dubridinium sp.	0.05
Batiacasphaera micropapillata	0.05
Nematosphaeropsis lativittata	0.03
Operculodinium janduchenei	0.03
Pyxidinopsis reticulata	0.02
Tuberculodinium vancampoae	0.02
Corrudinium harlandii	0.02
Batiacasphaera hirsuta	0.01
Nematosphaeropsis cf *rigida*	0.01
Operculodinium sp.	0.00
Nematosphaeropsis labyrinthus	0.00
Operculodinium israelianum	-0.03
Capisocysta sp.	-0.04
Invertocysta lacrymosa	-0.04
Hystrichokolpoma rigaudiae	-0.06
Cysts *of Protoceratium reticulatum*	-0.11
Polysphaeridium zoharyi	-0.12
Lingulodinium machaerophorum	-0.37
Achomosphaera/Spiniferites spp.	-0.51

Table 3. Scores of samples on PC2

Age sample	PC2 scores
2.96	-0.077
2.99	-0.107
3.05	0.000
3.07	-0.100
3.09	-0.144
3.16	0.222
3.19	-0.121
3.23	-0.161
3.28	-0.133
3.30	-0.128
3.32	0.046
3.36	0.048
3.38	0.155
3.41	-0.125
3.46	-0.647
3.47	-0.229
3.49	0.100
3.53	0.125
3.54	0.156
3.56	0.185
3.60	-0.142
3.66	-0.744
3.68	-0.540
3.73	-0.046
3.84	0.016
3.88	-0.107
3.90	-0.192
3.92	-0.491
4.56	-0.006
4.58	0.134
4.60	0.348
4.65	0.216
4.66	0.371
4.69	0.348
4.70	0.318
4.74	0.352
4.76	0.266
4.79	0.251
4.83	0.458
4.91	0.063
4.94	0.060

Table 4: taxa used for calculation of N/O index

Oceanic taxa (O)	**Neritic taxa (N)** **inner neritic - outer neritic**	
Impagidinium spp.	*T. vancampoae*	*Spiniferites* spp.
Impagidinium aculeatum	*Tectatodinium*	*Achomosphaera* spp.
Impagidinium patulum	*O. israelianum*	
Impagidinium paradoxum	*L. machaerophorum*	
Impagidinium sp.		

4.6. Discussion

4.6.1 Pliocene environmental changes at Site 959

The difference between the early (4.94–4.56 Ma) and later Pliocene (3.92–2.96 Ma) dinoflagellate cyst assemblages can likely be explained by different paleoceanographic conditions in the Gulf of Guinea. The assemblages of the early Pliocene interval (4.94 and 4.56 Ma) can be separated from those of the late Pliocene intervals by the different scores on the second principal component PC2 (Table 3). The statistical separation between both intervals is explained by the presence of *B. hirsuta, N. lativittata, N. cf. rigida,* and *B. micropapillata* in the early Pliocene and also by the absence of *Capisocysta* and the little abundance of cysts of *P. reticulatum*. With exception of the maximum at 4.91 Ma, the average total dinocyst accumulation rate is lower (~$1.3*10^3$ cysts*cm^{-2}*kyr^{-1}) lower before 4.5 Ma than after 4.0 Ma (~$2*10^3$ cysts*cm^{-2}*kyr^{-1}) suggesting lower productivity during the early Pliocene in line with the TOC record of Site 959, which shows lower values with small variations between 4.7 and 3.8 Ma than after 3.7 Ma (Wagner, 2002). Maximum accumulation rates at 4.91 Ma are found for all dinocysts but are dominated by *L. maecharophorum* indicating strong influence of river discharge.

B. hirsuta and *B. micropapillata* are recorded only in 4.94 -4.56 Ma interval. The genus *Batiacasphaera* has not been attributed to a specific environment (Zegarra and Helenes, 2011). Here, the *B. hirsuta* curve shows a pattern opposite to the one of *Brigantedinium* spp. *B. micropapillata* shows a peak both in relative abundances (Figure 3) and in influx values (Figure 4) at 4.56 Ma and it is not present in the interval after 3.92 Ma. *Batiacasphaera* spp. (including *B. hirsuta* and *B. sphaerica*) were abundant in the Middle Miocene to early Late Pliocene assemblages off southwest Africa, in association with *Impagidinium* spp., *Nematosphaeropsis* spp., *Spiniferites ramosus* and *Operculodinium* spp. (Udeze and Oboh-Ikuenobe, 2005). *B. hirsuta* is found in sediment cores off Namibia until 4.5 Ma, before upwelling intensification occurred (Hoetzel et al. 2016). *B. micropapillata* is considered as warm-to cool temperate species within outer-neritic to oceanic environments in the North Atlantic (Schreck and Matthiessen, 2013). However, it also has been found in warm-poor nutrient waters off Namibia (Hoetzel et al. 2016). Thus, available evidences imply that early Pliocene, surface waters at Site 959 were warm and low in nutrients. The N/O index also supports this interpretation.

Different assemblages in the Early and Late Pliocene were expected based on earlier hydrography reconstructions by Norris (1998). Between 4.94 and 4.56 Ma, surface waters in the Gulf of Guinea were warmer and more stratified than after 4.5 Ma suggesting reduced seasonal upwelling (Norris, 1998). This condition has been associated to a northern than today's summer position of the ITCZ (Norris, 1998; Billups, 1999) that was limiting the transport of warm surface waters from the tropical to subtropical regions and reducing the transport of cool waters back to the east equatorial Atlantic (Billups, 1999).

4.6.2 Upwelling and vegetation dynamics during the late Pliocene

After 3.92 Ma the dinoflagellate cyst record indicates several phases with upwelling and nutrient-rich surface waters in the Gulf of Guinea. This is reflected in the high relative abundances and accumulation rates of heterotrophic taxa like *Brigantedinium* spp. and *Selenopemphix* spp. and the

high P/G ratio (Figure 5). In modern surface sediments samples of the Gulf of Guinea, high percentages of the heterotrophic *Brigantedinium* spp. are found in upwelling areas off Ivory Coast (up to 2000 m water depth), especially after diatom blooms (Marret, 1994). Upwelling off the Ivory Coast/Ghana occurs during summer when the ITCZ is at its northern position. The SE trade winds are stronger then and strengthen the countercurrent system, formed by the Northern Equatorial Countercurrent and the Equatorial Undercurrent (EUC). The EUC brings cool waters into the Gulf of Guinea and provide the source for upwelled waters (Hisard and Merle, 1980; Verstraete, 1992; Norris, 1998). Upwelling implies shoaling of the thermocline corresponding to a reduced oxygen isotope gradient between planktonic foraminifera that dwell at the thermocline and those of the surface waters (Norris, 1998).

Between 4 and 3.6 Ma, an interval occurred (Ep 4), in which *Brigantedinium* spp. and *Selenopemphix* spp. dominate the assemblage indicating nutrient-rich surface waters. On the other hand, the N/O index indicates more oceanic conditions until 3.7 Ma. The total dinocyst accumulation rates ($1.6*10^3$ cysts*cm^{-2}*kyr^{-1}) increase slightly compared to Ep 3 ($1.2*10^3$ cysts*cm^{-2}*kyr^{-1}) and an increase in R cyst accumulation rates indicate higher productivity (Versteegh and Zonneveld, 2002; Zonneveld et al., 2007; Zonneveld et al. 2010). The combination of higher productivity and increasing nutrients in the surface water (Figure 4 and 5) suggest increased upwelling, which might be the result of stabilisation of the Guinea Current in the Gulf of Guinea since 4.5 Ma (Norris, 1998). Since then, the modern circulation developed and SSTs of the eastern Atlantic Ocean started to show seasonal variations. Billups et al. (1999) demonstrated that between 4.4 and 4.3 Ma (with age uncertainty of ~100 ka) a southwards shift of the ITCZ could have been the cause of thermocline depth changes in eastern equatorial oceans resulting in upwelling. Moreover, today's upwelling in the Gulf of Guinea is not restricted to the coastal areas but has a considerable latitudinal range (Verstraete, 1992).

Stronger seasonality, implying enhanced seasonal upwelling, has been recorded at ODP Site 959 from 3.2 Ma (Vallé et al. submitted to IJES). Starting from 3.6 Ma, the upwelling intervals (from 3.5 to 3 Ma) are compared with late Pliocene pollen records from ODP Sites 659 and 658 located offshore of Mauritania at subtropical latitudes (18-21°N) (Leroy and Dupont 1994, Vallè et al. 2014) (Figure 6). Higher percentages of Chenopodiacaeae-Amaranthaceae (CA) in marine sediments at Site 659 indicate aridity and enhanced wind activity, while higher percentages of woodland forests represent more humidity in the Sahel zone (Vallé et al., 2014). Upwelling intervals recorded at ODP Site 959 correspond to intervals of increased aridity in the Sahel zone (Figure 6, yellow rectangles). Between 3.3 Ma and 3.2 Ma, after the cold stage M2, we observe low values of total dinocyst accumulation rates (Figures 4, 6 and 7) and reduced *Brigantedinium* spp. suggesting reduced productivity off Ivory Coast/Ghana during this interval (green rectangle in Figures 6 and 7). During this interval offshore NW Africa, the reduced dust signal and pollen record from ODP Site 659 indicated a wetter interval in the Sahel zone, within the Mid-Pliocene warm period (Vallè et al. 2014). This is comparable to the modern situation in which cold SST during upwelling intervals in the Gulf of Guinea occur during the dry season in West Africa, while longer intervals of warm surface waters cause increasing precipitation and seasonal upwelling is reduced (Verstraete, 1992;

Norris, 1998). Also, during the last 190 ka, the arid and cold isotopic stages corresponded to intervals of stronger upwelling in the eastern equatorial Atlantic (Dupont et al., 1999).

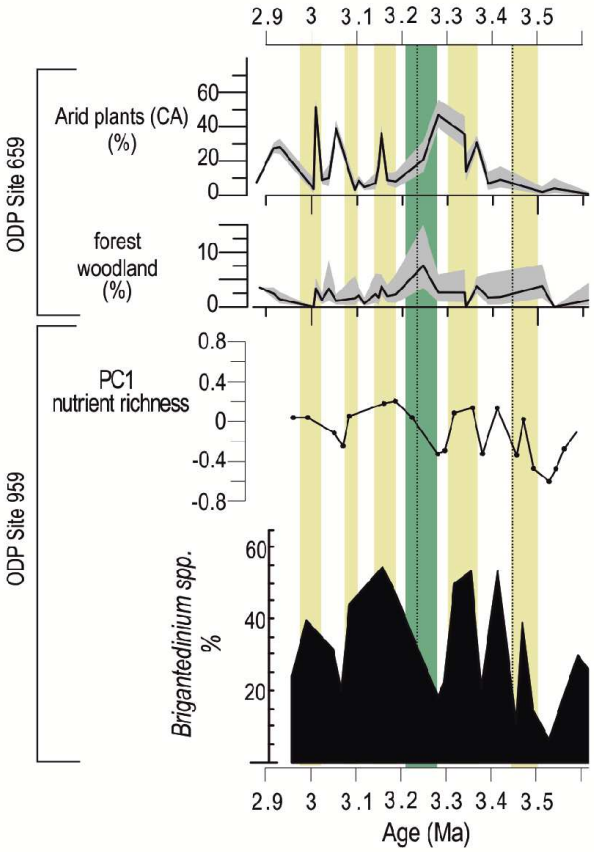

Figure 6: Comparison between upwelling intervals (pale yellow rectangles) recorded at Site 959 during the Late Pliocene and pollen results from ODP Site 659 (18°N, 21°W). Green rectangle indicates a wetter interval in subtropical Africa and reduced upwelling at ODP site 959.

4.6.3 Evidences for sea level changes

We observe distinct intervals in which the relative abundance of typical low saline estuarine cysts *O. israelianum*, *P. zoharyi*, *T. vancampoae* and *L. machaerophorum*, mostly corresponding to maxima of *Achomosphaera/Spiniferites* spp., is mainly opposed to the abundance of oceanic taxa such as *Nematosphaeropsis* and *Impagidinium*. Today, the innermost shelf zone near Abidjan on the Ivory Coast of West Africa is characterized by different species of *Spiniferites* together with cysts *Protoceratium reticulatum* and *T. vancampoae* representing a low salinity estuarine-coastal subsystem with alternating periods of upwelling and annual stratification (Wall et al. 1977). Morzadec-Kerfourn (1992) documented climatic changes during the Pleistocene off the Ivory Coast based on variations of estuarine dinoflagellate cysts. Oboh-Ikuenobe et al. (1999) suggested that the presence of neritic species in the deep-sea sediments of ODP Site 959 during the Oligocene to early Miocene is most probably the result of transport via currents or sea level fluctuations. To check for transportation from the continent to the ocean site we compared the Site 959 proxies

representing input from the continent to changes in sea level (Figure 7). Variations of ODP Site 959 Ti/Al ratios are used as indicator for terrigenous transport sources; higher values indicate aeolian transport and lower values suggest increasing fluvial transport (Vallè et al. submitted).
It has been suggested that fern spore accumulation rates in the Gulf of Guinea could serve as an indicator of fluvial activity during lower sea levels (Poumot, 1989) and that the ratio of terrestrial palynomorphs over dinoflagellate cysts is related to the continental influence at the oceanic site (e.g. Versteegh, 1994). Four glaciation events, at ~4.9-4.8 Ma, ~4 Ma, ~3.6 Ma, ~3.3 Ma are associated with lower sea levels recognised globally during the Pliocene (indicated in Figure 7) (De Schepper et al. 2014). For the three glaciation events covered by our dinoflagellate cyst records, we find higher relative abundance of estuarine cysts associated with increased spore accumulation rates. This indicates enhanced transport from the neritic zone bringing more neritic and estuarine dinoflagellate cysts to the deep-sea location through fluvial discharge closer to the site as a result of lower sea level. The river transport signal in the dinoflagellate cyst record (Figure 7) is clearer before 3.5 Ma. From 3.5 Ma on, the Ti/Al record indicates enhancement of the winter trade winds signal suggestive of a southward shift of the southernmost ITCZ position allowing the NE trade winds to reach the Gulf of Guinea (Vallé et al., submitted).

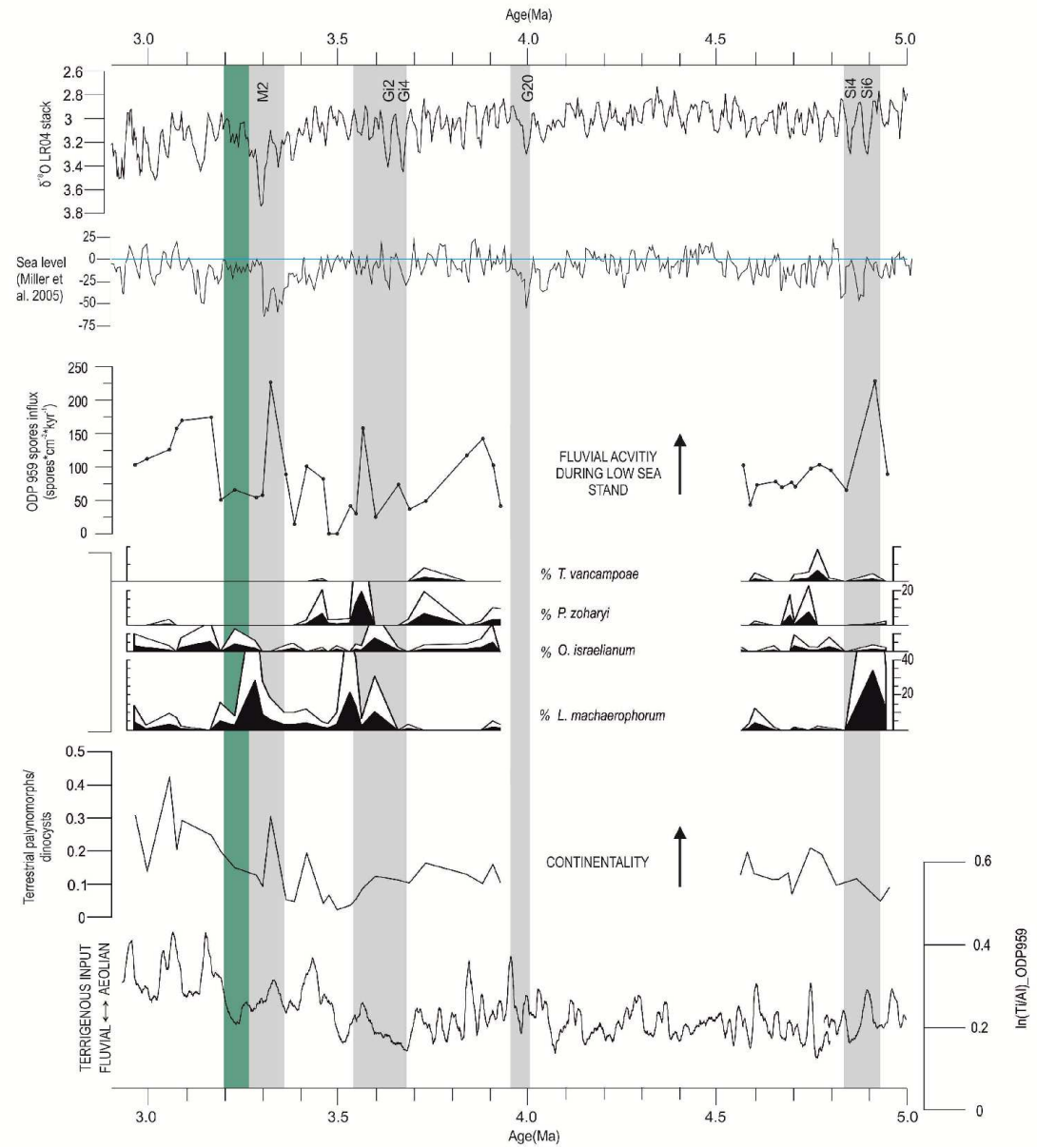

Figure 7: (from top to bottom) Oxygen isotope stack from Lisiecki and Raymo 2005, sea level changes from Miller et al. 2005. Site 959 spore accumulation rates, estuarine cyst percentages, ratio of terrestrial palynomorphs over dinocysts, Ti/Al ratios (from Vallè et al., submitted). Grey rectangles indicate the four Pliocene glaciations events and consequent lower sea level (after De Schepper et al. 2014).

4.7 Conclusions

Our dinoflagellate cyst record from ODP Site 959 (off Ivory Coast) in combination with pollen and spore accumulation rates and Ti/Al ratios provides new evidence about environmental changes in the Gulf of Guinea during the Pliocene. By comparing dinoflagellate records and pollen results from ODP Site 659, we could associate late Pliocene upwelling intervals with arid phases in West Africa. Between 3.3 and 3.2, a wetter interval recorded by a change in vegetation, corresponded to an interval of reduced upwelling in the Gulf of Guinea. Dinoflagellate cyst record weaker seasonal upwelling and more oceanic conditions during the early Pliocene interval, between 4.94 and 4.5 Ma, when sea surface waters were warmer and the thermocline of the Gulf of Guinea may have been stronger. This supports what has been previously inferred from oxygen isotope gradients. Two extinct species are present during this interval, *B. hirsuta* and *B. micropapillata* that likely have an affinity with warm and nutrient-poor waters. After 3.9 Ma the dinocyst record indicates increased coastal upwelling. The occurrence of *I. lacrymosa* with relative abundances of ~15% suggests warmer waters during certain intervals. A comparison between the dinocyst record, terrestrial palynomorphs and the Ti/Al ratios allowed the recognitions of increased river input at Site 959 during periods of low sea level associated with Pliocene glaciation events.

4.8 Acknowledgements

The study was financially supported by the Deutsche Forschungsgemeinschaft (DFG), grant DU221/5. FV thanks GLOMAR (Bremen International Graduate School for Marine Sciences) and the Department of Earth Science, University of Bergen for the hospitality. We are grateful to Martin Head, Michael Schreck and Jan Hennissen for help with identifications. Ocean Drilling Program is acknowledged for providing the samples.

Chapter 5

Thesis synthesis and Outlook

5.1 Synthesis

The main goal of this thesis was to investigate the long-term environmental change and climatic evolution in West Africa and in the surface waters of the eastern equatorial Atlantic during the Pliocene epoch, in order to improve understanding of the linkages between low-latitude environmental variability and the climate driving forces during this interval.

Pliocene environmental changes in west Africa have been investigated by studying changes in vegetation development (Chapter 2) and in variation of geochemical proxy records (Chapters 2 and 3). Sea surface conditions have been analysed by means of dinoflagellate proxy records (Chapter 4). By comparing palynological results with geochemical proxy records, vegetation dynamics and pollen transport have been linked to changes in continental humidity/aridity, to which (respectively) less dust supply/more dust supply correspond (Chapter 2). Good agreement between dust proxy records from the equatorial and subtropical regions (Chapter 3) indicated that after 3.5 Ma the Intertropical Convergence Zone shifted southward during winter. Moreover, continent-wide aridity or larger climate variability has been proposed between 3.2 and 2.9 Ma (Chapter 3). By analysing the time series of high-resolution terrestrial proxies, it has been possible to identify the influence of eccentricity (405 kyr and 100 kyr) and precession forcings on the east equatorial Atlantic sedimentation throughout the Pliocene (Chapter 3). Difference in upwelling intensity between the early and the late Pliocene, have been reconstructed and possibly related to different position of the ITCZ and to conditions in the thermocline in the Gulf of Guinea. Moreover, sea level drops in the Gulf of Guinea, associated to the Pliocene glaciation events, have been recorded in the dinoflagellate and pollen records at ODP Site 959 (Chapter 4).

The specific questions addressed were answered:

1. Was the MPWP characterized by a generally warmer and wetter West African climate or were arid events just less intense?

A short but continuous wet time interval between ~3.25 and 3.2 Ma has been identified within the so-called mid-Pliocene warm period (~3.3-3 Ma, Dowsett et al., 2007). Notably, it has been identified in all our records (Chapter 2, 3, 4). This short interval represent a distinct wet interval, during when, woodlands expanded northwards (Chapter 2) and reduced aeolian activity (Chapters 2 and 3) cause reduced pollen transport off northwest Africa. In the Gulf of Guinea, this interval corresponds to reduced coastal upwelling, thus indicating warm sea surface temperatures (Chapter 4).

2. What were the triggers of dust export events and how do they relate to West African climate variability?

Results presented in Chapter 2 regarding vegetation change, pollen transport, and the evolution of the trade wind system allow the identification of the important forcings for Pliocene west African climate variability. Our findings link the NE trade wind development with the intensification of the Northern Hemisphere glaciations (iNHG). Prior to the iNHG, little or no systematic relation could be found between sea surface temperatures of the North Atlantic with aridity and dust in West Africa.

3. Before the CAS closure, i.e., before intensification of the AMOC, was West Africa generally drier and less vegetated?

Pollen content off northwest Africa is very low during the early Pliocene (Chapter 2). Minimal dust was found at ODP Site 959 in agreement with other dust records between 4.9 and 4.7 Ma. This minimum corresponds to one of the very long eccentricity minima in the eccentricity amplitude modulation of the early Pliocene implying smaller amplitudes of precession cycles (Chapter 3). Dinoflagellate records in the Gulf of Guinea indicate reduced upwelling during early Pliocene, probably associated to warm sea surface temperature. This is in agreement with the suggested reduced equatorial-tropical gradient and the reduced activity of the Guinea Current (Chapter 4). In our records, there are no evidences of less vegetation conditions; it is instead suggested a long-term decrease in river supply in the Gulf of Guinea, after 5.4 Ma (Chapter 3).

4. Which were the land-sea connections during the Pliocene?

Comparison between results obtained from pollen records and dinoflagellate cysts records (Chapters 1 and 4) indicate a link between late Pliocene upwelling intervals in the Gulf of Guinea, after establishment of the Guinea Current, and increasing aridity in northwest Africa (southern Sahel zone). While, during the wet interval between 3.24 and 3.2 Ma, upwelling is reduced.

Basic hypotheses were: 1) the MPWP is the result of the closure of the CAS, redirecting warm tropical waters to the North Atlantic. It caused elevated humidity and extensions of woodland and forest biomes in NW Africa; 2) NW African aridity and vegetation changes are mainly driven by AMOC variations as recently postulated by Mulitza et al. (2008), Castañeda et al. (2009) and others. Both hypotheses regard the connections between low-latitudes environmental and climate variability and the high-latitude systems. During the Quaternary, AMOC intensification has been suggested as cause of increased precipitation in west Africa. Recently, a model study for the last deglaciation have linked decreased AMOC intensity to suppressed precipitation both in southwest and northwest Africa, changing to wetter conditions once the AMOC re-established in response to high summer insolation (Otto-Bliesner et al. 2014). The shoaling of the CAS after 4.6 Ma, modified the oceanic circulation, intensifying the thermohaline circulation (Haug and Tiedemann, 1998) and thus the AMOC. Based on results obtained in this thesis, the first hypothesis is acceptable; though only a short interval of the so-called mid-Pliocene warm period in west Africa can be considered wetter and warmer (Chapter 2 and 4). A long-term decrease of river supply in equatorial Africa after 5.4 Ma towards the early Pleistocene (Chapter 3) might be linked to local changes in the Gulf of Guinea. Dust activity increased after 3.5 Ma, probably linked to a southwards shift of the ITCZ at

least during winter is linkable with increased seasonality, which is shown after 3.4 Ma (Chapter 3). Enhanced continental aridity or larger climate variability corresponding with eccentricity maxima occurred in west Africa between 3.2 and 2.9 Ma. After the intensification of the Northern Hemisphere Glaciation (iNHG) at 2.75 Ma, NE trade winds over west Africa are enhanced. Prior to the iNHG little or no systematic relation were established between aridity, dust in west Africa and sea surface temperatures in the north Atlantic. Thus, from this thesis it resulted that strong connections between west African climate variability and high-latitudes systems, are present since the iNHG. Thus, main forcings of the west African Pliocene climate are related to low-latitude processes involving the thermocline evolution, west African monsoon variations, influenced by precession (eccentricity modulated).

5.2. Outlook

Proxy records obtained for this thesis underline different environmental conditions during the early Pliocene and the late Pliocene, especially in the east equatorial Atlantic. The early Pliocene has been less investigated, than the mid-Pliocene interval (De Schepper et al., 2014). Where possible, more direct upwelling proxies are necessary to extend the knowledge of sea surface waters conditions in the global upwelling regions. This thesis suggest the use of dinoflagellate cysts records, which could be associated to study of other proxies, such as diatoms (Marlow et al., 2000).

The combination of palynological results and continental climate proxy records obtained from XRF-scanning, used in this thesis, allowed the investigation of relationships between pollen transport, dust supply reflecting wind systems change. This approach could be used also useful for southwest Africa or south American margin.

Unfortunately, in this thesis it has not been possible to have high-resolution vegetation records or organic-walled dinoflagellate cysts records because of the poor contents, especially during the early Pliocene. New high-resolution records might be better achieved in sites located closer to the African continent, where dust supply is integrated with river supply, and probably, in upwelling areas, where sedimentation rates are higher and preservation of organic material is increased (Hooghiemstra et al. 2006).

Combination of palynological results focusing on vegetation development, and proxies obtained from plant waxes ($\delta^{13}C$ proxy for C_3/C_4 plants and δD_{wax} as precipitation proxy) allow detailed environmental reconstructions. Pliocene palynological results from this thesis might be compared with results obtained from Küchler et al., (unpublished results) at ODP Site 659. Furthermore, this comparison might be also interesting in order to check the role of fire as a driver of the C4 grassland expansion (Hoetzel et al., 2013) in west Africa.

References

Arz, H., Pätzold, J., Wefer, G., 1999. The deglacial history of the western tropical Atlantic as inferred from high resolution stable isotope records off northern Brazil. Earth and Planetary Science Letters 167, 105-117.

Balsam, W.L., Otto-Bliesner, B.L., Deaton, B.C., 1995. Modern and last glacial maximum eolian sedimentation patterns in the Atlantic Ocean interpreted from sediment iron oxide content. Paleoceanography 10, 493-507.

Bartoli, G., Hönisch, B., Zeebe, R.E., 2011. Atmospheric CO2 decline during the Pliocene intensification of Northern Hemisphere Glaciations. Paleoceanography 26, PA4213, 14. doi:10.1029/2010PA002055.

Bartoli, G., Sarnthein, M., Weinelt, M., Erlenkeuser, H., Garbe-Schönberg, D. and Lea, D.W., 2005. Final closure of Panama and the onset of Northern Hemisphere glaciation. Earth and Planetary Science Letters, 237: 33-44.

Beckmann, B., Flögel, S., Hofmann, P., Schulz, M., Wagner, T., 2005. Orbital forcing of Cretaceous river discharge in tropical Africa and ocean response. Nature, 437, 241-244.

Billups K., Ravelo A.C., Zachos J.C. and Norris R.D., 1999. Link between oceanic heat transport, thermohaline circulation, and the Intertropical Convergence Zone in the early Pliocene Atlantic. Geology 27, 319-322.

Boko, M., I. Niang, A. Nyong, C. Vogel, A. Githeko, M. Medany, B. Osman-Elasha, R. Tabo and P. Yanda, 2007: Africa. Climate Change 2007: Impacts, Adaptation and Vulnerability. Contribution of Working Group II to the Fourth Assessment Report of the Intergovernmental Panel on Climate Change, M.L. Parry, O.F. Canziani, J.P. Palutik of, P.J. van der Linden and C.E. Hanson, Eds., Cambridge University Press, Cambridge UK, 433-467.

Bonnefille, R., Potts, R., Chalié, J., D., Peyron, O., 2004. High-resolution vegetation and climate change associated with Pliocene *Australopithecus afarensis*. Proceedings of the National Academy of Sciences 101, 12125-12129.

Bonnefille, R., Riollet, G., 1980. Pollens des savanes d'Afrique orientale. Éditions du Centre National de la Recherche Scientifique Paris, 140p. 113pl.

Borcard D., Gillet F., Legendre P., 2011. Numerical ecology with R. Springer-Verlag New York.

Bremer, K., 1994. Asteraceae, cladistics & classification. Timber Press Portland Oregon, 752p.

Brierley C.M., Fedorov A.V., Liu Z., Herbert T.H., Lawrence K.T., Lariviere J.P., 2009. Greatly Expanded Tropical Warm Pool and Weakened Hadley Circulation in the Early Pliocene. Science 323, 1714-1718.

Castañeda, I.S., Mulitza, S., Schefuß, E., Lopes dos Santos, R.A., Sinninghe Damsté, J.S., Schouten, S., 2009. Wet phases in the Sahara/Sahel region and human migration patterns in North Africa. Proc. Natl. Acad. Sci. USA 106(48), 20159–20163.

CIESM, 2008. The Messinian salinity crisis from mega-deposits to microbiology. In: Briand, F. (Ed.), A consensus report, in 33ème CIESM Workshop Monographs, 33. CIESM, 16, bd de Suisse, MC-98000, Monaco, pp. 1–168.

Clemens, S.C., 1999. An astronomical tuning strategy for Pliocene sections: implications for global-scale correlation and phase relationships. Philosophical Transactions, Mathematical Physical and Engineering Sciences 357, 1949-1973.

Cohen, K.M., Finney, S.C., Gibbard, P.L., Fan, J.-X., 2013. The International Chronostratigraphic Chart. Episodes 36, 199-204.

COHMAP, 1988. Climatic changes of the last 18,000 years: observations and model simulations. Science 241, 1043-1052.

Collins, J.A., Govin, A., Mulitza, S., Heslop, D., Zabel, M., Hartmann, J., Röhl, U., Wefer, G., 2013. Abrupt shifts of the Sahara–Sahel boundary during Heinrich stadials. Climate of the Past 9, 1181-1191.

Contoux, C., Ramstein, G., Jost, A., 2012. Modelling the mid-Pliocene Warm Period climate with the IPSL coupled model and its atmospheric component LMDZ5A. Geoscientific Model Development 5, 903-914.

De Schepper S., Fischer E., Groeneveld J., Head M.J, Matthiessen J., 2011. Deciphering the paleoecology of the Late Pliocene and Early Pliocene dinoflagellate cysts. Paleogeography, Palaeoclimatology, Palaeoecology 309, 17-32.

De Schepper S., Gibbard P. L., Salzmann U., Ehlers J., 2014. A global synthesis of the marine and terrestrial evidence for glaciation during the Pliocene Epoch. Earth-Science Reviews 135, 83–102.

De Schepper S., Groeneveld J., Naafs, BDA, Van Renterghem C., Hennissen J., Head M. J., Louwye S., Fabian K, 2013. Northern Hemisphere Glaciation during the Globally Warm Early Late Pliocene. PLoS ONE 812: e81508. doi:10.1371/journal.pone.0081508.

De Schepper S., Head M.J., 2009. Pliocene and Pleistocene dinoflagellate cyst and acritarch zonation of DSDP Hole 607A, eastern North Atlantic. Palynology 33, 179-218.

Dekens P.S., Ravelo A.C., McCarthy M.D., 2007. Warm upwelling regions in the Pliocene warm period. Paleoceanography, Vol. 22, PA3211, doi:10.1029/2006PA001394.

deMenocal, P.B., 1995. Plio-Pleistocene African Climate. Science, 270, 53-59.

deMenocal, P.B., 2004. African climate change and faunal evolution during the Pliocene-Pleistocene. Earth and Planetary Science Letters 220, 3-24.

deMenocal, P.B., 2011. Climate and Human Evolution. Science, 331, 540-542.

deMenocal, P.B., Ortiz, J., Guilderson, T., Adkins, J., Sarnthein, M., Baker, L., Yarusinsky, M., 2000. Abrupt onset and termination of the African Humid Period: rapid climate responses to gradual insolation forcing. Quaternary Science Reviews 19, 347-361.

deMenocal, P.B., Ortiz, J., Guilderson, T., Sarnthein, M., 2000. Coherent high- and low- latitude climate variability during the Holocene warm period. Science 288, 2198-2202.

deMenocal, P.B., Rind, D., 1993a. Sensitivity of Asian and African climate to variations in seasonal insolation, glacial ice cover, sea surface temperature, and Asian orography. J. Geophys. Res. 98(D4), 7265–7287.

deMenocal, P.B., Ruddiman, W.F., Pokras, E.M., 1993b. Influences of high- and low-latitude processes of African terrestrial climate: Pleistocene eolian records from equatorial Atlantic Ocean Drilling Program Site 663. Paleoceanography 8, 209-242.

Dowsett, H.J., 2007. The PRISM palaeoclimate reconstruction and Pliocene sea-surface temperature. In: Deep-time perspectives on climate change: marrying the signal from computer models and biological proxies (eds. Williams, M., Haywood, A.M., Gregory, J., and Schmidt, D.N.), London, UK, Micropalaeontological Society (Special Publication), Geological Society of London, 459–480.

Dowsett, H.J., Barron, J., and Poore, R., 1996. Middle Pliocene sea surface temperatures: a global reconstruction, Marine Micropaleontolology, 27, 13–25.

Dowsett, H.J., Chandler, M.A, Robinson, M.M, 2009. Surface temperatures of the Mid-Pliocene North Atlantic Ocean: implications for future climate. Philosophical Transactions of the Royal Society A, 367, 69-84.

Driscoll, N.W. and Haug, G.H., 1998. A short circuit in thermohaline circulation: A cause for Northern Hemisphere Glaciation? Science, 282: 436-438.

Dupont L.M, Behling H., Jahns S., Marret F., Kim J. 2007. Variability in glacial and Holocene marine pollen records offshore from west southern Africa. Vegetation History and Archaeobotany 16:87–100. DOI 10.1007/s00334-006-0080-8.

Dupont L.M., 1999a. Pollen and spores in marine sediments from the East Atlantic. A view from the ocean into the African continent. In Fisher G., and Wefer G. (Eds). Use of Proxies in Paleoceanography: examples from the South Atlantic. Springer Verlag Berlin: 523-546.

Dupont L.M., Marret F., Winn K., 1998. Land-sea correlation by means of terrestrial and marine palynomorphs from the equatorial East Atlantic: phasing of SE trade winds and the oceanic productivity. Palaeogeography, Palaeoclimatology, Palaeoecology 142, 51-84.

Dupont L.M., Schmüser A. Jahns S., Schneider R., 1999b. Marine-terrestrial interaction of climate changes in West Equatorial Africa of the last 190,000 years. Paleoecology of Africa, 26, 61-84.

Dupont, L.M., 2011. Orbital scale vegetation change in Africa. Quaternary Science Reviews 30, 3589-3602.

Dupont, L.M., Agwu, C.O.C., 1991. Environmental control of pollen grain distribution patterns in the Gulf of Guinea and offshore NW -Africa. Geologische Rundschau 80, 567-589.

Dupont, L.M., Leroy, S.A.G., 1995. Steps toward drier climatic conditions in northwestern Africa during the Upper Pliocene. E.S. Vrba, G.H. Denton, T.C. Partridge, L.H. Burckle (eds.). Paleoclimate and evolution with emphasis on human origins. Yale University Press New Haven, 289-298.

Durugbo E. U., Ogundipe O. T., and Ulu O.K., 2011. Preliminary reports on Middle Miocene-Early Pleistocene dinoflagellate cysts from the Western Niger Delta, Nigeria. Ozean Journal of Applied Sciences 4 (4). ISSN 1943-2429.

Etourneau, J., Ehlert, C., Frank, M., Martinez, P., Schneider, R., 2012. Contribution of changes in opal productivity and nutrient distribution in the coastal upwelling systems to Late Pliocene/Early Pleistocene climate cooling. Climate of the Past 8, 1435-1445.

Etourneau, J., Schneider, R., Blanz, T., Martinez, P., 2010. Intensification of the Walker and Hadley atmospheric circulations during the Pliocene–Pleistocene climate transition. Earth and Planetary Science Letters 297, 103-110.

Evans, H.F., Westerhold, T., Channell, J.E.T., 2004. ODP Site 1092: revised composite depth section has implications for Upper Miocene "cryptochrons."Geophysical Journal International, 156,195-199.

Faegri, K., Iversen, J., 1989. Textbook of pollen analysis. IV Edition by Faegri, K., Kaland, P.E., Krzywinski, K.Wiley, New York.

Falkowski, P.G., Barber R.T., and Smetacek V., Biogeochemical controls and feedbacks on ocean primary production, Science, 281, 200–206.

Faugères, J.C., Legigan, P., Maillet, N., Latouche, C., 1989. Pelagic, turbiditic, and contouritic sequential deposits on the Cape Verde Plateau (Leg 108, Site 659, Northwest Africa): sediment record during Neogene time. Ruddiman W.F., Sarnthein M. et al. Proceedings ODP, Scientific Results 108, 311-327.

Fedorov, A.V., Brierley C.M., Lawrence K.T., Liu, Z., Dekens P.S., Ravelo A.C., 2013. Patterns and mechanisms of early Pliocene warmth. Nature 496, 43–49.

Fedorov, A.V., Dekens, P.S., Mccarthy, M., Ravelo, A.C., deMenocal, P.B., Barriero, M., Pacanowski, R.C., Pilander, S.G., 2006. The Pliocene paradox (mechanisms for a permanent El Nino). Science 312, 1485-1489.

Fensome R.A., MacRae R.A., Williams, G.L., 2008. DINOFLAJ2, Version 1. American Association of Stratigraphic Palynologists, Data Series no. 1. Available online at: http:// http://dinoflaj.smu.ca/wiki/Main_Page.

Fensome, R.A., Riding, J.B., Taylor, F.J.R., 1996. Dinoflagellates. In: Jansonius, J., McGregor, D.C. (Eds.), Palynology: Principles and Applications, vol. 1. AASP Foundation, Salt Lake City, UT, pp. 107-169.

Fensome, R.A., Taylor, F.J.R., Norris, G., Sarjeant, W.A.S., Wharton, D.I. and Williams, G.L., 1993: A classification of fossil and living dinoflagellates. Micropaleontology Press Special Paper, no.7, 351 p.

Gasse, F., 2000. Hydrological changes in the African tropics since the Last Glacial Maximum. Quaternary Science Reviews 19, 189-211.

Ghil, M., Allen M.R, Dettinger, M.D., Ide, K., Kandrashov, D., Mann, M.E., Robertson, A.W., Sanders, A., Tian, Y., Varadi, F., Yiov, P., 2002. Advanced spectral methods for climatic timeseries. Reviews of Geophysics, 40, 1003, doi:10.1029/2001RG000092.

Giresse P., Gadel F., Serve L., Barusseau J. P., 1998. Indicators of climate and sediment-source variations at Site 959: Implications for the reconstruction of the paleoenvironments in the Gulf of Guinea through Pleistocene times. In: Mascle, J., Lohmann, G.P., and

Moullade, M. (Eds.) Proceedings of the Ocean Drilling Program, Scientific Results, 159. Ocean Drilling Program, College Station TX, pp. 585-603.

Giresse P., Gadel F., Serve L., Barusseau J.P., 1998. Indicators of climate and sediment-source variations at Site 959: Implications for the reconstruction of the paleoenirvonments in the Gulf of Guinea through Pleistocene times. In: Mascle, J., Lohmann, G.P., Moullade, M. (eds.), Proceedings of the Ocean Drilling Program, Scientific Results Vol. 159, College Station, TX (Ocean Drilling Program), 585-683.

Govin, A., Holzwarth, U., Heslop, D., Ford-Keeling, L., Zabel, M., Mulitza, S., Collins, J.A., Chiessi, C.M., 2012. Distribution of major elements in Atlantic surface sediments (36°N–49°S): Imprint of terrigenous input and continental weathering. Geochemistry, Geophysics, Geosystems 13, Q01013, 1-23.

Gradstein, F. M., Ogg, J. G., Schmitz M., Ogg, G., 2012. The Geologic Time Scale 2012.

Grimm EC (1987) CONISS: a FORTRAN 77 program for stratigraphically constrained cluster analysis by the method of incremental sum of squares. *Computer & Geosciences* 13(1): 13-35.

Grimm EC (2004) TGView version 2.0.2. Springfield Illinois State Museum, Research and Collection Center.

Hammer, Ø., Harper, D.A.T., Ryan, P.D., 2001. PAST: Paleontological Statistics Software Package for Education and Data Analysis. Palaeontologia Electronica 4(1), 1-9.

Haug, G.H., Ganopolski, A., Sigman, D.M., Rosell-Mele, Swann, G.A., Tiedemann, R., Jaccard, S.L., Bollmann, J., Maslin, M.A., Leng, M.J., Eglinton, G., 2005. North Pacific seasonality and the glaciation of North America 2.7 million years ago. Nature 433, 821-825.

Haug, G.H., Sigman, D.M., Tiedemann, R., Pedersen, T., Sarnthein, M., 1999. Onset of permanent stratification in the subarctic Pacific Ocean. Nature 401, 779-782.

Haug, G.H., Tiedemann, R., 1998. Effect of the formation of the Isthmus of Panama on Atlantic Ocean thermohaline circulation. Nature 393, 673–676.

Haywood, A.M., Dowsett, H.J., Otto-Bliesner, B., Chandler, M. A., Dolan, A.M., Hill, D.J., Lunt, D. J., Robinson, M.M., Rosenbloom, N., Salzmann, U., Sohl, L., E, 2010. Pliocene Model Intercomparison Project (PlioMIP): experimental design and boundary conditions (Experiment 1). Geoscientific Model Development, 3, 227-242.

Haywood, A.M., Dowsett, H.J., Valdes, P.J., Lunt, D.J., Francis, J.E., Sellwood, B.W., 2009. Introduction. Pliocene climate, processes and problems. Royal Society of London Philosophical Transactions, ser. A 367, 3–17.

Head M.,J., Westphal I., 1999. Palynology and Paleoenvironments of a Pliocene Carbonate Platform: The Clino Core, Bahamas. Journal of Paleontology, Vol. 73, No. 1, pp. 1-25.

Head M.J., 1997. Thermophilic dinoflagellate assemblages from the mid Pliocene of eastern England. Journal of Paleontology, 71, pp 165-193.doi:10.1017/S0022336000039123.

Head M.J., Norris G., Mudie P.J, 1989. New species of dinocysts and a new species of acritarch from the upper Miocene and lowermost Pliocene, ODP Leg 105, Site 464, Labrador Sea. In:

Srivastava S.P., Arthur M., Clement B. et al. (eds.), Proceedings of the Ocean Drilling Program, Scientific Results Vol. 105, College Station, TX (Ocean Drilling Program), 453-466.

Head, M.J., Norris, G. and Mudie, P.J., 1989: 27. Palynology and dinocyst stratigraphy of the Miocene in ODP Leg 105, Hole 645E, Baffin Bay. In: Srivastava, S.P. et al., Ocean Drilling Program, Proceedings, Scientific Results, Leg 105, College Station, Texas, . 467-514.

Hennissen, J.A.I., Head, M.J., De Schepper, S., Groeneveld, J., 2014. Palynological evidence for a southward shift of the North Atlantic Current at ~2.6 Ma during the intensification of late Cenozoic Northern Hemisphere glaciations. Paleoceanography: 2013PA002543.

Herbert, T., Premoli Silva, I., Erba, E., Fischer, A.G., 1995. Orbital chronology of Cretaceous-Paleocene marine sediments. Geochronology Time Scales and Global Stratigraphic Correlation, SEPM Special Publication No. 54.

Herbert, T.D., Cleaveland Peterson, L., Lawrence, K.T., Lui, Z., 2010. Tropical ocean temperatures over the past 3.5 million years. Science 328, 1530-1534.

Hisard P., and Merle J., 1980. Onset of summer surface cooling in the Gulf of Guinea during GATE. Deep-Sea Research, Suppl. II, 26, 325−341.

Hodell D.A., Curtis J.H., Sierro J.F., Raymo M.E., 2001. Correlation of the late Miocene to early Pliocene sequences between the Mediterranean and North Atlantic. Paleoceanography, 16, 164-178.

Hötzel, S., Dupont, L., Schefuß, E., Rommerskirchen, F., Wefer, G., 2013. The role of fire in Miocene to Pliocene C4 grassland and ecosystem evolution. Nature geoscience 6, 1027–1030.

Hoetzel S., Dupont L.M., Marret F., Jung G., Wefer G., 2016. Miocene–Pliocene stepwise intensification of the Benguela upwelling over the Walvis Ridge off Namibia. International Journal of Earth Sciences, in press.

Holzwart U., Esper O., Zonneveld K.A.F., 2010. Organic-walled dinoflagellate cysts as indicators of oceanographic conditions and terrigenous input in the NW African upwelling region. Review of Palaeobotany and Palynology 159, 35–55.

Hooghiemstra, H., 1988. Palynological records from northwest African marine sediments: a general outline of the interpretation of the pollen signal. Philosophical Transactions of the Royal Society of London B 318, 431-449.

Hooghiemstra, H., Agwu, C.O.C., Beug H.-J., 1986. Pollen and spore distribution in recent marine sediments: a record of NW-African seasonal wind patterns and vegetation belts. "Meteor" Forschungs-Ergebnisse C 40, 87-135.

Hooghiemstra, H., Bechler, A., Beug, H.-J., 1987. Isopollen maps for 18,000 yr BP of the Atlantic offshore of Northwest Africa: evidence for palaeo-wind circulation. Paleoceanography 2, 561-582.

Hooghiemstra, H., Lézine, A.-M., Leroy, S.A.G., Dupont, L., Marret, F., 2006. Late Quaternary palynology in marine sediments: A synthesis of the understanding of pollen distribution patterns in the NW African setting. Quaternary International 148, 29–44.

Ivanovic, R. F., Valdes, P. J., Flecker, R., and Gutjahr, M., 2014. Modelling global-scale climate impacts of the late Miocene Messinian Salinity Crisis. Climate of the Past, 10, 607-622.

Jansen, E., Fronval, T., Ranck, F. & Channel, J.E.T., 2000. Pliocene-Pleistocene ice rafting history and cyclicity in the Nordic Seas during the last 3.5 Myr. Paleoceanography, 15: 709-721.

Jansen, E., Overpeck J., Briffa K.R., Duplessy J.-C., Joos F., Masson-Delmotte V., Olago D., Otto-Bliesner B., Peltier W.R., Rahmstorf S., Ramesh R., Raynaud D., Rind D., Solomina O., Villalba R. and Zhang D., 2007: Palaeoclimate. In: Climate Change 2007: The Physical Science Basis. Contribution of Working Group I to the Fourth Assessment Report of the Intergovernmental Panel on Climate Change [Solomon, S., D. Qin, M. Manning, Z. Chen, M. Marquis, K.B. Averyt, M. Tignor and H.L. Miller (eds.)]. Cambridge University Press, Cambridge, United Kingdom and New York, NY, USA.

Jansen, E., Raymo., M.E., Blum, P., et al., 1996. Site 982 Proceedings ODP Initial Reports 162. Ocean Drilling Program College Station TX, 91-138.

Jansen, J.H.F., Gaast, S.J. van der, Koster, B., Vaars, A.J., 1998. CORTEX, a shipboard XRF-scanner for element analyses in split sediment cores. Marine Geology 151, 143-153.

Kalu A.E., 1979. The African dust plume: its characteristics and propagation across West Africa in Winter. In: Morales, C. (ed.), Saharan dust: Mobilization, transport, deposition. John Wiley, New York, 95-118.

Kalu, A.E., 1979. The African dust plume: its characteristics and propagation across West Africa in Winter. In: Morales, C. (Ed.), Saharan dust: Mobilization, transport, deposition. John Wiley, New York, pp. 95-118.

Knapp, R., 1973. Die Vegetation von Afrika. Fischer Stuttgart, 626p.

Krijgsman, W., Hilgen, F.J., Raffi, I., Sierro, F.J., Wilson, D.S., 1999. Chronology, causes and progression of the Messinian salinity crisis. Nature, 400, 652-655.

Kröpelin, S., Verschuren, D., & Lezine, A.M., 2008. Response to Comment on "Climate-Driven Ecosystem Succession in the Sahara: The Past 6000 Years". Science, 322: 1326.

Kutzbach, J.E., Liu, Z., 1997. Response of the African monsoon to orbital forcing and ocean feedbacks in the middle Holocene. Science, 278, 440-443.

LaRiviere, J.P., Ravelo, A.C., Crimmins, A., Dekens, P.S., Ford, H.L., Lyle, M., Wara, M.W., 2012.Late Miocene decoupling of oceanic warmth and atmospheric carbon dioxide forcing. Nature 486, 97–100.

Larrasoaña, J. C., Roberts, A. P., Rohling, E. J., 2013. Dynamics of green Sahara periods and their role in hominin evolution. PLoS ONE, 8, e76514. doi:10.1371/journal.pone.0076514.

Laskar, J., Robutel, P., Joutel, F., Gastineau, M., Correia, A. C. M., Levrard, B., 2004. A long-term numerical solution for the insolation quantities of the Earth. Astronomy and Astrophysics, 285, 261-285.

Laskar, J., Robutel, P., Joutel, F., Gastineau, M., Correia, A.C.M., Levrard, B., 2004. A long-term numerical solution for the insolation quantities of the Earth. Astronomy and Astrophysics, 285, 261–285.

Lawrence, K.T., Herbert, T.D., Brown, C.M., Raymo, M.E., Haywood, A.M., 2009. High-amplitude variations in North Atlantic sea surface temperature during the early Pliocene warm period. Paleoceanography 24, PA2218, 1-15.

Lawrence, K.T., Liu, Z., Herbert, T.D., 2006. Evolution of the eastern tropical Pacific through Plio-Pleistocene glaciation. Science 312, 79-83.

Lawrence, K.T., Sosdian, S.M., White, H.E., Rosenthal, Y., 2010. North Atlantic climate evolution through the Plio-Pleistocene climate transitions. Earth and Planetary Science Letters 300, 329-342.

Leroux, M. 1983. Le climat de l'Afrique tropicale (texte & atlas). Edition Champion, Paris: 633p.

Leroy, S.A.G., Dupont, L.M., 1994. Development of vegetation and continental aridity in northwestern Africa during the Late Pliocene: the pollen record of ODP 658. Palaeogeography, Palaeoclimatology, Palaeoecology 109, 295-316.

Leroy, S.A.G., Dupont, L.M., 1997. Marine palynology of the ODP Site 658 (N-W Africa) and its contribution to the stratigraphy of Late Pliocene. Geobios 30, 351-359.

Lisiecki L.E., Raymo M.E., 2005. A Pliocene-Pleistocene stack of 57 globally distributed benthic $\delta^{18}O$ records. Paleoceanography 20, PA1003, doi: 10.1029/2004PA001071.

Lunt, D.J., Haywood, A.M., Schmidt, G.A., Salzmann, U., Valdes, P.J., Dowsett, H.J., 2010. Earth system sensitivity inferred from Pliocene modelling and data. Nature Geoscience. 3, 60–64.

Lunt, D.J., Valdes, P.J., Haywood, A.M. & Rutt, I.C., 2007. Closure of the Panama Seaway during the Pliocene: implications for climate and Northern Hemisphere glaciations. Climate Dynamics, 30: 1-18.

Maher, L.J. Jr., 1972. Nomograms for computing 0.95 confidence limits of pollen data. Review of Palaeobotany and Palynology 13, 85-93.

Maley, J., 1970. Contributions à l'étude du bassin tchadien. Atlas de pollens du Tchad. Bulletin du Jardin botanique national de Belgique 40, 29-48.

Mann, M. E., Lees, J. M., 1996. Robust estimation of background noise and signal detection in climatic time series. Climate Change, 33, 409–445, doi:10.1007/BF00142586.

Manzi, V., Gennari, R., Hilgen, F., Krijgsman, W., Lugli, S., Roveri, M., Sierro, F.J., 2013. Age refinement of the Messinian salinity crisis onset in the Mediterranean. Terra Nova, 25, 315-322.

Marlow J.R., Lange C.B., Wefer G., Rosell-Melé A., 2000. Upwelling intensification as part of the Pliocene-Pleistocene climate transition. Science 290, 2288-2291.

Marret F., 1994. Distribution of dinoflagellate cysts in recent marine sediments from the east Equatorial Atlantic (Gulf of Guinea). Review of Palaeobotany and Palynology 84, 1-22.

Martínez-Botí M.A., Foster G.L., Chalk T.B., Rohling E.J., Sexton P.F., Lunt D.J., Pancost R.D., Badger M.P.S., Schmidt D., 2015. Plio-Pleistocene climate sensitivity evaluated using high-resolution CO_2 records. Nature 518, 49-54.

Marzocchi, A., Lunt, D. J., Flecker, R., Bradshaw, C. D., Farnsworth, A., Hilgen, F. J., 2015. Orbital control on late Miocene climate and the North African monsoon: insight from an ensemble of sub-precessional simulations. Climate of the Past Discussions, 11, 2181-2237.

Mascle J., Lohmann G.P., Clift P.D., et al., 1996. Proceedings of the Ocean Drilling Program, Initial Reports Vol. 159. Ocean Drilling Program, College Station, TX.

McGee, D., Donohoe, A., Marshall, J., Ferreira, D., 2014. Changes in ITCZ location and cross-equatorial heat transport at the Last Glacial Maximum, Heinrich Stadial 1, and the mid-Holocene. Earth and Planetary Science Letters, 390, 69–79.

McMinn, A. 1992. Neogene dinoflagellate distribution in the eastern Indian Ocean from Leg 123, Site 765. In: Gradstein F.M., Ludden J.N. et al. (eds.), Proceedings of the Ocean Drilling Program, Scientific Results Vol. 123, College Station, TX (Ocean Drilling Program), 429-441, doi:10.2973/odp.proc.sr.123.120.1992.

Miller K.G, Kominz M.A., Browning JV., Wright J.D., Mountain G.S., Sugarman P.J., Cramer B.S., Christie-Blick N., Pekar S.F., 1995. The Phanerozoic Record of Global Sea-Level Change. Science, 310, 1293-1298.

Mittelstaedt E., 1991. The ocean boundary along the northwest African coast: Circulation and oceanographic properties at the sea surface. Prog. Oceanog. Vol. 26, pp. 307-355.

Moreno, T., Querol, X., Catillo, S., Alastuey, A., Cuecas, E., Herrmann, L., Mounkaila, M., Elvira, J., Gibbons, W., 2006. Geochemical variations in aeolian mineral particles from the Sahara–Sahel Dust Corridor. Chemosphere 65, 261-270.

Morley, R. J., 2000. Origin and Evolution of Tropical Rain Forest. London: Wiley & Sons, 378 p.

Morzadec-Kerfourn M.T., 1992. Estuarine dinoflageflagellate cysts among oceanic assemblages of Pleistocene deep-sea sediments from the west African margin and their paleoenvironmental significance. In: Head M.J., Wrenn, J.H. (eds.), Neogene and Quaternary Dinoflagellate cysts and Acritarchs. American Association of Stratigraphic Palynologists Foundation, Dallas, 133-146.

Moussa A., Novello A., Lebatard A-E., Decarreau A., Fontaine C., Barboni D., Sylvestre F., Bourlès D.L., Paillès C., Buchet G., Duringer P., Ghienne J-F., Maley J., Mazur J-C., Roquin C., Schuster M., Vignaud P., Brunet M., 2016. Lake Chad sedimentation and environments during the late Miocene and Pliocene: new evidence from mineralogy and chemistry of the Bol core sediments. Journal of African Earth Sciences (in press), doi:10.1016/j.jafrearsci.2016.02.023.

Mulitza, S., Prange, M., Stuut, J.-B., Zabel, M., von Dobeneck, T., Itambi, A.C., Nizou, J., Schulz, M., Wefer, G., 2008. Sahel megadroughts triggered by glacial slowdowns of Atlantic meridional overturning. Paleoceanography 23, PA4206, 1-11.

Murphy, L N., Kirk-Davidoff, D. B., Mahowald, N., Otto-Bliesner, B. L., 2009. A numerical study of the climate response to lowered Mediterranean Sea level during the Messinian Salinity Crisis. Palaeogeography, Palaeoclimatology, Palaeoecology, 279, 41-59

Naafs, B.D.A., Hefter, J., Acton, G., Haug, G.H., Martínez-Garcia, A., Pancost, R., Stein, R., 2012. Strengthening of North American dust sources during the late Pliocene (2.7 Ma). Earth and Planetary Science Letters 317-318, 8-19.

Naafs, B.D.A., Stein, R., Hefter, J., Khélifi, De Schepper, S., Haug, G.H., 2010. Late Pliocene changes in the North Atlantic Current. Earth and Planetary Science Letters 298, 434-442.

Nicholson S.E., and Grist J.P, 2003. The Seasonal Evolution of the Atmospheric Circulation over West Africa and Equatorial Africa. Journal of Climate 16, 1013-1030.

Nicholson, S.E., 2009. A revised picture of the structure of the "monsoon" and land ITCZ over West Africa. Climate Dynamics 32, 1155-1171.

Nicholson, S.E., 2013. The West African Sahel: A Review of Recent Studies on the Rainfall Regime and Its Interannual Variability. ISRN Meteorology, Vol. 2013, Article ID 453521,32 pages. http://dx.doi.org/10.1155/2013/453521.

Nicolás, J., Chiari, M., Crespo, J., Garcia Orellana, I., Lucarelli, F., Nava, S., Pastor, C., Yubero, E., 2008. Quantification of Saharan and local dust impact in an arid Mediterranean area by the positive matrix factorization (PMF) technique. Atmospheric Environment 42, 8872-8882.

Niedermeyer, E.M., Prange, M., Mulitza, S., Mollenhauer, G., Schefuß, E. & Schulz, M., 2009. Extratropical forcing of Sahel aridity during Heinrich Stadials. Geophysical Research Letters, 36, L20707: 1-4.

Norris, R.D., 1998. Miocene-Pliocene surface-water hydrography of the eastern equatorial Atlantic. In: Mascle, J., Lohmann, G.P., Moullade, M. (eds.), Proceedings of the Ocean Drilling Program, Scientific Results Vol. 159, College Station, TX (Ocean Drilling Program), 539-555.

Norris, R.D., 1998. Planktonic foraminifer biostratigraphy: eastern equatorial Atlantic. In: Mascle, J., Lohmann, G.P., Moullade, M. (Eds.), Proceedings of the Ocean Drilling Program, Scientific Results, 159. Ocean Drilling Program, College Station TX, pp. 445-479.

Oboh-Ikuenobe F.E., Hoffmeister A.P. Chrisfield R.A., 1999. Cyclical distribution of dispersed organic matter and dinocysts, ODP site 959 (early Oligocene-early Miocene, côte d'Ivoire-Ghana transform margin), Palynology, 23:1, 87-96.

Oboh-Ikuenobe F.E., Yepes O., ODP Leg 159 Scientific Party, 1997. Palynofacies analysis of sediments from the C ôte d'Ivoire-Ghana transform margin: Preliminary correlation with some regional events in the Equatorial Atlantic. Palaeogeography, Palaeoclimatology, Palaeoecology 129 291-314.

Oksanen J., Blanchet F. G, Kindt R., Legendre P., Minchin P. R, O'Hara R. B., Simpson G. L., Solymos P., Stevens M. H. H. and Wagner H., 2015. Vegan: Community Ecology Package. R package version 2.2-1.

Otto-Bliesner, B.L., Russell, J.M., Clark, P.U., Liu, Z., Overpeck, J.T., Konecky, B., deMenocal, P., Nicholson, S.E., He, F., Lu, Z., 2014. Coherent changes of southeastern equatorial and northern African rainfall during the last deglaciation. Science, 346 (6214), 1223–1227.

Paez-Reyes M., Head J.M. 2013. The Cenozoic Gonyaulacacean Dinoflagellate Genera Operculodinium Wall, 1967 and Protoceratium Bergh, 1881 and Their Phylogenetic Relationships. Journal of Paleontology 87(5):786-803.

Paez-Reyes M., Head J.M., 2013. The Cenozoic Gonyaulacacean Dinoflagellate genera Operculodinium Wall, 1967 and Protoceratium Bergh, 1881 and their phylogenetic relationships. Journal of Paleontology 87, 786-803.

Pagani M., Liu Z., Lariviere J.P., Ravelo A.C., 2010. High Earth-system climate sensitivity determined from Pliocene carbon dioxide concentrations. Nature Geoscience 3, 27-30, doi: 10.1038/ngeo724.

Paillard, D., Labeyrie, L., Yiou, P., 1996. Macintosh program performs time-series analysis. EOS Transactions AGU 77(39), 379, doi:10.1029/96EO00259.

Peterson R.G. and Stramma L., 1991. Upper-level circulation in the south Atlantic ocean. Progress in Oceanography, 26, 1-73.

Peyrillé P. and Lafore J.P., 2007. An idealized two-dimensional framework to study the West African Monsoon—part II: largescale advection and the diurnal cycle. Journal of the Atmospheric Sciences, vol. 64(8) pp. 2783–2803.

Philander S.G., 2001. Atlantic Ocean Equatorial Currents. In Encyclopedia of Ocean Sciences, 188-191.

Poumot C. 1989. Palynological evidence for eustatic events in the tropical Neogene. Bull. Centres Rech. Explor-Prod. Elf-Aquitaine, 13,2,437-453.

Prange, M., 2008. The low-resolution CCSM2 revisited: new adjustments and a present-day control run. Ocean Sciences, 4: 151-181.

Prescott, C. L., Haywood, A. M., Dolan, A. M., Hunter, S. J., Popoe, J. O., Pickering, S. J., 2014. Assessing orbitally-forced interglacial climate variability during the mid-Pliocene Warm Period. Earth and Planetary Science Letters, 400, 261-271.

Prospero, J. M., Ginoux, P., Torres, O., Nicholson, S. E., Gill, T. E., 2002. Environmental characterization of global sources of atmospheric soil dust identified with the Nimbus 7 total ozone mapping spectrometer (TOMS) absorbing aerosol product. Reviews of Geophysics. 40, 1002, doi:10.1029/2000RG000095.

Prospero, JM., Glaccum, R.A, Nees R.T., 1981. Atmospheric transport of soil dust from Africa to south America. Nature, Vol. 289, 570-572.

R Development Core Team 2008. R: A language and environment for statistical computing. R Foundation for Statistical Computing, Vienna, Austria. ISBN 3-900051-07-0, URL http://www.R-project.org.

Radi T., Pospelova V., de Vernal A., Barrie J. V., 2007. Dinoflagellate cysts as indicators of water quality and productivity in British Columbia estuarine environments. Marine Micropalaeontology, Vol. 62 (4), 269–297.

Rahmstorf, S., 2006. Thermohaline Ocean Circulation. In: Encyclopeda of Quaternary Sciences, edited by S.A., Elias. Elsevier, Amsterdam.

Ratmeyer, V., Fischer, G., Wefer, G., 1999. Lithogenic particle fluxes and grain size distribution in the deep ocean off northwest Africa: Implications for seasonal changes of aeolian dust input and downward transport. Deep-Sea Research I 46, 1289−1337.

Ravelo, A.C., 2006. Walker Circulation and global warming: Lessons from the geologic past. Oceanography, Vol.19 (4), 114-122.

Ravelo, A.C., Andreasen, D.H., 2000. Enhanced circulation during a warm period. Geophysical Research Letters, 27, 1001–1004.

Ravelo, A.C., Andreasen, D.H., Lyle, M., Olivarez Lyle, A., Wara, M.W., 2004. Regional climate shifts caused by gradual global cooling in the Pliocene epoch. Nature 429, 263- 267.

Rea, D.K, 1994. The paleoclimatic record provided by eolian deposition in the deep-sea: the geologic history of wind. Reviews of geophysics, 32(2), 159-195.

Resh F., Sunnu A., Afeti G., 2007. Saharan dust flux and deposition rate near the Gulf of Guinea. Tellus (2008), 60B, 98–105.

Richter, T.O., Gaast, S. van der, Koster, B., Vaars, A., Gieles, R., Stichter, H.C. de, Haas, H. De, Weering, T.C. van, 2006. The Avaatech XRF Core Scanner: technical description and applications to NE Atlantic sediments. Geological Society, Special Publication 267, 39-50.

Röhl, U., Abrams, L.J., 2000. High resolution, downhole, and nondestructive core measurements from Site 999 and 1001 in the Carribean Sea: application to the Late Paleocene thermal maximum. Leckie R.M., Sigurdsson H., Acton G.D., Draper G. (eds.). Proceedings ODP, Scientific Results 165. College Station TX (Ocean Drilling Program), 191-203.

Röhl, U., Westerhold, T., Bralower, T. J., Zachos, J. C., 2007. On the duration of the Paleocene-Eocene thermal maximum (PETM), Geochemistry, Geophysics, Geosystems, 8, Q12002, doi:10.1029/2007GC001784.

Rosell-Melé A., Martínez-Garcia A., McClymont E.L., 2014. Persistent warmth across the Benguela upwelling system during the Pliocene epoch. Earth and Planetary Science Letters 386, 10-20.

Roveri, M., Flecker, R., Krijgsman, W., Lofi, J., Lugli, S., Manzi, V., Sierro, F.J., Bertini, A., Camerlenghi, A., de Lange, G., Govers, R., Hilgen, F.J., Hübscher, C., Meijer, P.Th., Stoica, M., 2014. The Messinian Salinity Crisis: Past and future of a great challenge for marine sciences, Marine Geology, 352, 25-58.

Roveri, M., Lugli, S., Manzi, V., Schreiber, C. B., 2008. The Messinian Sicilian stratigraphy revisited: new insights for the Messinian salinity crisis. Terra Nova, 20, 483-488.

Ruddiman, W. F, and Janecek, T., 1989. Pliocene-Pleistocene biogenic and terrigenous fluxes at equatorial Atlantic Sites 662, 663, and 664, In: Ruddiman, W., Sarnthein, M. et al.(Eds.), Proceedings Ocean Drilling Program, Scientific Results, 108. Ocean Drilling Program, College Station TX, pp. 211-240.

Ruddiman, W.F., Sarnthein, M. et al., 1987. Initial Reports of the DSDP/ODP, 108A. U.S. Governmental Printing Office Washington, 657-668.

Ruddiman, W.F., Sarnthein, M., Backman, J., Baldauf, J.G., Curry, W., Dupont, L.M., Janecek, T., Pokras, E.M., Raymo, M.E., Stabell, B., Stein, R., Tiedemann, R., 1989. Late Miocene to Pleistocene evolution of climate in Africa and the low-latitude Atlantic: overview of Leg 108 results. Ruddiman W.F., Sarnthein M. et al. Proceedings ODP Scientific Results 108. College Station TX (Ocean Drilling Program), 463-484.

Salzmann U., Haywood A.M and Lunt D.J, 2009. The past is a guide to the future? Comparing Middle Pliocene vegetation with predicted biome distributions for the twenty-first century. Phil. Trans. R. Soc. A. 367, 189–204.

Salzmann U., Haywood A.M., Lunt D.J., Valdes P.J., Hill D.J., 2008. A new global biome reconstruction and data-model comparison for the Middle Pliocene. Global Ecology and Biogeography 17, 432-447.

Salzmann, U., Williams, M., Haywood, A.M., Johnson, A.L.A., Kender, S., Zalasiewicz, J., 2011. Climate and environment of a Pliocene warm world. Palaeogeography, Palaeoclimatology, Palaeoecology 309, 1-8.

Sarnthein M., Tetzlaff G., Koopmann B., Wolter K., Pflaumann U., 1981. Glacial and interglacial wind regimes over the eastern subtropical Atlantic and North-West Africa. Nature 293, 193-196.

Sarnthein, M., Thiede, J., Pflaumann, U., Erlenkeuser, H., Fütterer, D., Koopmann, B. Lange, H., Seibold, E., 1982. Atmospheric and oceanic circulation patterns off Northwest Africa during the past 25 million years. U. von Rad et al. (eds.), Geology of the Northwest African Continental Margin. Springer Heidelberg, 545-604.

Sarnthein, M., Winn, K., Jung, S.J.A., Duplessy, J.-C., Labeyrie, L., Erlenkeuser, H., Ganssen, G. 1994. Changes in east Atlantic deep-water circulation over the last 30000 years: Eight time slice reconstructions. Paleoceanography 9, 209–267.

Scheuvens, D., Schütz, L., Kandler, K., Ebert, M., Weinbruch, S., 2013. Bulk composition of northern African dust and its source sediments — A compilation. Earth-Science Reviews 116, 170-194.

Schmidt, D.N., 2007.The closure history of the Central American seaway: evidence from isotopes and fossils to models and molecules. In: Williams, M., Haywood, A.M., Gregory, F.J., Schmidt, D.N. (Eds.),Deep-Time Perspectives on Climate Change: Marrying the Signal from Computer Models and Biological Proxies. The Micropalaeontological Society, Special Publications. The Geological Society, London, pp. 427–442.

Schneck, R., Micheels, A., Mosbrugger, V., 2010. Climate modelling sensitivity experiments for the Messinian Salinity Crisis. Palaeogeography, Palaeoclimatology, Palaeoecology, 286, 149-163.

Schreck M., and Matthiessen J. 2013. *Batiacasphaera micropapillata*: paleobiogeographic distribution and paleoecological implications of a critical Neogene species complex. From: Lewis, J.,M., Marret F., & Bradley, L., (eds). Biological and Geological Perspectives of Dinoflagellates. The Micropaleontological Society, Sp. Publ. Geological Society, London, 301-134.

Schreck M., Matthiessen J., Head M.J., 2012. A magnetostratigraphic calibration of Middle Miocene through Pliocene dinoflagellate cyst and acritarch events in the Iceland Sea (Ocean Drilling Program Hole 907A), Review Palaeobotany and Palynology 187, 66-94.

Schreck, M., Meheust, M., Stein, R., Matthiessen, J., 2013. Response of marine palynomorphs to Neogene climate cooling in the Iceland Sea (ODP Hole 907A). Marine Micropaleontolology, 101, 49–67.

Schulz, M., Mudelsee. M., 2002. REDFIT: estimating red-noise spectra directly from unevenly spaced paleoclimatic time series. Computers & Geosciences, 28, 421-426.

Seki O., Foster G., Schmidt D., Mackensen A., Kawamura K., Pancost R., 2010, Alkenone and boron-based Pliocene pCO_2 records. Earth and Planetary Science Letters 292, 201-211, doi: 10.1016/j.epsl.2010.01.037.

Shackleton, N.J., Crowhurst, S., 1997. Sediment fluxes based on an orbitally tuned time scale 5 Ma to 14 Ma, Site 926. In: Shackleton, N.J., Curry, W.B., Richter, C., Bralower, T. (Eds.), Proceedings of the Ocean Drilling Program, Scientific Results, 154: Ocean Drilling Program, College Station TX, pp. 69-82.

Shackleton, N.J., M. A. Hall, Pate, D., 1995. Pliocene stable isotope stratigraphy of Site 846, In: Pisias, N.G., Mayer, L.A., Janecek, T.R., Palmer-Julson, A., van Andel, T.H. (Eds.), ,Proceedings of the Ocean Drilling Program, Scientific Results. 138. Ocean Drilling Program, College Station TX, pp. 337-355.

Shafik, S., Watkins, D. K. Shin, I. C., 1998. Upper Cenozoic calcareous nannofossil biostratigraphy, Cote D'Ivoire-Ghana Margin, eastern equatorial Atlantic. In: Mascle, J., Lohmann, G.P., Moullade, M. (Eds.), Proceedings of the Ocean Drilling Program, Scientific Results, 159. Ocean Drilling Program, College Station TX, pp. 509-523.

Shin, I. C., 1998. Pliocene-Pleistocene paleoclimatic and paleoceanographic history of the site 959, Eastern equatoria AtlanticOcean. In: Mascle, J., Lohmann, G.P., Moullade, M. (Eds.), Proceedings of the Ocean Drilling Program, Scientific Results, 159. Ocean Drilling Program, College Station TX, pp. 575-583.

Shin, I. C., Shafik, S., Watkins, D. K., 1998. High resolution Pliocene-Pleistocene biostratigraphy of Site 959. In: Mascle, J., Lohmann, G.P., Moullade, M. (Eds.), Proceedings of the Ocean Drilling Program, Scientific Results, 159. Ocean Drilling Program, College Station TX, pp.533-538.

Sowunmi, M.A., 1973. Pollen grains of Nigerian plants. Grana 13, 145-186.

Sowunmi, M.A., 1995. Pollen of Nigerian plants 2. Woody species. Grana 34, 39-44.

Stein, R., Haven, H.L., Littke, R., Rullkötter, J.,Welte, D.H., 1989. Accumulation of marine and terrigenous organic carbon at upwelling Site 658 and nonupwelling Sites 657 and 659: implications for the reconstruction of paleoenvironments in the eastern subtropical Atlantic through late Cenozoic times. Ruddiman W.F., Sarnthein M. et al. Proceedings ODP Scientific Results 108. College Station TX (Ocean Drilling Program), 361-385.

Steph, S., Tiedemann, R., Prange, M., Groeneveld, J., Nürnberg, D., Reuning, L., Schulz, M.,Haug, G.H., 2006. Changes in Caribbean surface hydrography during the Pliocene shoaling of the Central American Seaway. Paleoceanography 21, PA4221.

Steph, S., Tiedemann, R., Prange, M., Groeneveld, J., Schulz, M., Timmermann, A., Nürnberg, D., Rühlemann, C., Saukel, S., Haug, G., 2010. Early Pliocene increase in thermohaline overturning: A precondition for the development of the modern equatorial Pacific cold tongue. Paleoceanography 25, PA2202, 1-17.

Stuut, J. B., Zabel, M., Ratmeyer, V., Helmke, P., Schefuß, E., Lavik, G., Schneider, R., 2005. Provenance of present-day eolian dust collected off NW Africa, J. Geophysical Research, 110, D04202, doi:10.1029/2004JD005161.

Tiedemann, R., 1991. Acht Millionen Jahre Klimageschichte von Nordwest Afrika und Paläo-Ozeanographie des angrenzenden Atlantiks: Hochauflösende Zeitreihen von ODP Sites 658-661. Thesis Universität Kiel, 127p.

Tiedemann, R., Sarnthein, M., Shackleton, N.J., 1994. Astronomic timescale for the Pliocene Atlantic $\delta^{18}O$ and dust flux records of Ocean Drilling Program site 659. Paleoceanography 9, 619-638.

Tiedemann, R., Sarnthein, M., Stein, R., 1989. Climatic changes in the western Sahara: aeolo-marine sediment record of the last 8 M.Y. (ODP-Sites 657-661). Ruddiman W.F., Sarnthein M. et al. Proceedings ODP Scientific Results 108. College Station TX (Ocean Drilling Program), 241-277.

Tjallingii, R., 2006. Application and quality of X-Ray Fluorescence core scanning in reconstructing late Pleistocene NW African continental margin sedimentation patterns and paleoclimate variations. Thesis University of Bremen, 114p.

Tjallingii, R., Rohl U., Kolling M., and Bickert T., 2007. Influence of the water content on X-ray fluorescence core-scanning. Marine Geology 151, 143–153.

Torrence, C., Compo, G.P., 1998. A practical guide to wavelet analysis. Bulletin of the American Meteorological Society, 79, 61-78.

Trauth, M.H., Larrasoana, J.C., Mudelsee, M., 2009. Trends, rhythms and events in Plio-Pleistocene African climate. Quaternary Science Reviews 28, 399-411.

Tuenter, E., Weber, S.L., Hilgen, F.J., Lourens, L.J., 2003. The response of the African summer monsoon to remote and local forcing due to precession and obliquity. Global and Planetary Change, 36, 219-235.

Tuenter, E., Weber, S.L., Hilgen, F.J., Lourens, L.J., Ganopolski, A., 2005. Simulation of climate phase lags in response to precession and obliquity forcing and the role of vegetation. Climate Dynamics, 24, 279-295.

Udeze C.U, Oboh-Ikuenobe F.E., 2005. Neogene palaeoceanographic and palaeoclimatic events inferred from palynological data: Cape Basin off South Africa, ODP Leg 175. Palaeogeography, Palaeoclimatology, Palaeoecology 219, 199 – 223.

Vallé F., Dupont L.M., Leroy S.A.G., Schefuß E., Wefer G., 2014. Pliocene environmental change in West Africa and the onset of strong NE Trade winds (ODP Sites 659 and 658). Palaeogeography, Palaeoclimatology,Palaeoecology 414, 403-414.

Vallè F., Dupont, L.M., Westerhold, T. submitted to IJES. Orbitally-driven environmental changes recorded at ODP Site 959 (eastern equatorial Atlantic) from the Late Miocene to the Early Pleistocene. (under review)

Versteegh G.J.M, 1994. Recognition of cyclic and non-cyclic environmental changes in the Mediterranean Pliocene: A palynological approach. Marine Micropaleontology, 23, 147-183.

Versteegh G.J.M., Zonneveld K.A.F, 2002. Use of selective degradation to separate preservation from productivity. Geology; 20, 615-618.

Verstraete, J.M., 1992. The seasonal upwellings in the Gulf of Guinea. Progress in Oceanography 29, 1-60.

Vidal, L., Bickert, T., Wefer, G., Röhl, U., 2002. Late Miocene stable isotope stratigraphy of SE Atlantic ODP Site 1085: Relation to Messinian events. Marine Geology, 180, 71-85.

Vizy E., and Cook, K.H., 2001. Mechanisms by Which Gulf of Guinea and Eastern North Atlantic Sea Surface Temperature Anomalies Can Influence African Rainfall. Journal of Climate, Vol.14, 795-821.

Wagner, T., 1998. Pliocene-Pleistocene deposition of carbonate and organic carbonate at Site 959: paleoenvironmental implications for the eastern Equatorial Atlantic off Ivory Coast/Ghana. In: Mascle, J., Lohmann, G.P., and Moullade, M. (Eds.), Proceedings of the Ocean Drilling Program, Scientific Results, 159. Ocean Drilling Program, College Station TX, pp. 557-574.

Wagner, T., 2002. Late Cretaceous to early Quaternary organic sedimentation in the eastern Equatorial Atlantic. Palaeogeography, Palaeoclimatology, Palaeoecology, 179, 113–147.

Wall D., Dale B., Lohmann G.P., Smith W. K., 1977. The environmental and climatic distribution of dinoflagellate cysts in modern marine sediments from regions in the North and South Atlantic oceans and adjacent seas.Marine Micropaleontology, 2, 121-200.

Wara, M.W., Ravelo, A.C., Delaney, M.L., 2005. Permanent El Nino–like conditions during the Pliocene Warm Period. Science 309, 758-761.

Warny S.A., and Wrenn J.H., 1997. New species of dinoflagellate cysts from the Bou Regreg core: a Miocene-Pliocene boundary section on the Atlantic coast of Morocco. Review of Palaeobotany and Palynology 96, 281-304.

Weedon, G. 2003. Time-Series Analysis and Cyclostratigraphy: Examining Stratigraphic Records of Environmental Cycles. Cambridge University Press, 252p.

Wefer G., and Fisher, G., 1993. Seasonal patterns of vertical particle flux in equatorial and coastal upwelling areas of the eastern Atlantic. Deep-Sea Research I, Vol.40 (8), pp.1613-1645.

Weltje, G.J., Tjallingii, R., 2008. Calibration of XRF core scanners for quantitative geochemical logging of sediment cores: Theory and application. Earth and Planetary Science Letters 274, 423-438.

Westerhold, T., and Röhl, U., 2006. Data report: Revised composite depth records for Shatsky Rise Sites 1209, 1210, and 1211. In Bralower, T.J., Premoli Silva, I., and Malone, M.J. (Eds.), Proc. ODP, Sci. Results,198, 1–26.

Westerhold, T., and Röhl, U., 2013. Orbital pacing of Eocene climate during the Middle Eocene Climate Optimum and the chron C19r event: Missing link found in the tropical western Atlantic. Geochemistry, Geophysics, Geosystems, 14, 4811-4825.

Westerhold, T., Bickert, T., Röhl, U., 2005. Middle to late Miocene oxygen isotope stratigraphy of ODP site 1085 (SE Atlantic): new constrains on Miocene climate variability and sea-level fluctuations. Palaeogeography, Palaeoclimatology, Palaeoecology, 217, 205–222.

Westerhold, T., Röhl, U., Wilkens, R., Pälike, H., Lyle, M., Jones, T. D., Bown, P., Moore, T., Kamikuri, S., Acton, G., Ohneiser, C., Yamamoto, Y., Richter, C., Fitch,, P., Scher, H., Liebrand, D. and the E. 320/321 Scientists, 2012. Revised composite depth scales and integration of IODP Sites U1331-U1334 and ODP Sites 1218-1220. In: Pälike, H., Lyle,

M., Nishi, H., Raffi, I., Gamage, K., Klaus, A., and the Expedition 320/321 Scientists, Proceedings IODP, 320/321, Tokyo (Integrated Ocean Drilling Program Management International, Inc.), doi:10.2204/iodp.proc.320321.201.2012

Westerhold,T., Röhl, U., Laskar, J., Raffi, I., Bowles, J., Lourens, L. J., Zachos, J. C., 2007. On the duration of magnetochrons C24r and C25n and the timing of early Eocene global warming events: Implications from the Ocean Drilling Program Leg 208 Walvis Ridge depth transect. Paleoceanography, 22, PA2201, doi:10.1029/2006PA001322.

White, F., 1983. The vegetation of Africa. Natural Resourses Research 20. UNESCO, 356p. 3 maps.

Ybert, J.P., 1979. Atlas des pollens de Côte d'Ivoire. ORSTOM, Paris. Initiations Documentation Technique 40, pp.40.

Zabel, M., Schneider, R.R., Wagner, T., Adegbie, A.T., De Vries, U., Kolonic, S., 2001. Late Quaternary climate changes in Central Africa as inferred from terrigenous input to the Niger Fan. Quaternary Research 56, 207-217.

Zachos J., Pagani M., Sloan L., Thomas E., Billups K., 2001. Trends, Rhythms, and Aberrations in Global Climate 65 Ma to Present. Science, Vol 292, 686-693.

Zeeden, C.; Hilgen, F.J.; Westerhold, T., Lourens, L.J., Röhl, U.; Bickert, T., 2013: Revised Miocene splice, astronomical tuning and calcareous plankton biochronology of ODP Site 926 between 5 and 14.4 Ma. Palaeogeography, Palaeoclimatology, Palaeoecology, 369, 430-451.

Zegarra M., and Helenes, J., 2011. Changes in Miocene through Pleistocene dinoflagellates from the Eastern Equatorial Pacific (ODP Site 1039), in relation to primary productivity. Marine Micropaleontology 81, 107–121.

Zhang Y.G., Pagani, M., Lui, Z., 2014. A 12-million-year temperature history of the tropical Pacific Ocean. Science 344, 84-87.

Zhang Z., Ramstein, G., Schuster, M., Li, C., Contoux, C., Yan, Q., 2014. Aridification of the Sahara desert caused by Tethys Sea shrinkage during the Late Miocene Nature, 513, 401-404.

Zonneveld K.A.F, Versteegh G.J.M, Kasten S., Eglinton T.I., Emeis K-C., Huguet C., Koch B.P., de Lange, G.J., de Leeuw J.W., Middelburg J.J., Mollenhauer G., Prahl F.G., Rethemeyer J., Wakeham S.G., 2010. Selective preservation of organic matter in marine environments; processes and impact on the sedimentary record. Biogeosciences 7, 483–511.

Zonneveld K.A.F, Versteegh G.J.M., de Lange G.J., 1997. Preservation of organic-walled dinoflagellate cysts in different oxygen regimes: a 10000 year natural experiment. Marine Micropaleontology, 29,393-405.

Zonneveld K.A.F., Bockelmann F-D., Holzwarth U., 2007. Selective preservation of organic walled dinoflagellate cysts as a tool to quantify past net primary production and bottom water oxygen concentrations, Marine Geolohy 237, 109-126.

Zonneveld K.A.F., Marret F., Versteegh G.J.M., Bogus K., Bonnet S., Bouimetarhan I., Crouch E., de Vernal A., Elshanawany R., Edwards L., Esper O., Forke S., Grøsfjeld K., Henry M., Holzwarth U., Kielt J-F., Kim S-Y., Ladouceur S., Ledu D., Chen L., Limoges A., Londeix L.,

Lu S-H., Mahmoud M.S., Marino G., Matsouka K., Matthiessen J., Mildenhal D.C., Mudie P., Neil H.L., Pospelova V., Qi Y., Radi T., Richerol T., Rochon A., Sangiorgi F., Solignac S., Turon J-L., Verleye T., Wang Y., Wang Z., Young M., 2013. Atlas of modern dinoflagellate cyst distribution based on 2405 datapoints, Review Palaeobotany and Palynology 191, 1-197.

Acknowledgements

First, I am indebted to Prof. Wefer who gave me the chance to work in the international community at the Marum and who gave precious advices during PhD meetings and for being understanding when I needed it.

I am deeply grateful to Lydie Dupont. She was always calm and smiling, supporting and cheering me up me when I was stressed. Lydie, thank you for having faith in me and for your great help, also after I left Bremen.

Sincere thanks to Enno Schefuß and Matthias Prange who dedicated part of their time to actively participate in my committee meetings with helpful discussions.

I am thankful to Thomas Westerhold, Vera Lukies and Ursula Röhl, "my xrf guides", for assisting me with patience during my scanning sessions. Thomas, thank you also for the time you took to explain and discuss with me the age model "problems"; that was a big help for my thesis.

Many thanks to Alex Wülbers and Walter Hale for their helpfulness in the core repository.

I thank GLOMAR and its staff for support and for the funding that allowed me to take part in several conferences and especially to have my research stay in Bergen.

My warmest gratitude is for all friends I have met in Bremen. It is also thanks to you, if I never felt alone. Mariem, Zsuzsi, Will, Claudia, Domenico, Sebastian, James, Hendrik, Ling, Raul, Jeroen, Amanda, Heather, Yancheng, Stefan, Luisa...thanks for having enriched my life in Bremen and for all your support!! Many thanks to Anna, Rony and Tim for "crazy" office moments and to Lélia, Janna, Katja, Maria for have been sharing their PhD experiences with me.

Stijn and Petra, thank you for your support and happy moments when I was in Bergen. Stijn, thanks also for sharing your dinoflagellate and Pliocene knowledge.

Grazie Fede, Fra, Paolo, Enrico, Anna, Boris, Stefania, Micol, Sara e agli amici di Bucci per essere sempre stati con me, specialmente quando ero lontano. Grazie Roberta per lo "psychiatric help" degli ultimi tempi.

Grazie Luca, che hai scelto di aspettarmi con pazienza e condividere con me tutto questo.

Un GRAZIE immenso e speciale ai miei genitori ed ai miei fratelli, mio instancabile sostegno e fonte di forza.

My entire PhD time has been a complex and long one, but for sure, it has been a very good life experience, during which I have met many nice persons that will be always in my thoughts. Thanks to all of you! Vielen Dank!

Appendix: Own contributions to Chapters 2, 3 and 4

Chapter 2: F.V. analysed part of the total samples presented in the pollen record of ODP Site 659 and combined those with previously counted samples by in the complete record. F.V. did the xrf-scanning of the cores sections and calibrated them afterwards. She elaborated and interpreted the pollen and elemental ratios results and wrote the draft of the article.

Chapter 3: F.V. scanned the core sections and developed the composite depth record and the astronomical age model. She elaborated ad interpreted the results; and drafted the manuscript.

Chapter 4: F.V. analysed the dinoflagellate cysts content of all samples presented in this chapter. She elaborated the results and interpreted the dinocysts record. F.V. drafted the manuscript.